Alma Mater Studiorum · Università di Bologna

Scuola di Scienze
Corso di Laurea magistrale in Fisica della materia

Characterization of organic thin film devices for direct X-ray photoconversion

Relatore:
Prof.Beatrice Fraboni

Presentata da:
Francesco Mariotti

Correlatori:
Ing. Carlo Dalla Val
Dott.Lorenzo Giuliani

Sessione III
Anno Accademico 2017/2018

"Dedicato ai miei genitori"

Contents

Introduction

The main purpose of this thesis is to present the fundamental characteristics of organic thin film devices for direct X-ray photoconversion. In the first part of this study will be presented the theoretical background of X-rays, X-rays detection and the theory organic devices.

In the second part will be considered in details the process of fabrication and characterization of organic devices projected for X-rays detection. The subjects of this thesis are some samples realized at the laboratories of the Department of Physics and Astronomy of Bologna: their fabrication and their electrical and X-rays characterization will be analised in this work. These samples have been realized on 5 different "substrates" in order to study their effect on the behaviour of the device.

In the third and last part will be presented the characterization of a TIPGe device (acronym of bis(triisopropylgermylethynyl)), realized at the laboratories of the Department of Physics and Astronomy of Bologna, and tested at Skan-X Radiology Devices S.p.A., a X-ray tube factory situated in San Lazzaro di Savena (Bo). The collaboration with this company offered the possibility to test the device with a complete different sets of parameters, in energy and dose range typical of dental medical applications.

Moreover it was a constructive collaboration under the aspect of further developments of the device: physicists and experts from Skan-X Radiology Devices S.p.A. and from SkanRay S.p.A. defined the key points that organic thin film devices for direct X-rays photoconversion should have to work as a X-rays detectors for radiographic imaging.

The encouraging results placed the bases for further analysis such as testing

the device with other X-rays machine or/and trying to better understand the effect of the substrates on the behaviour of the device.

In addition they represent the starting point for the beginning of the process of scaling of the device in order to move towards the fabrication of a prototype of X-ray detector for radiographic imaging.

First Part

Chapter 1

The X-rays

Nowadays X-rays are part of our life: luggage scanning at the airports, non-destructive analysis of materials and all the applications related to the medical field. In this first chapter, the fundamental characteristics and the principal methods of X-rays production are presented.

1.1 The X-rays nature

X-rays or Roentgen rays are ionizing electromagnetic radiation whose wavelength is included between 10 nanometers e 10^{-4} nanometers (1 picometeres); There are "soft" X-rays which are characterised by a wavelength greater than 0.1nm and "hard" X-rays where the wavelength is smaller than 0.1nm (Figure 1).

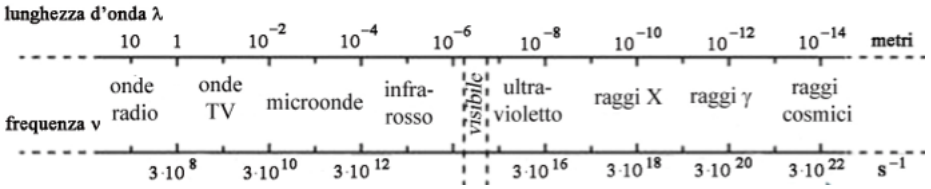

Figure 1 - Electromagnetic spectrum

Due to their short wavelength, X-rays are highly energetic radiations; this characteristic makes them a powerful instrument for deep internal analysis of object in a low invasive way. For this reason, in the last century, X-rays have been applied in medical field, chemical analysis and in the study of the internal structure of materials.

1.2 Historical informations

The studies of Willian Crookes represent the basis for the understanding of X-rays; in detail he invented the Crookes tube, father of the modern X-ray tubes (Figure 2).

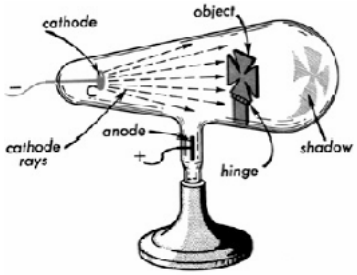

Figure 2 - Crookes tube

It is a glass cilinder, with vacuum inside, where contained electrodes aimed to produce electrical current with the application of a high voltage. He noticed that, covering the tube with photografic films, some of them were impressed. However, he did not deeply analyzed this phenomenon.

By the end of the nineteenth century, many physicists, such as Hertz, Lenard, Tesla, Righi Helmholt, studied and worked (directly or indirectly) with X-rays; though the patronage of the discovery of X-rays belongs to the German Physicists Wilhelm Konrad Röntgen (Figure 3).

Figure 3 - Wilhelm Konrad Rontgen

The discovery of X-rays is dated november, the eighth, 1895, when Roentgen, studying the properties of cathodic rays produced by an Hittorf-Crookes tube covered with opaque dark paper noticed fluorescence phenomena in a

fluorescent screen placed few meters away from the tube.

Roentgen understood that the fluorescence phenomena could not be induced by the cathodic rays. In fact those rays are able to move trough the air for smaller distances (order of centimeter). Roentgen guessed that those phenomena needed to be related to a different radiation. He called that radiation "radiation X" because he was not able to understand its characteristics. Roentgen's discovery represented a scientific revolution, in particular in the medical science field. (Figure 4).

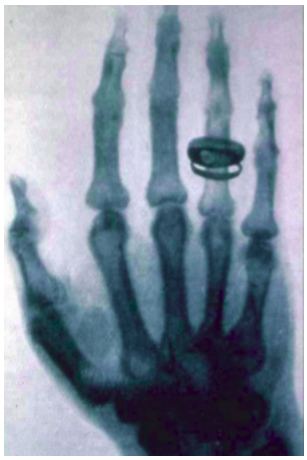

Figure 4 - First radiography by Roentgen, done on his wife's hand

1.3 The X-rays tube

The most common devices for X-rays production are the X-rays tubes. They are high vacuum tubes with a cathode and an anode placed at high voltage. The cathode is composed by the heating filament which acts as a generator of electrons.

The anode is composed by a disk of an heavy metal (with high atomic number). It can be stationary or rotating, in particular the second one allows to have a better dissipation of the heat generated by the impact of the electrons coming from the cathode.

The X-rays tube is placed inside a metallic sheat (usually alluminum with lead shielding) filled with dielectric oil which ensures heat dissipation on the

anode side and electric insulation on the cathode side. The X-rays windows is the region of the tube from which X-rays come out and it is obviously not shielded. In some X-rays tubes there are copper or berillium filter needed for screening low energy rays. The filament, powered by a huge electrical current, is heated and emits electron because of thermoionic effect; those electrons are accellerated towards the anode via high voltage potential applied. To ensure the complete focalization of the electrons is possible to use a focalizing grid which is negatively polarized by the anodic current and acts as an optical focalizer for the electrons because of the coulombian repulsion (Figure 5).

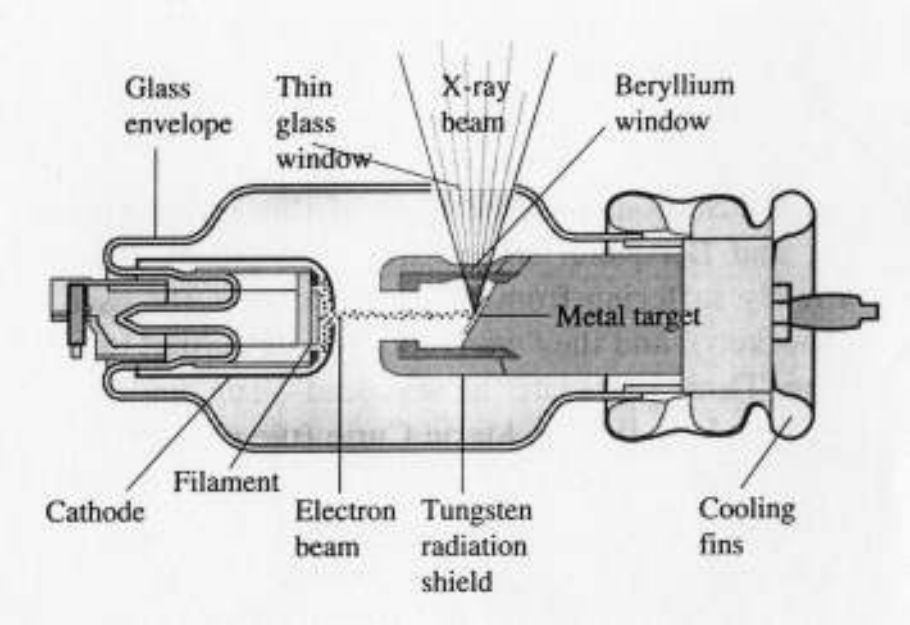

Figure 5 - Schematic representation of an X-rays tube

In the impact between electrons and the anode only 5% of the kinetic energy of the electrons is available for X-rays production. The rest of the energy is converted into thermal dissipation which can cause the deterioration or even the fusion of the tungsten disk. This is the main reason which brought to the production of rotating anode X-rays tubes (Figure 6).

The area on the tungsten disk on which electrons are shot is called target. It is not perpendicular to the electrons beam in fact it is inclined with respect to the beam accordingly to the desired angular acceptance of the tube. This inclination is necessary also to ensure that the electrons interact with a relatively great rectangular area while the X-rays photons coming out of the tube are generated by a small effective squared area called the focal spot. (Figure 7).

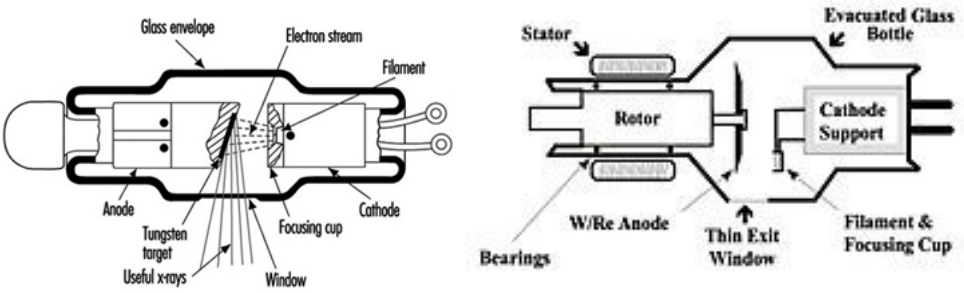

Figura 6 - Schematic of an X-rays stationary anode tube and of an X-ray rotating anode tube

By increasing the anodic angle, the focus area increases as well, inducing an increment in the intensity of X-rays; however it makes the effective focal spot bigger which implies a loss of resolution in the radiographic image. Therefore it is necessary to achieve a compromise between focal area increment and reduction of focal spot (Figure 7).

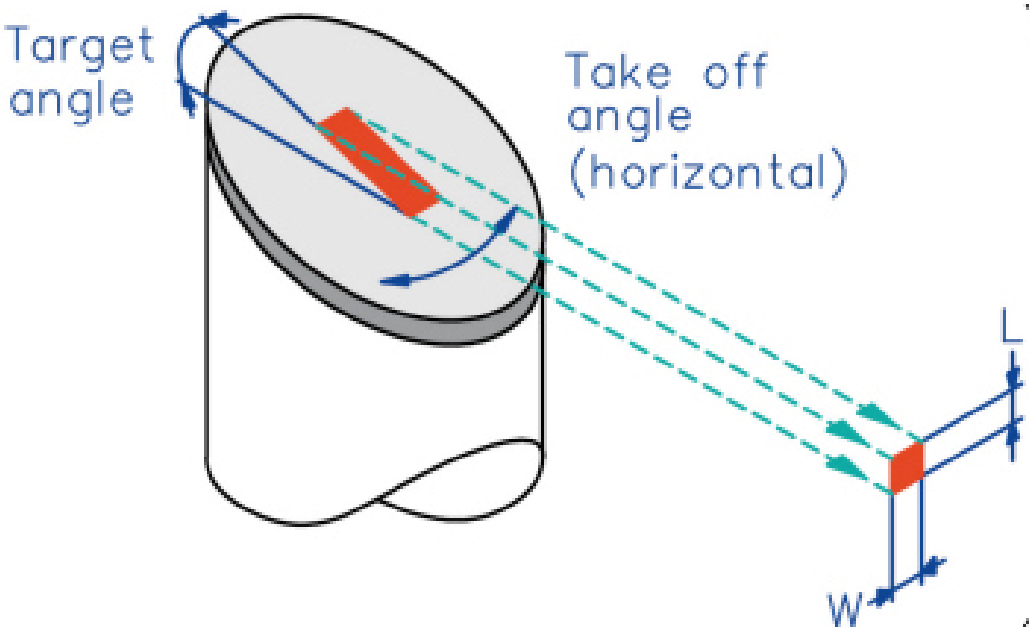

Figure 7 - X-rays tubes focal spot

1.4 X-rays tube's spectrum

The X-rays tube's spectrum represents the distribution, with respect to the energy, of the intensity of the electromagnetic radiation emitted. It is divided into two components:

- The characteristic radiation
- The continuos radiation

The last one also known as "Bremssthralung radiation" represents the radiation emitted by charged particle in a decelartion process.

The loss of energy due to Bremssthralung is relevant when treating with highly energetic electrons (hundreds of MeV in air or water tens of MeV in heavy materials). The loss of energy per unit of length is approximately calculated as:

$$-\frac{dE}{dx} = \frac{4N_a Z^2 \alpha^3 E(hc)^2}{m_e^2 c^4} ln\left(\frac{183}{z^1/3}\right) \tag{1.1}$$

where N_a is the atomic number per unit volume, Z is the atomic number of the material, α is the fine structure constant and m_e is the electron mass.

The energetic spectrum of the emitted radiation is a continuum because the energy of the X-rays depends on the distance between electron and nucleus. This means that its value can vary with continuity from 0 to the maximum value equal to the kinetic energy of electrons.

In addition to that continuum spectrum there are single lines which are due to the emission of electrons from the internal atomic level of the target. When electrons from outer atomic levels cover the holes induced by the bombarding electrons, there is an emission of specific X-rays (fluorescence X-rays).

The resultant X-rays tube's spectrum is composed by the overlapping of continuum and specific component (Figure 8).

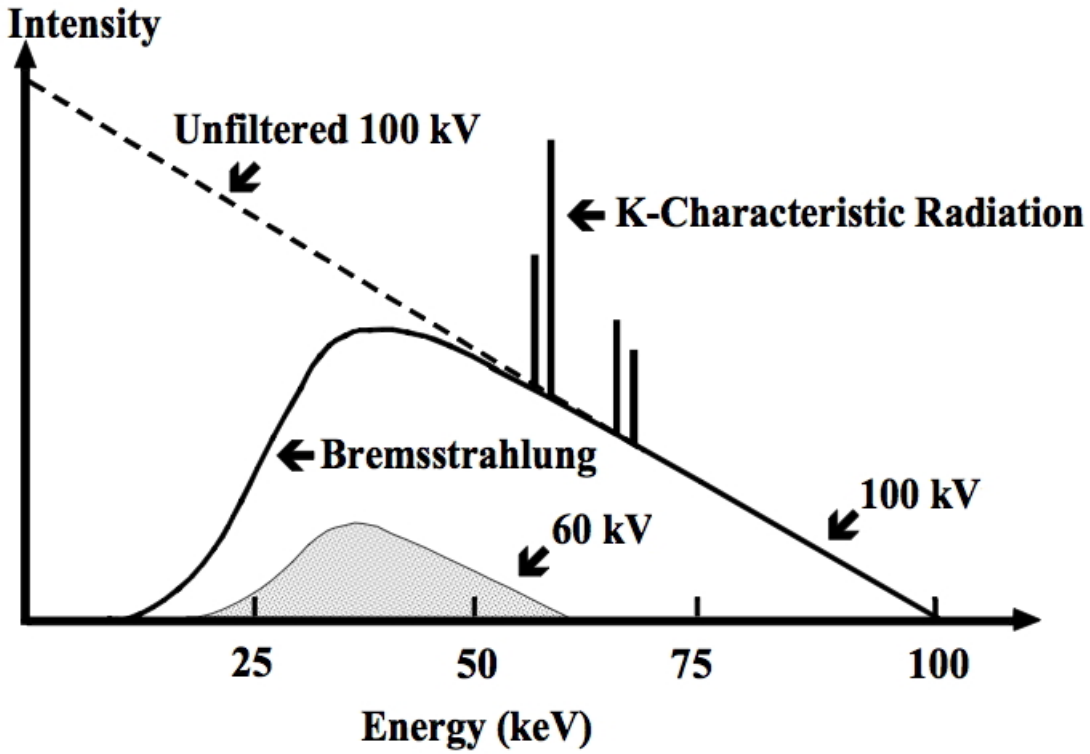

Figure 8 - X-rays tube's spectrum

1.5 Interaction with matters

X-rays are ionizing radiation, whose interaction with matter is accomplished by energy exchange between X-rays photon and the target object. This process, intrinsically probabilistic, of energy exchange between photon and the object, may induce the generation of secondary charged particles.

There are different possible interactions:

- Photoelectric effect
- Compton effect
- Couple creation
- Rayleigh coerent diffusion

- Photonuclear effect

each of them characterized by a total, partial or naught loss of energy in the interaction.

Many variables influence the type of interactions which will occur. The most relevant are:

- the atomic number of target atoms
- the energy of the beam
- the nature of the target atom itself

Figure 9 shows the range of dominant interaction (Photoelectric effect, couple production, Compton effect) as a function of both X-rays beam's energy and atomic number Z.

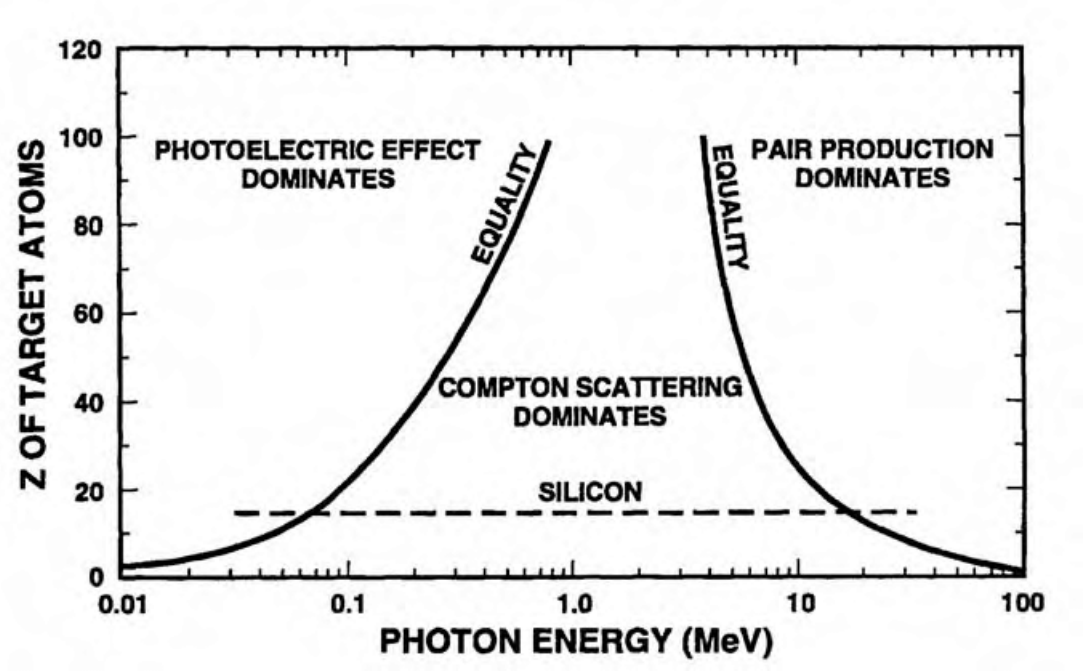

Figure 9 - Range of predominance of different effects in the interaction between photons and matters

Looking at the graph it is evident that, for low energy photons, the photoelectric effect is predominant as well as couple production is for high energy photons. The Compton effect lies in the middle between these two effects. The amplitude of the region of occurrence increases with an increment of the

atomic number Z.

The total cross section offers a quantitatively measure of the probability of interactions between photons and matters. It will take into account the contributes held by the single effects in all the possible interactions:

$$\sigma_{tot} = \sigma_{p.e} + \sigma_{C.e} + \sigma_R + \sigma_{nucl} + \kappa \tag{1.2}$$

where it is :

- $\sigma_{p.e}$ cross section linked with Photoelectric effect
- $\sigma_{C.e}$ cross section linked with Compton effect
- σ_R cross section linked with Rayleigh effect
- σ_{nucl} cross section linked with Photonuclear effect
- κ cross section linked with couple production

1.5.1 Photoelectric effect

The Photoelctric effect is the phenomenon in which the electrons of an atom, hit by low energy photon, are emitted due to the total absorption of photon energy (Figure 10). The emitted electron (photoelectron) will have a kinetic energy K_{e^-} equal to the difference between photon energy and binding energy.

$$K_{e^-} = K_f - E_b = h\nu - E_b \tag{1.3}$$

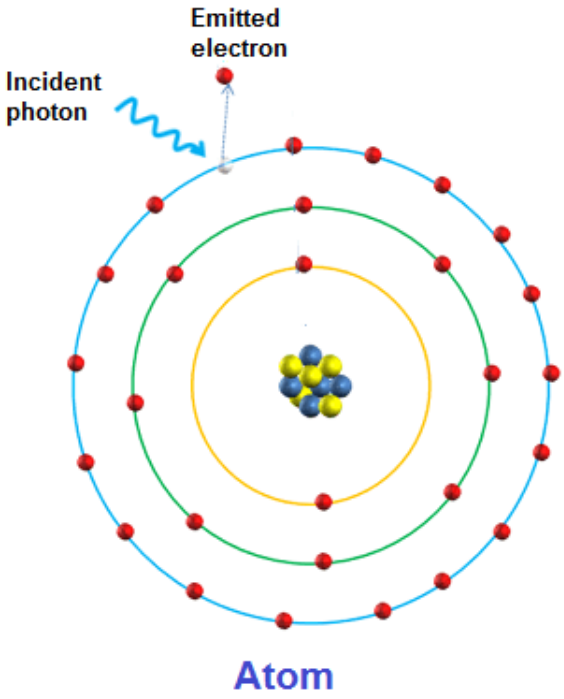

Figure 10 - Photoelectric effect

The cross section related to the Photoelectic effect will be:

$$\sigma_{p.e.} \propto Z^4 (h\nu)^{-7/2} \tag{1.4}$$

The probability of interaction via Photoelectric effect is greater the stronger the electron is bond to the atom. It happens more frequently with K-orbit electrons which are almost 80% of the total photoelectrons emitted. The probability per orbit increases when the photon energy is enough to extract the electron from the atom.

The cross section trend, due to Photoelectric effect, is characterized by sudden discontinuity corresponding to the edge energy of the orbits. This discontinuity are greater the bigger is the atomic number Z. The edge energy value can be calculated by:

$$E = \frac{13,6(Z-\sigma)^2}{n^2} eV \tag{1.5}$$

Due to the strong dipendence of the cross section to the atomic number Z, the photoelectric effect is more relevant for those heavy atoms with which the photoelectron emission induces the re-arrangement of the electrons in the atomic orbitals with consequently characteristic X-rays emission.

1.5.2 Compton effect

The compton effect represents the anelastic collision between the incident photon and an electron in the outer atomic level.

In this interaction the photon is deflected with respect to its original direction and it transmits part of its energy to the electron inducing the emission (scattering). The Compton effect is also defined as incoherent scattering because the photon is interacting with the single electron instead of the entire atom (Figure 11).

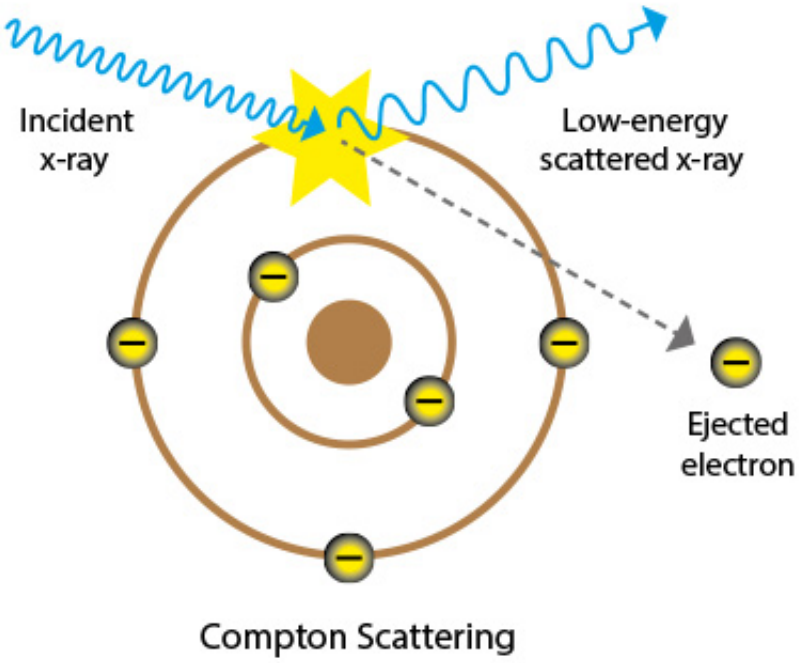

Figure 11 - Compton effect

From energy andmomentum conservation it is possible to obtain the photon energy ater the collision $E_f = h\nu^{'}$, known the initial energy $E_i = h\nu$ and the deflection angle θ:

$$h\nu^{'} = \frac{h\nu}{1 + \gamma(1 - cos(\theta))} \tag{1.6}$$

While the kinetic energy K_e will be:

$$K_e = Ei - Ef = h\nu - h\nu^{'} = h\nu \frac{\gamma(1 - cos(\theta))}{1 + \gamma(1 - cos(\theta))} \tag{1.7}$$

where:

$$\gamma = \frac{h\nu}{mc^2} \tag{1.8}$$

The photon initial energy is the key parameter determining the dynamic of the scattering:

- low energy photon: almost isotropic angular distribution.
- high energy photon: smaller deflection angles.

The electron's emission angle depends on the energy of the incident photon; however this angle is always smaller than 90 degrees. The calculation of the contribute of the Compton effect to the total cross section requires the quantistic electrodynamic; it gives for the Compton effect a cross section $\sigma_{C.e}$ proportional to Z:

$$\sigma_{C.e} \propto Z \tag{1.9}$$

1.5.3 Rayleigh diffusion

The coherent diffusion or Rayleigh diffusion is characteristic of those X-rays whose energy is smaller than bonding energy of the electrons. This consists of the elastic collision between incident low energy photons and the atoms.

Photon and atom do not exchange energy so there is no electrons emission though the photon is slightly deflected with respect to the direction of incidence.

The cross section linked with Rayleigh diffusion is proportional to a power of the atomic number Z, in details we have:

$$\sigma_R \propto Z^{5/2}(h\nu)^{-2} \tag{1.10}$$

Its contribution, in particular at high energy, is negligible compared to that brought by the Photoelectric effect.

1.5.4 Photonuclear effect

Photonuclear effect is characterized by the direct interaction between photon and nucleus; it happens when higly energetic photon (order of some MeV), able to escape from the interaction with the electron cloud and nucleus field, interacts directly with the nucleus itself.

The nucleus, assorbing photon's energy, is excited and emits a proton (reaction γ, p^+) or a neutron (reaction γ, n^0).

1.5.5 Couple creation

This process consists of the total absorption of a photon by an atom; as a consequence there is the production of a couple electron-positron. This process happens, as well as Photonuclear effect, when the energy of the photon is high enough to escape the electron cloud and to reach the nucleus of the target atom (Figure 12).

The strong dependence from energy makes the process of creation of electron-positron couple a threshold process. The minimum energy to ensure the couple creation is equal to the sum of rest energy of electron and positron:

$$E = mc^2 = m_e c^2 + m_p c^2 = 2m_e c^2 = 1.022 MeV \tag{1.11}$$

In couple production, photon's energy is absorbed and partially converted into kinetic energy and partly transformed in rest energy of the new couple of particles. However the energy is not equally split between the particles because of the nuclear repulsion.

The cross section related to this process is proportional to the squared value of the atomic number Z:

$$k = Z^2 \tag{1.12}$$

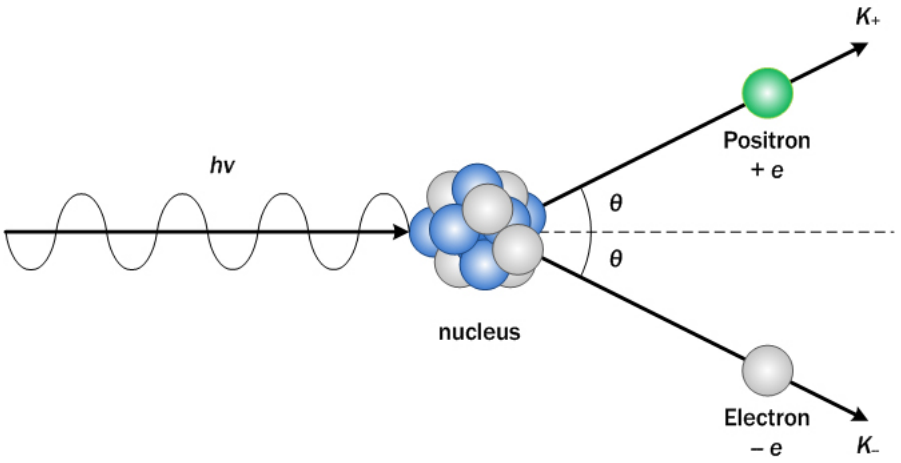

Figure 12 - Couple creation

Chapter 2

Physics of X-Ray detection in semiconductors detectors

2.1 Semiconductor properties and Semiconductor Detectors

The periodic lattice of crystalline materials establishes allowed energy bands for electrons that exist within the solid. The energy of any electron within the pure material must be confined to one of these energy bands, which may be separated by gaps of forbidden energies. A simplified representation of the bands of interest in insulators or semiconductors is shown in Figure 13.

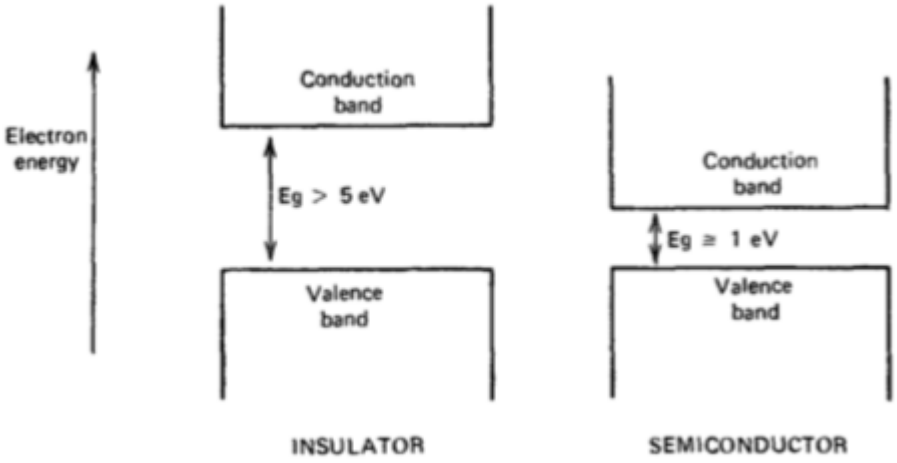

Figure 13 - Band structure for electron energies

The lower band, called the valence band, corresponds to those outer-shell electrons that are bound to specific lattice sites within the crystal. In the case of silicon or germanium, they are parts of the covalent bonding that constitutes the interatomic forces within the crystal. The next higher-lying band is called the conduction band and represents electrons that are free to migrate through the crystal. Electrons in this band contribute to the electrical conductivity of the material. The two bands are separated by the bandgap, the size of which determines whether the material is classified as a semiconductor or an insulator.

The number of electrons within the crystal is just adequate to fill completely all available sites within the valence band. In the absence of thermal excitation, both insulators and semiconductors would therefore have a configuration in which the valence band is completely full and the conduction band completely empty. Under these circumstances, neither would theoretically show any electrical conductivity.

In a metal, the highest occupied energy band is not completely full. Therefore, electrons can easily migrate throughout the material because they need to achieve only small incremental energy to be above the occupied states as shown in Figure 14.

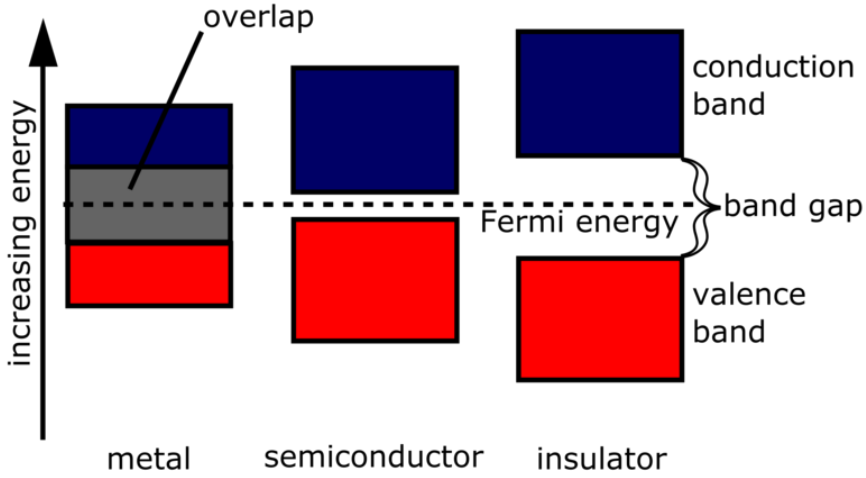

Figure 14 - Band structure comparison between metal, semiconductor and insulator

At any nonzero temperature, some thermal energy is shared by the electrons in the crystal. It is possible for a valence electron to gain sufficient thermal

energy to be elevated across the bandgap into the conduction band. Physically, this process simply represents the excitation of an electron that is normally part of a covalent bond such that it can leave the specific bonding site and drift throughout the crystal. The excitation process not only creates an electron in the otherwise empty conduction band, but it also leaves a vacancy (called a hole) in the otherwise full valence band. The combination of the two is called an electron-hole pair and is roughly the solid-state analogue of the ion pair in gases [30].

The electrons in the conduction band can be made to move under the influence of an applied electric field. The hole, representing a net positive charge, will also tend to move in an electric field, but in a opposite direction respect to the electron. The motion of both of these charges contributes to the observed conductivity of the material(4). The probability per unit time that an electron-hole pair is thermally generated is given by [8]:

$$p(T) = CT^{\frac{3}{2}} \exp\left(- \frac{E_g}{2kT} \right) \tag{2.1}$$

where:

- T is the absolute temperature
- E_g is the Band gap energy
- K is the Boltzmann constant
- C is the proportionality constant characteristic of the material

As reflected in the exponential term, the probability of thermal excitation is critically dependent on the ratio of the bandgap energy to the absolute temperature.

After their formation, both the electron and the hole take part in a random thermal motion that results in their diffusion away from their point of origin. If all electrons (or holes) were initially created at a single point, this diffusion leads to a broadening distribution of the charges as a function of time. A cross section through this distribution would be approximated by a Gaussian

function with a standard deviation σ given by:

$$\sigma = \sqrt{2Dt} \tag{2.2}$$

where D is the diffusion coefficient and t is the elapsed time. Values for D can be predicted from the relationship [8]:

$$D = \mu \frac{kT}{q} \tag{2.3}$$

where μ is the mobility of the charge carrier,q is the elementary charge, k is the Boltzmann constant, and T is the absolute temperature. At 20C (293K), the numerical value of $\frac{kT}{q_e} \approx 0.0253$eV.

If an electric field is applied to the semiconductor material, both the electrons and holes will undergo a net migration. The motion will be the combination of a random thermal velocity and a net drift velocity parallel to the direction of the applied field. The motion of the conduction electrons is a relatively easy process to visualize, but the fact that holes also contribute to conductivity is less obvious. A hole moves from one position to another if an electron leaves a normal valence site to fill an existing hole [30].

The vacancy left behind by the electron then represents the new position of the hole. Because electrons will always be drawn preferentially in an opposite direction to the electric field vector, holes move in the same direction as the electric field.

This behavior is consistent with that expected for a point positive charge, since the hole actually represents the absence of a negatively charged electron. At low-to-moderate values of the electric field intensity, the drift velocity v is proportional to the applied field. Then a mobility p for both electrons and holes can be defined by[30]:

$$v_h = \mu_h E \tag{2.4}$$

$$v_e = \mu_e E \tag{2.5}$$

Many semiconductor detectors are operated with electric field values sufficiently high to result in saturated drift velocity for the charge carriers. Because these saturated velocities are of the order of $10^7 \frac{cm}{s}$, the time required to collect the carriers over typical dimensions of 0.1cm or less will be under 10ns. Semiconductor detectors can therefore be among the fastest-responding of all radiation detector types.

In addition to their drift, the charge carriers will also undergo the influence of diffusion mentioned in the previous section. Without diffusion, all charge carriers would travel to the collecting electrodes following exactly the electric field lines that connect their point of origin to their collection point. The effect of diffusion is to introduce some spread in the arrival position that can be characterized as a Gaussian distribution whose standard deviation is[30]:

$$\sigma = \sqrt{\frac{2kTx}{q_e E}} \tag{2.6}$$

where x represents the drift distance. In small-volume detectors, a typical value for the drift distance would be less than 100 pm. This diffusion broadening of the charge distribution limits the precision to which position measurements can be made using the location at which charges are collected at the electrodes in semiconductor detectors.

Once electrons and holes are formed in a semiconductor, they will tend to migrate either spontaneously or under the influence of an applied electric field until they are either collected at an electrode or they are combine. There are theoretical predictions that the average lifetime of charge carriers before recombination in perfectly pure semiconductors could be as large as a second. In practice, lifetimes at least three or four orders of magnitude smaller than a second, are actually observed as dominated entirely by the very low level

of impurities remaining in the material.

Some of these impurities, such as gold, zinc, cadmium, or other metallic atoms occupying substitutional lattice positions, introduce energy levels near the middle of the forbidden gap. They are therefore classified as "deep impurities" (as opposed to acceptor or donor impurities whose corresponding energy levels lie near the edges of the forbidden band. are called shallow impurities). These deep impurities can act as traps for charge carriers in the sense that if a hole or electron is captured, it will be immobilized for a relatively long period of time. Although the trapping center ultimately may release the carrier back to the band from which it came, the time delay is often sufficiently long to prevent carrier from contributing to the measured pulse [30].

Other types of deep impurities can act as recombination centers. These impurities are capable of capturing both majority and minority carriers, causing them to annihilate. An impurity level near the center of the forbidden gap might, for example, first capture a conduction electron. At a slightly later time, a hole from the valence band might also be captured, with the electron then filling the hole.

The impurity site is thus returned to its original state and is capable of causing another recombination event. In most crystals recombination through such centers is far more common than direct recombination of electrons and holes across the full bandgap.

Both trapping and recombination contribute to the loss of charge carriers and tend to reduce their average lifetime in the crystal. For the material to serve as a good radiation detector, a large fraction (preferably 100%) of all the carriers created by the passage of the incident radiation should be collected. This condition will hold provided the collection time for the carriers is short compared with their mean lifetime. Collection times of the order of 10^7s to 10^8s are fairly common, so that carrier lifetimes of the order of 10^5s or longer are usually sufficient.

When radiation interacts in a semiconductor, the energy deposition always leads to the creation of equal numbers of holes and electrons. This statement holds regardless of whether the host semiconductor is pure or intrinsic,

or doped as p-type or n-type. Just as equal numbers of free electrons and positive ions are created in a gas, every conduction electron produced in a semiconductor must also create a hole in the valence band, leading to an exact balance in the initial number of created charges.

It should also be emphasized that the doping levels typical in p- or n-type semiconductors are so low that these atoms play no significant role in determining the nature of the radiation interactions in the material. Thus p-type or n-type silicon of equal thickness will present identical interaction probabilities for gamma rays, and the range of charge particles in either type will also be the same [30].

The dominant advantage of semiconductor detectors lies in the smallness of the ionization energy.The value of E for either silicon or germanium is about 3 eV, compared with about 30 eV required to create an ion pair in typical gas-filled detectors. Thus, the number of charge carriers is 10 times greater for the semiconductor case, for a given energy deposited in the detector. The increased number of charge carriers has two beneficial effects on the attainable energy resolution.

The statistical fluctuation in the number of carriers per pulse becomes a smaller fraction of the total as the number is increased. This factor is often predominant in determining the limiting energy resolution of a detector for medium to high radiation energy. At low energies, the resolution may be limited by electronic noise in the preamplifier, and the greater amount of charge per pulse leads to a better signal/noise ratio.

2.2 Semiconductor direct detectors

Starting from 1970s, silicon or germanium doped with lithium (Si(Li) or Ge(Li)) semiconductor detectors have been developed. X-rays photons are converted to electron-hole pairs in the semiconductor and are collected to directly detect the X-rays.

When the temperature is low enough (the detector is cooled by Peltier cells or even cooler liquid nitrogen), it is possible to directly determine the X-ray energy spectrum; this method is called energy dispersive X-rays spectroscopy

(EDX or EDS); it is often used in small X-ray fluorescence spectrometers.

Silicon drift detectors[44] (SDDs, Figure 15), produced by conventional semiconductor fabrication, now provide a cost-effective and high resolving power radiation measurement. Unlike conventional X-rays detectors, such as Si(Li), they do not need to be cooled with liquid nitrogen. These detectors are rarely used for imaging and are only efficient at low energies.

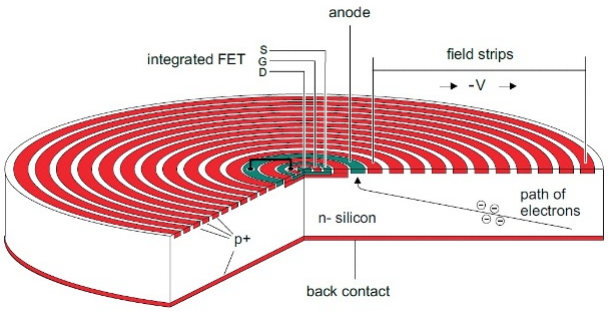

Figure 15 - Silicon drift detectors

Practical application in medical imaging started in the early 2000s. Amorphous selenium is used in commercial large area flat panel X-rays detectors for mammography and general radiography due to its high spatial resolution and x-ray absorbing properties[61]. However Selenium's low atomic number requires a thick layer to achieve sufficient sensitivity.

Cadmium telluride (CdTe) and its alloy with zinc, cadmium zinc telluride, are considered one of the most promising semiconductor materials for X-rays detection due to its wide band-gap and high quantum number resulting in room temperature operation with high efficiency[42]. Current applications include bone densitometry and SPECT but flat panel detectors suitable for radiographic imaging are not yet in production. Current research and development is focused around energy resolving pixel detectors, such as CERN's detector and Science and Technology Facilities Council's HEXITEC detector[42].

A typical semiconductor diode, such as a 1N4001, will produce a small amount of current when placed in an X-ray beam[53]. A test device once used by medical imaging service personnel was a small project box that contained several diodes of this type connected in series, which could be connected to an oscilloscope as a quick diagnostic.

2.3 Indirect detectors

Indirect detectors are made up of a scintillator to convert X-rays to visible light and a phosphor to convert the light to electrons, which is read by a TFT array.

This can provide sensitivity advantages over current (amorphous selenium) direct detectors, albeit with a potential tradeoff in sensitivity. Indirect flat panel detectors (FPDs) are in widespread use today in medical, dental, veterinary, and industrial applications.

The TFT array consists of a sheet of glass covered with a thin layer of silicon that is in an amorphous or disordered state. At a microscopic scale, the silicon has been imprinted with millions of transistors arranged in a highly ordered array, like the grid on a sheet of graph paper[46]. Each of these thin-film transistors (TFTs) is attached to a light-absorbing photodiode making up an individual pixel as shown in Figure 16.

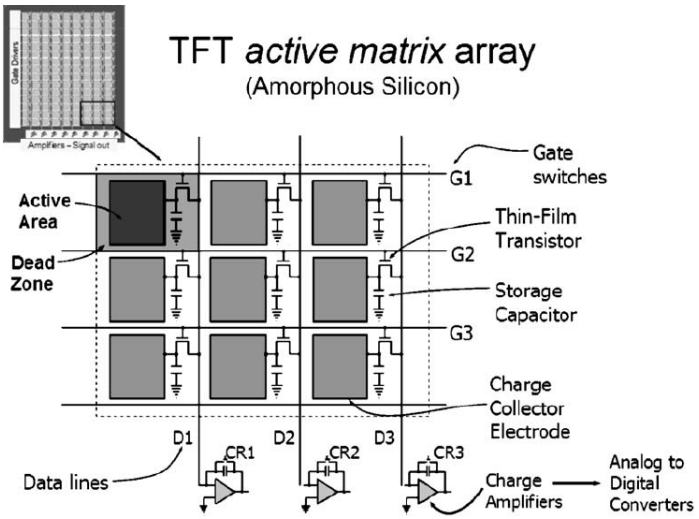

Figure 16 - TFT Matrix array

Photons striking the photodiode are converted into two carriers of electrical charge, called electron-hole pairs. Since the number of charge carriers produced will vary with the intensity of incoming light photons, an electrical pattern is created that can be swiftly converted to a voltage and then a digital signal, which is interpreted by a computer to produce a digital image.

Although silicon has outstanding electronic properties, it is not a particularly good absorber of X-ray photons. For this reason, X-rays first impinge upon scintillators made from such materials as gadolinium oxysulfide or caesium iodide. The scintillator absorbs the X-rays and converts them into visible light photons which then pass onto the photodiode array[32].

The physics behind these different detectors is almost the same. The detectors are made of higly doped semiconductors which are reactive to X-ray radiation; In semiconductor detectors, ionizing radiation is measured by the number of charge carriers set free in the detector material which is arranged between two electrodes, by the radiation. Ionizing radiation produces free electrons and holes.

The number of electron-hole pairs is proportional to the energy of the radiation to the semiconductor. As a result, a number of electrons are transferred from the valence band to the conduction band, and an equal number of holes are created in the valence band.

Under the influence of an electric field, electrons and holes travel to the electrodes, where they result in a pulse that can be measured in an outer circuit, as described by the Shockley-Ramo theorem[21]. The holes travel in the opposite direction and can also be measured. As the amount of energy required to create an electron-hole pair is known, and is independent of the energy of the incident radiation, measuring the number of electron-hole pairs allows the intensity of the incident radiation to be determined.

This phenomena represents the conjunction between a microscopic reality, creation of electron-hole pair, and a macroscopic quantity, the photo-inducted current.

The energy required to produce electron-hole-pairs is very low compared to the energy required to produce paired ions in a gas detector. Consequently, in semiconductor detectors the statistical variation of the pulse height is smaller and the energy resolution is higher. As the electrons travel fast, the time resolution is also very good, and is dependent upon rise time.

The density of a semiconductor detector, compared to gaseous ionization detectors, is very high, and charged particles of high energy can give off their

energy in a semiconductor of relatively small dimensions. Carrier concentration is one of the key parameter in a semiconductor device; it is a function of temperature which varies approximately linearly near room temperature. Some detectors are operated cold for the following reason:

- Low noise operation (e.g. fast imaging/astro applications)
- Mitigate the issue of thermal run-away while irradiating detectors (i.e. stop noise swamping signal when radiation damaged).

Chapter 3

X-Rays detection

Somehow the detection of X-rays was born with the discovery of X-rays itself. Under a certain point of view it can be said that Roentgen has done the first X-rays detection of human history.

The detection of X-rays is done using materials which are reactive to X-rays. The X-rays hitting the materials leave a trace of their passage. This process is the one characterizing the commonly known radiographic films as shown in the Figure 17. This sheet (analogous to a photographic film) is a strip of transparent plastic film coated on one side with a gelatin emulsion containing microscopically small light-sensitive silver halide crystals. The size and other characteristics of the crystals determine the sensitivity, contrast and resolution of the film.

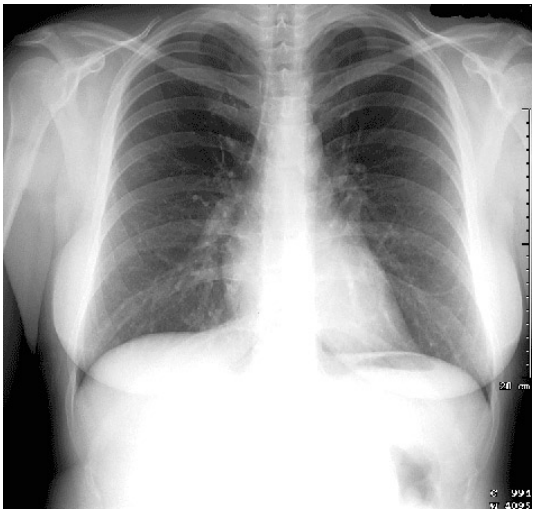

Figure 17 - Radiographic films showing a woman chest

The radiation will impress the film accordingly to the intensity of the X-rays photon. Since the body is made up of various substances with differing densities, X-rays can be used to reveal the internal structure of the body on film by highlighting these differences using attenuation, or the absorption of X-rays photons by the denser substances.

The creation of images by exposing an object to X-rays or other high-energy forms of electromagnetic radiation and capturing the resulting remnant beam (or "shadow") as a latent image is known as "projection radiography".

There are many analogical types of X-rays detectors such as the Chemical dosimeters, based on the concept of a radiation sensitive chemical reaction in which the amount of reaction products is correlated with the absorbed dose to their active elements (Figure 18). Among them, coloration dosimeters have a rich and interesting history in dosimetry[45]. For example, polyacetylenes (PDAs) form a unique class of polymeric materials that upon irradiation join-up aligned and their conjugated backbones and grow in length with the level of exposure.

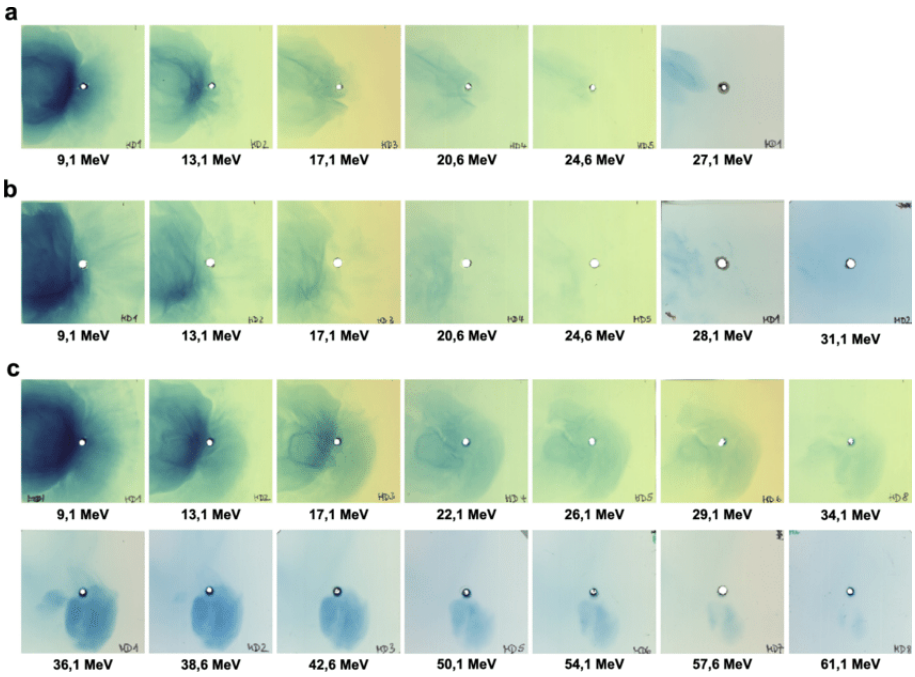

Figure 18 - Radiochromic films

Moreover the Radiochromic (RC) films are self-developing coloration passive detectors (no chemical processing is required, as opposed to silver halide films, however they need some time for full development) consisting of one or more radiation sensitive-layers of diacetylene microcrystals on a thin organic base. Under irradiation of the initially almost colourless monocrystals, chromophores become coloured through a chemical reaction due to the energy imparted to them. In principle, but not always in practice, the degree of colour formation is proportional to the energy imparted to them[45].

The detection of X-rays radiation in the latest years moved toward a digitalization of the process. This objective has been accomplished with the implementation of new X-rays detectors.

Digital radiography is a form of X-rays imaging, where digital X-rays sensors are used instead of traditional photographic film[58]. Advantages include time efficiency through bypassing chemical processing and the ability to digitally transfer and enhance images. Also, less radiation can be used to produce an image of similar contrast to conventional radiography.

On the place of X-rays films, digital radiography uses a digital image capture

device[58]. This gives many advantages such as:

- immediate image preview and availability
- avoidance of costly film processing steps
- wider dynamic range
- ability to apply special image processing techniques that enhance overall display quality of the image.

3.1 X- rays Flat Panel Detectors: FPDs

Flat panel detectors (FPDs) are the most common kind of digital detectors. They are classified in two main categories(Figure 19):

- Indirect FPDs
- Direct FPDs

In the first categories, amorphous silicon (a-Si) is the most common semiconducting material of commercial FPDs[61]. Combining a -Si detectors with a scintillator in the detector's outer layer, which is made from caesium iodide (CsI) or gadolinium oxysulfide (Gd2O2S), converts X-rays to light. Because of this conversion the a-Si detector is considered an indirect imaging device. The light is channeled through the a-Si photodiode layer where it is converted to a digital output signal. The digital signal is then read out by thin film transistors (TFTs) or fiber- coupled CCDs.

In the second case the amorphous selenium (a-Se) FPDs[61] are known as "direct" detectors because X-ray photons are converted directly into charge carriers. The outer layer of the flat panel in this design is typically a high-voltage bias electrode[49]. X-ray photons create electron-hole pairs in a-Se, and the transit of these electrons and holes depends on the potential of the bias voltage charge.

As the holes are replaced with electrons, the resultant charge pattern in the selenium layer is read out by a TFT array, active matrix array, electrometer probes or microplasma line addressing.

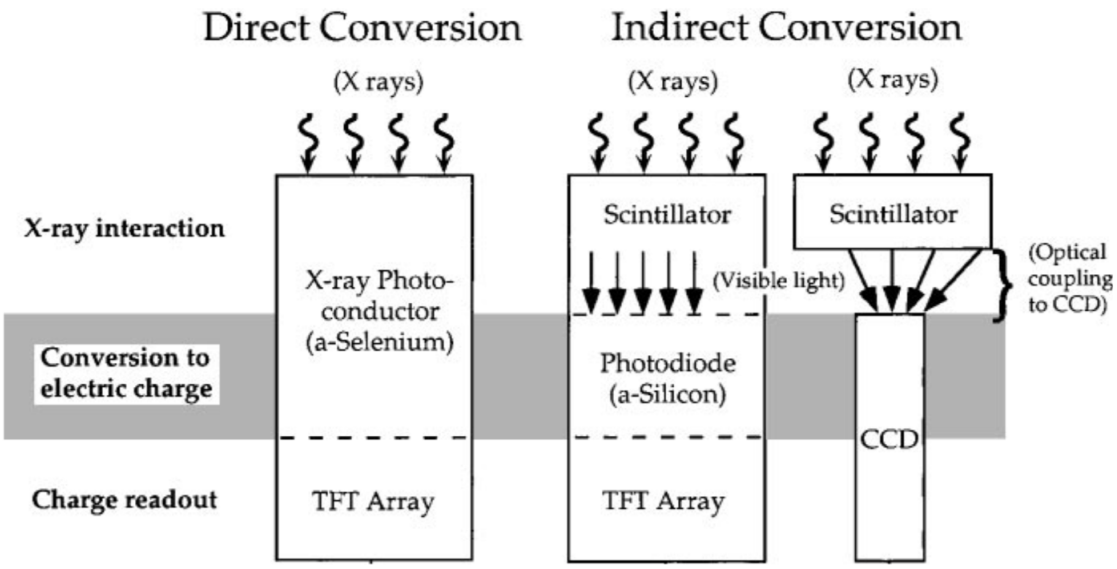

Figure 19 - Schematic of indirect and direct detectors

3.1.1 Advantages and disadvantages of Direct and Indirect detectors

Common to both the indirect and direct X-ray conversion technologies, the basic architecture of an a-Si TFT device is arranged as a row and column array of detector element. Within each detector element are the TFT, a charge collection electrode and a charge collection capacitor. Interconnecting each element via the TFT and capacitor are 'gate–and 'drain–lines.

By keeping the TFT switch closed during the exposure, incident X-rays interact with the converter and produce a corresponding charge that is stored in the local capacitor[46]. When the X-rays exposure is terminated, one gate line at a time is set high to activate all connected TFTs along the row, where the charge flows from the local capacitors through the transistors and down the drain lines in parallel to the output charge amplifiers at each column of the matrix.

Digitization of the output signal occurs and the digital image is built up one row at a time. Deactivating the gate line resets the TFTs for the next exposure, and the adjacent gate line is activated for the next row of data,

with the process continuing until the whole array is analyzed [48].

For real-time fluoroscopic imaging, the readout procedure must occur fast enough to acquire data from all detector elements over a period of 33 ms or 30 frames per second, which places high demands on the switching characteristics of the TFTs, charge/discharge rate of the capacitors, and the speed of the charge amplifiers and digitizers of the output stage.

The "fill-factor" is a characteristic of the TFT and represents the fraction of each detector element that efficiently collects charges from the energy deposited by the absorbed X-rays signal in the converter material above it. Dead areas of the element include the gate, drain, TFT, and capacitor electronics[46].

As the detector element gets smaller, the fill factor gets smaller and less efficient, ultimately setting a lower limit on the achievable spatial resolution. Typical fill factors (1 is ideal) range from about 0.5 to 0.8 for indirect detectors and are larger for direct detectors because of the ability to redirect the charge using "mushroom electrodes".

Although the TFT array and associated electronics are common to FPD systems, significant differences in the X-rays detection and signal conversion exist. Indirect detectors use also phosphor (scintillator) material that absorbs X-rays and produces a proportionate number of light photons that subsequently interact with a photodiode on the TFT array, to produce the corresponding charge in the detector element capacitor.

Scintillators are either unstructured, such as gadolinium oxysulfide (Gd2O2S), or structured (Figure 20), such as cesium iodide (CsI). Benefits of the unstructured phosphors are low cost and inert physical characteristics; however, the classic tradeoff of spatial resolution versus absorption efficiency is a distinct disadvantage.

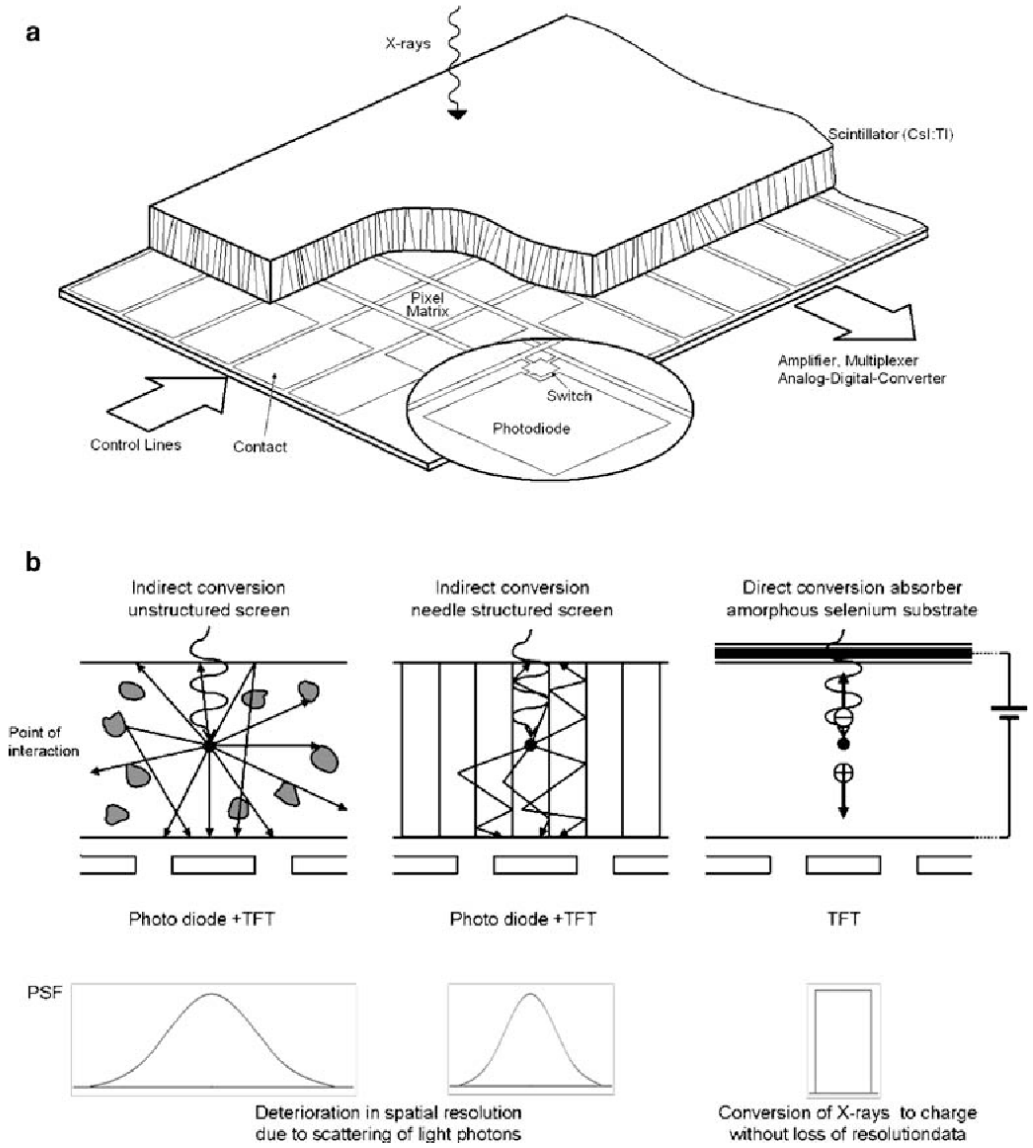

Figure 20 - Flat Panels detectors[23]

The achievement of good absorption efficiency typically requires a thick scintillator, but to achieve good spatial resolution requires a thin scintillator, and thus a compromise must be struck between these two opposite factors[23].

Benefits of the structured scintillator are the ability to confine the light photons in the needle structure, thus limiting lateral light spread and providing high resolution, while being at the same time able to deposit a thick phosphor layer, thus achieving good absorption efficiency.

Fragility of the CsI scintillator[46] and slight hygroscopic (water absorbing) characteristics are disadvantages. Because of good absorption and good resolution, the structured phosphor is widely employed.

Direct detectors use a semiconductor material sandwiched between two electrodes to absorb and convert the X-ray energy directly into ion pairs (electrons and positively charged entities). Currently, amorphous selenium (a-Se) is the only clinical choice for a direct FPD, even though there are other semiconductors under investigation in research laboratories[61].

To collect the charge confined to the detector element with minimal spread, and to keep the ion pairs from recombining, a large voltage bias is placed between the electrodes. Active collection of the X-ray-induced charges allows a relatively thick substrate material with reasonable absorption efficiency despite the low atomic number of selenium.

Advantages of the direct conversion FPD include the simpler TFT structure (no photodiode is necessary but just a charge collection electrode, simplifying the production process), and high intrinsic spatial resolution achieved by the active collection of ion pairs under a high voltage with minimal resolution-reducing lateral spread.

Disadvantages are:

- charge-trapping within the thick a-Se absorber, which reduces absorption efficiency, increases signal retention, and causes a greater amount of lag
- potential destruction of a TFT in a detector element by overcharging caused by high X-ray exposures.

Until recently, indirect detection methods have been the only flat-panel technology available for clinical fluoroscopy. Direct FPD systems for fluoroscopy are now available since technological advances have reduced the effects of lag caused by charge trapping in the semiconductor and because overcharging protection circuits have been implemented.

3.2 CMOS and CCD visible light detectors

Detectors based on CMOS and charge coupled device (CCD) have also been developed, but despite lower costs compared to FPDs of some systems, bulky designs and low quality image have precluded widespread adoption[23].

CCD (charge coupled device) and CMOS (complementary metal oxide semiconductor) image sensors are two different technologies for capturing images digitally. Each has unique strengths and weaknesses giving advantages in different applications.

Both types of imagers convert light into electric charge and process it into electronic signals (Figure 21). In a CCD sensor, every pixel's charge is transferred through a very limited number of output nodes (often just one) to be converted to voltage, buffered, and sent off-chip as an analog signal.

All of the pixel can be devoted to light capture, and the output's uniformity (a key factor in image quality) is high[45].

In a CMOS sensor, each pixel has its own charge-to-voltage conversion, and the sensor often also includes amplifiers, noise-correction, and digitization circuits, so that the chip outputs digital bits. These other functions increase the design complexity and reduce the area available for light capture.

With each pixel doing its own conversion, uniformity is lower, but it is also massively parallel, allowing high total bandwidth for high speed.

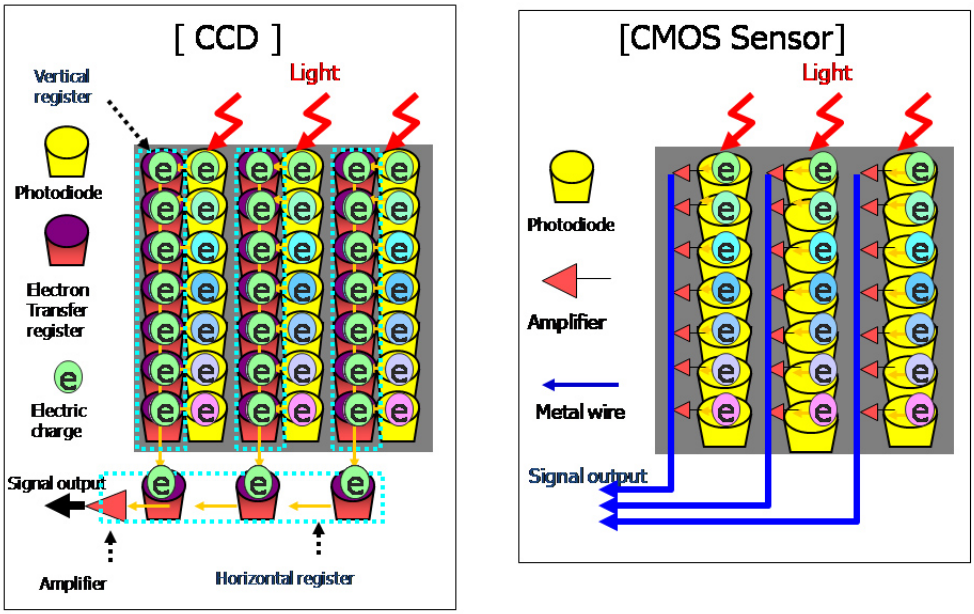

Figure 21 - CMOS and CCD detectors

CCDs and CMOS imagers were both invented in the late 1960s and 1970s (DALSA founder Dr. Savvas Chamberlain was a pioneer in developing both technologies)[45]. CCD became dominant, primarily because they gave far superior images with the fabrication technology available. CMOS image sensors required more uniformity and smaller features than silicon wafer foundries could deliver at the time.

Not until the 1990s did lithography develop to the point that designers could begin making a case for CMOS imagers again. Renewed interest in CMOS was based on expectations of lowered power consumption, camera-on-a-chip integration, and lowered fabrication costs from the reuse of mainstream logic and memory device fabrication.

Achieving these benefits in practice while simultaneously delivering high image quality has taken far more time, money, and process adaptation than original projections suggested, but CMOS imagers have joined CCDs as mainstream, mature technology.

3.3 High Density Line-Scan Solid State Detectors

A high-density line-scan solid state detector is composed of a photostimulable barium fluorobromide doped with europium (BaFBr:Eu) or caesium bromide (CsBr) phosphor[58]. The phosphor detector records the X-ray energy during exposure and is scanned by a laser diode to excite the stored energy which is released and read out by a digital image capture array of a CCD.

Chapter 4

Organic devices for direct X-ray photoconversion

Organic semiconductors are a new class of materials whose building blocks are π-bonded molecules or polymers made up by carbon and hydrogen atoms and – at times – heteroatoms such as nitrogen, sulfur and oxygen. They exist in form of molecular crystals or amorphous thin films.

In general, they are electrical insulators but become semiconducting when charges are injected from appropriate electrodes, either upon doping, or by photoexcitation. Organic compounds are almost endless in number and range in size from small molecules to macromolecules. This greatly increases the range of screening and design possibilities for organic semiconductors and provides an advantage over inorganic semiconductors.

In molecular crystals the energetic separation between the top of the valence band and the bottom conduction band, i.e. the band gap, is typically 2.5–4 eV, while in inorganic semiconductors the band gaps are typically 1–2 eV. This implies that they are, in fact, insulators rather than semiconductors in the conventional sense.

They become semiconducting only when charge carriers are either injected from the electrodes or generated by intentional or unintentional doping. Charge carriers can also be generated in the course of optical excitation. It is important to realize, however, that the primary optical excitations are neutral excitons with a Coulomb-binding energy of typically 0.5–1.0 eV.

The reason is that in organic semiconductors their dielectric constants are as low as 3–4. This hampers efficient photogeneration of charge carriers in neat systems in the bulk. Efficient photogeneration can only occur in binary systems due to charge transfer between donor and acceptor moieties. Otherwise neutral excitons decay radiatively to the ground state – thereby emitting photoluminescence – or non-radiatively.

4.1 History of organic semicondtuctors

In 1862, Henry Letheby obtained a partly conductive material by anodic oxidation of aniline in sulfuric acid[38][54]. The material was probably polyaniline. In the 1950s, researchers discovered that polycyclic aromatic compounds formed semi-conducting charge-transfer complex salts with halogens[38][54]. In particular, high conductivity of 0.12 S/cm was reported in perylene–iodine complex in 1954. This finding indicated that organic compounds could carry current[25].

The fact that organic semiconductors are, in principle, insulators but become semiconducting when charge carriers are injected from the electrode(s) was discovered by Kallmann and Pope[2]. They found that a hole current can flow through an anthracene crystal contacted with a positively biased electrolyte containing iodine that can act as a hole injector[47]. This work was stimulated by the earlier discovery by Akamatu that aromatic hydrocarbons become conductive when blended with molecular iodine because a charge-transfer complex is formed [50].

Since it was readily realized that the crucial parameter that controls injection is the work function of the electrode, it was straightforward to replace the electrolyte by a solid metallic or semiconducting contact with an appropriate work function. When both electrons and holes are injected from opposite contacts, they can recombine radiatively and emit light (electroluminescence). It was observed in organic crystals in 1965 by [24].

In 1972, researchers found metallic conductivity in the charge-transfer complex TTF-TCNQ[51]. Superconductivity in charge-transfer complexes was

first reported in the Bechgaard salt (TMTSF)2PF6 in 1980[16].

In 1973 Dr. John McGinness produced the first device incorporating an organic semiconductor[27]. This occurred roughly eight years before the next such device was created. The "melanin (polyacetylenes) bistable switch" currently is part of the chips collection of the Smithsonian Institution[52].

In 1977, Shirakawa reported high conductivity in oxidized and iodine-doped polyacetylene[11]. They received the 2000 Nobel prize in Chemistry for "The discovery and development of conductive polymers". Similarly, highly conductive polypyrrole was rediscovered in 1979[17].

Rigid-backbone organic semiconductors are now used as active elements in optoelectronic devices such as organic light-emitting diodes (OLED, Figure 22), organic solar cells, organic field-effect transistors (OFET), electrochemical transistors and recently in biosensing applications[26]. Organic semiconductors have many advantages, such as easy fabrication, mechanical flexibility, and low cost.

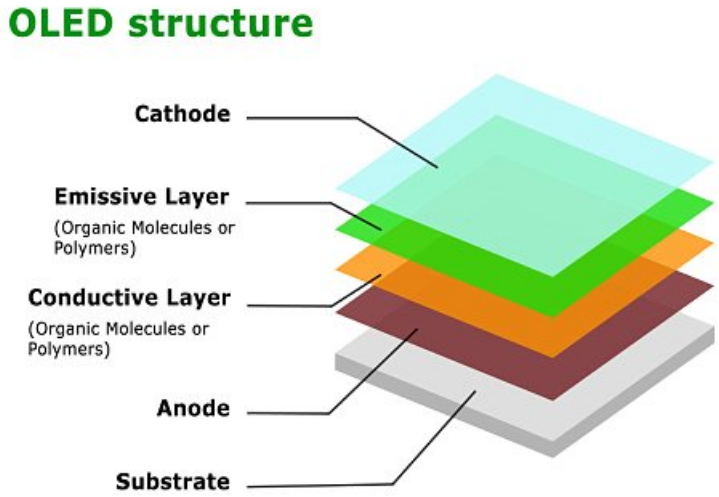

Figure 22 - OLED structure

The discovery by Kallman and Pope paved the way for applying organic solids as active elements in semiconducting electronic devices, such as organic light-emitting diodes (OLEDs) that rely on the recombination of electrons and hole injected from "ohmic" electrodes, which means electrodes with unlimited supply of charge carriers[7]. The next major step towards the

technological exploitation of the phenomenon of electron and hole injection into a non-crystalline organic semiconductor was the work by Tang and Van Slyke[19].

They showed that efficient electroluminescence can be generated in a vapor-deposited thin amorphous bilayer of an aromatic diamine (TAPC) and Alq3 sandwiched between an indium-tin-oxide (ITO) anode and an Mg:Ag cathode[56]. Another milestone towards the development or organic light-emitting diodes (OLEDs) was the recognition that also conjugated polymers can be used as active materials.

The efficiency of OLEDs was greatly improved when realizing that phosphorescent states (triplet excitons) may be used for emission when doping an organic semiconductor matrix with a phosphorescent dye, such as complexes of iridium with strong spin–orbit coupling.

Work on conductivity of anthracene crystals contacted with an electrolyte showed that optically excited dye molecules adsorbed at the surface of the crystal inject charge carriers. The underlying phenomenon is called sensitized photoconductivity. It occurs when photo-exciting a dye molecule with appropriate oxidation/reduction potential adsorbed at the surface or incorporated in the bulk. This effect revolutionized electrophotography, which is the technological basis of today's office copying machines. It is also the basis of organic solar cells (OSCs), in which the active element is an electron donor, and an electron acceptor material is combined in a bilayer or a bulk heterojunction.

Doping with strong electron donor or acceptors can render organic solids conductive even in the absence of light. Examples are doped polyacetylene and doped light-emitting diodes. Today organic semiconductors are used as active elements in organic light-emitting diodes (OLEDs), organic solar cells (OSCs) and organic field-effect transistors (OFETs)[56].

As detectors of ionizing radiation, organic semiconductors have so far been mainly proposed in the indirect conversion approach, for example, as scintillators, or as photodiodes. However, as stated before, the direct conversion of ionizing radiation into an electrical signal within the same device is a more effective process because it improves the signal to noise ratio and it reduces

the device response time.

In the last years, a few studies reported the proof-of-principle for direct X-ray detection based either on organic semiconducting single crystals or on polymer thin-films blended either with p-conjugated small molecules, inorganic high-Z nanocomponents or carbon nanotubes to enhance the sensitivity to X-rays improving the charge carriers mobility and the stopping power of the material.

However, it has been difficult to achieve a system that combines the use of an organic semiconductor in a direct approach of X-Rays detection, both flexible and working with ultra-low voltage bias. In 2016, it was discovered that this could all be possible using the 6,13-bis-(triisopropylsi- lylethynyl)pentacene (TIPS-pentacene) molecule (a standard material for the fabrication of organic devices onto flexible plastic substrates) deposited by drop casting onto flexible poly(ethyleneterephthalate) (PET) substrates. This molecule has been synthetised by prof.John Anthony from the University of Kentucky in collaboration with the Bologna semiconductor physics group of the Department of Physics and Astronomy of Bologna, in order to obtain an organic molecule which can be used to realize organic X-rays detectors. These devices revealed an unexpected high X-ray sensitivity.

In this project, the starting point was this last finding and the main goal was to investigate the influence of different parameters in the sensitivity and, therefore, in the performance of the X-Ray detector. There is a similar molecule to TIPS which is called 6,13-bis(triisopropylgermylethynyl)pentacene (TIPGe-pentacene) and it only differs in one atom, which in TIPS is silicon and in TIPGe is germanium (Figure 23). Given that the germanium has a higher Z number, it is expected that this second molecule delivers better results than the TIPS as a detector for its higher absorption rate.

Figure 23 - TIPS-Pentacene & TIPGe-Pentacene

4.2 Direct X-ray photoconversion in flexible organic thin film devices

The application of organic electronic materials for the detection of ionizing radiations is very appealing thanks to their mechanical flexibility, low-cost and simple processing in comparison to their inorganic counterpart.

The research brought up at the Department of Physics and Astronomy of Bologna[15] ended up with the realization of flexible organic thin film devices. The detectors realized consist of a 100 nm thick TIPS-pentacene organic active layer deposited by drop-casting onto interdigitated gold electrodes fabricated on 125mm thick PET film.

The deposition process, based on drop-casting of a solution containing TIPS-pentacene, gives rise to high-quality micro-crystalline films with crystallites extending a few tens of micrometres in length and width as measured by atomic force microscopy [15].

The average crystallite height is 100nm. The figure below shows the typical X-ray photocurrent signal of a device biased at 0.2V. While recording the current, three on/off switching cycles of a monochromatic synchrotron X-ray beam of 17 keV (dose rate 19.3$\frac{mGy}{s}$) are performed[15].

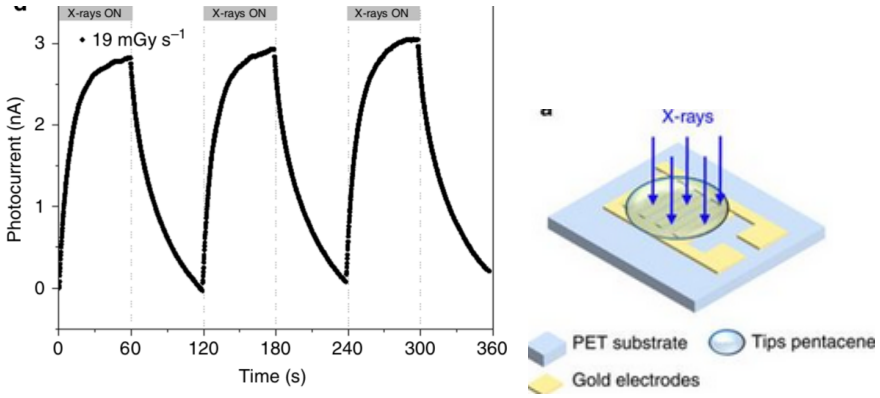

Figure 23 - X-ray-induced photocurrent signal[15] & Schematic of the device used[15]

The energy of radiation is chosen to be consistent with the typical values of medical diagnostic analysis (for example, mammography), to verify whether

the samples behave properly as X-rays detectors for medical applications. About 20 devices have been characterized with no significant differences in the detection performance[15].

As evidenced in the Figure 23, the X-ray-induced photocurrent saturates after 60s of X-ray exposure at a value of 2.8nA. The time required to return to the baseline value is usually comparable to the one needed to make the device saturate. The contribution of the electrodes and substrate to the X-ray-induced photocurrent can be evaluated by comparing the signal amplitude of detectors with metal electrodes with that of fully organic devices. Moreover it was proved that the X-ray-induced photocurrent is linearly proportional to the the applied bias voltage[15].

One of the key point of these devices is that they are meant to work in the low voltage range (0.2 V) to avoid possible instability issues due to bias stress effect and to avoid the decrease of the detector signal-to-noise ratio defined as the ratio between the current measured under X-rays exposure and the one measured with the devices not irradiated[15].

As it has been already written, the absorption of an X-ray photon in an inorganic semiconductor results in the creation of a high-energy primary electron, which dissipates its excess kinetic energy in the surrounding medium in the form of electron-hole pairs and phonons. Applying an electric field, the electron-hole pairs separate and drift to the respective electrodes, thus generating a photocurrent. Recombination and phonon formation represent losses in the process.

Organic semiconductor are characterized by a low phonon absorption, which implies that the calculated upper limit of the induced photocurrent is:

$$I_{cc} \approx 2pA \tag{4.1}$$

Even Though this value represents an upper limit, it is about two orders of magnitude smaller than the signal amplitude observed during the measurements held at the laboratories of the Department of Physics and Astronomy

of Bologna[15].

This evidence led to consider the possibility that other processes must be involved in the generation of such a large photocurrent. According to the study brought up at the Department of Physics and Astronomy of Bologna this phenomenon is related with the increase in conductivity due to a photoconductive gain[15], arising when X-ray generated.

Before recombination process sets in, the free charge carriers, photoinducted by the X-rays, flow in the organic material several times between the electrodes. This mechanism leads to an amplified photocurrent:

$$\Delta I_{pc} = I_{cc} \times G \tag{4.2}$$

where G represents the photoconductive gain. To exclude the possbility that this increment in the photocurrent can be ascribed to a modification of the hole mobility, μ_h has been calculated from transfer characteristic of TIPS-pentacene- based organic thin film transistors (OTFTs) both in the dark or under X-ray irradiation showing no significant differences[15].

The key point is that the organic thin film accumulates additional free carriers during X-rays exposition[15]. Since the devices are made by gold electrodes forming ohmic contacts with TIPS-pentacene an increase in carrier concentration ρ_X results in an increase of current ΔI_{pc} according to:

$$\Delta I_{pc} = W h \rho_X \mu E$$

with $E = V/L$ being the electric field and W being the active width of the interdigitated structure[15].

There are differences in hole and electron carrier transport in organic materials[36] from which it was possible to derive a model for the increase in free

carriers and its impact on photocurrent. Mainly the mobility of electrons and holes can be slightly different and, in addition, the possible presence of trap, for both electrons and holes, needs to be taken into account.

The availment of a polar substrate together with the presence of oxygen act as a trap for the electrons flowing in the devices as it is happened in the case of measurements held at the laboratories of the Department of Physics and Astronomy of Bologna.

The basis assumption proposed by the team of research of the Department of Physics and Astronomy of Bologna is that the additional electrons and holes generated by the interaction with the X-ray follow a different fate: holes drift along the electric field until they reach the collecting electrode while electrons remain trapped and act as 'doping centres'[15]. Charge neutrality needs to be guaranteed so mobile holes, that are collected at the collecting electrode, are continuously re-injected from the injecting electrode.

This evidence can be interpreted as a doping process which leads to a photoconductive gain: for each electron-hole pair the hole contribution to the photocurrent is "amplified".

Starting from the experimental saw-tooth shape of the X-ray photocurrent shown in Figure 23, considering the variation of photo-generated carrier concentration ρ_X in time[15] it has been obtained the following equation 4.3:

$$\frac{\partial \rho_X}{\partial t} = \frac{\Phi n q}{Ah} - \frac{\rho_X(t)}{\tau_r(\rho_X)} \tag{4.3}$$

where:

- n is the amount of generated charges per absorbed photon
- $\tau_r(\rho_X)$ is the free carrier lifetime
- Φ is the photon absorption rate
- q is the elementary charge

This Equation describes completely the dynamic of carrier photogeneration and recombination reflecting the experimental data. It is evident in Figure 24 how the upper equation well reproduces the saw-tooth shape of some of the experimental curves obtained at the laboratories of the Department of Physics and Astronomy of Bologna[15].

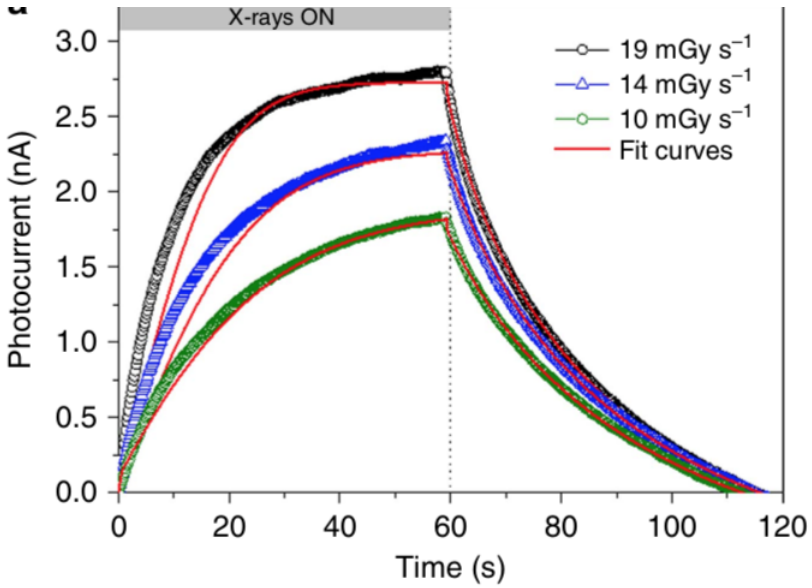

Figure 24 - Experimental and simulated curves of the dynamic response of the detector for three different dose rates of the radiation[15]

The kinetic model presented before is necessary to evaluate the dependence between the photocurrent and the dose rate. From this two quantities is possible to obtain the detector sensitivity defined as:

$$S = \frac{\partial I}{\partial S}$$

According to the data collected, the increment in the dose rate is followed by a monotone increase in the measured photocurrent (defined as $I_{ON} - I_{OFF}$). However, data collected show that the linear dependence tends to move to a sublinear one when the X-rays exposure time becomes longer (order of tens of seconds). The detector sensitivities S as a function of dose rate are obtained from the curves derivatives.

An other key parameter which may influence the behaviour of these devices is their geometrical configuration, In particular these devices have one of their strongest peculiarity in their mechanical flexibility. For such reason, the model afore presented, refers to devices characterized in a bent configuration. The bending radius was set to $0.3cm$, a value chosen to be conformable to most of the human body curves in view of possible medical diagnostic applications, by means of the experimental setup[15].

Second Part

Chapter 5

Fabrication of organic thin film devices for direct X-ray photoconversion

In this chapter the process of fabrication of the organic thin film devices that were used for this study will be presented, including samples preparation method, description of materials and employed tools.

The fabrication process is composed by:

- Substrate cleaving
- Substrate evaporation
- Organic molecules preparation
- Drop Casting

5.1 Substrate Cleaving

The Substrate cleaving consists of the notch of the substrate disk to realize small pieces on which electrodes and the organic layer will be placed. The cleaving is done firstly chipping the substrate disk in correspondence of the main axis of the crystal and then beating it softly until the crack runs along the axis splitting the disk(Figure 25).

Repeating this procedure it is possibile to obtain the desired shape for the substrate.

For the study analyzed in this dissertation were used Silicon substrates with three different SiO_2 growth process:

- PECVD, **P**lasma **E**nhanced **C**hemical **V**apor **D**eposition
- TEOS, **T**etra**E**thyl **O**rtho**S**ilicate
- THERMAL

For each substrate 3 cleaved pieces were used.

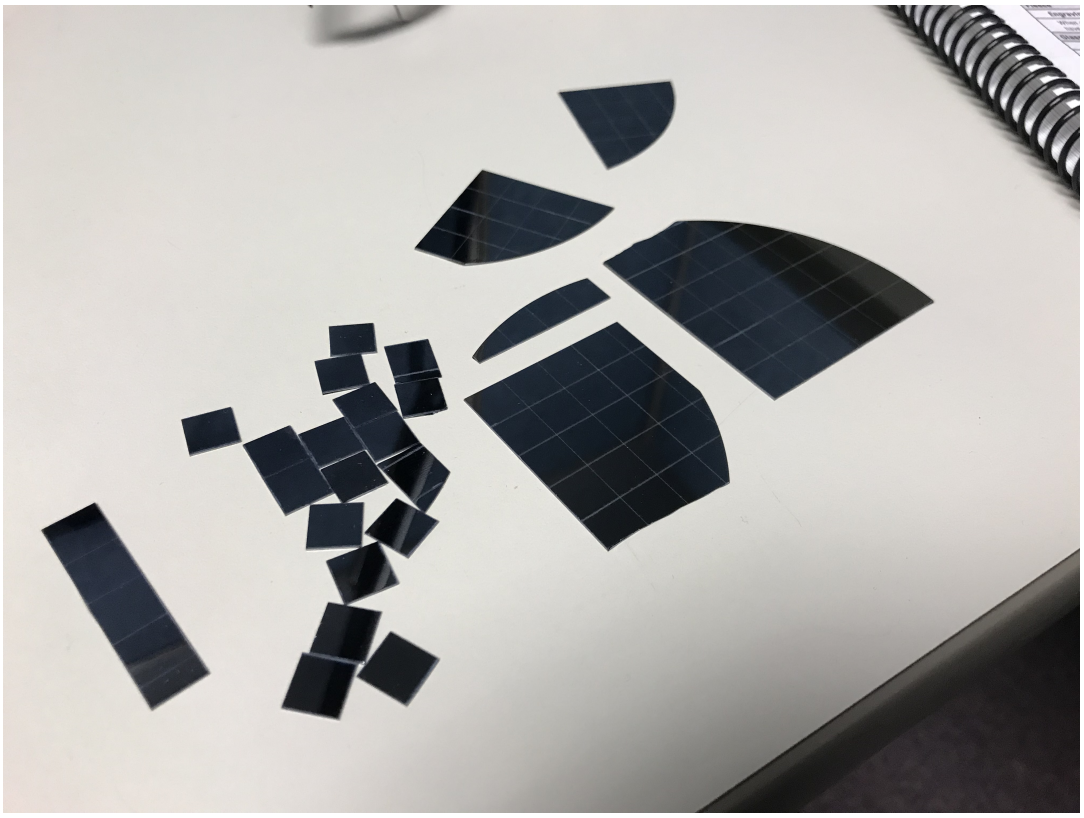

Figure 25 - Substrate cleaved pieces

5.1.1 PECVD SiO_2 growth process

The PECVD SiO_2 growth process is the acronym for **P**lasma **E**nhanced **C**hemical **V**apor **D**eposition.

Generally Plasma-enhanced chemical vapor deposition (PECVD) is a chemical vapor deposition process used to deposit thin films from a gas state (vapor) to a solid state on a substrate. Chemical reactions are involved in the process, which occurs after creation of a plasma of the reacting gases. The plasma is generally created by radio frequency (RF), alternating current (AC) or direct current (DC) discharge between two electrodes, the space between them is filled with the reacting gases.

5.1.2 TEOS SiO_2 growth process

Tetra**E**thyl **O**rtho**S**ilicate, formally named tetraethoxysilane and abbreviated TEOS, is the chemical compound with the formula $Si(OC_2H_5)_4$; it is a colorless liquid that degrades in water. TEOS is mainly used as a crosslinking agent in silicone polymers and as a precursor to silicon dioxide in the semiconductor industry.

The deposition of SiO_2 with TEOS is a complex pyrolytical chemical reaction. In this process TEOS is transported via a carrier gas to the hot surface of the wafer, where TEOS is dissociated. A certain amount of the decomposition products sticks on the surface and builts a SiO_2 layer while the other particles are reflected from the surface.

Those are in general highly reactive by-products of TEOS decomposition. In particular, more than 40 secondary reactions have been reported in this complex reaction. A rigorous simulation would cover all possible by-products and their secondary and ternary reactions but it would also require a considerable amount of computational power and memory to calculate and investigate this TEOS reaction.

5.1.3 THERMAL Substrate

The THERMAL substrate is a semiconductor substrate realized by thermal oxidation. This is one of the most basic deposition technologies. It is simply oxidation of the substrate surface in an oxygen rich atmosphere. The temperature is raised to 800°C -1100 °C to speed up the process. This is also the only deposition technology which actually consumes some of the substrate

as it proceeds.

The growth of the film is spurned by diffusion of oxygen into the substrate, which means the film growth is actually downwards into the substrate. As the thickness of the oxidized layer increases, the diffusion of oxygen to the substrate becomes more difficult leading to a parabolic relationship between film thickness and oxidation time for films thicker than 100nm. This process is naturally limited to materials that can be oxidized, and it can only form films that are oxides of that material.

This is the classical process used to form silicon dioxide on a silicon substrate. A schematic diagram of a typical wafer oxidation furnace is shown in the Figure 26 below.

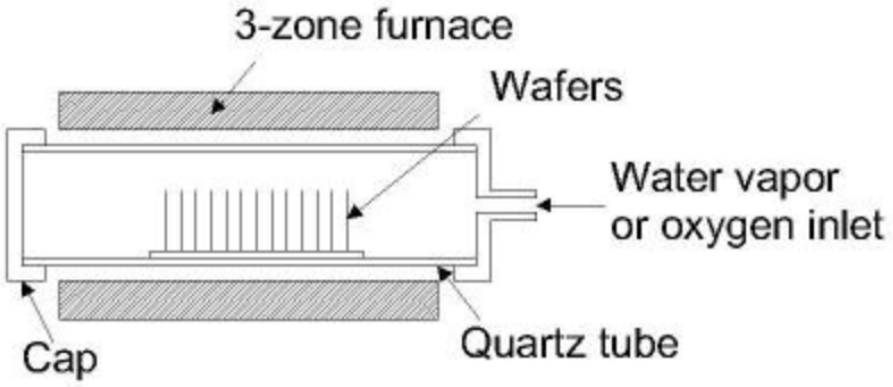

Figure 26 - Schematic diagram of a typical wafer oxidation furnace

In this study will be also analyzed few devices realized on two others substrates:

- PEN, **P**oly**E**thylene **N**aphthalate (poly(ethylene 2,6-naphthalate)
- Glass

5.1.4 PEN Substrate

Polyethylene naphthalate (poly(ethylene 2,6-naphthalate) is a polyester derived from naphthalene-2,6-dicarboxylic acid and ethylene glycol. As such it is related to poly(ethylene)terephthalate, but with superior barrier properties.

Two major manufacturing routes exist for PEN: an ester or an acid process, named according to whether the starting monomer is a diester or a diacid derivative, respectively. In both cases for PEN, the glycol monomer is ethylene glycol. Solid-state polymerization (SSP) of the melt-produced resin pellets is the preferred process to increase the average molecular weight of PEN.

5.1.5 Glass Substrate

The Glass substrate is composed by a thin film Borosilicate glass. It is a type of glass with silica and boron trioxide as the main glass-forming constituents. Borosilicate glasses are known for having very low coefficients of thermal expansion making them resistant to thermal shock, more so than any other common glass.

Borosilicate glass is created by combining together and melting boric oxide, silica sand, soda ash,[4] and alumina. Since borosilicate glass melts at a higher temperature than ordinary silicate glass, some new techniques were required for industrial production. The manufacturing process depends on the product geometry and can be differentiated between different methods like floating, tube drawing, or moulding

5.2 Electrode deposition

The process of substrate evaporation is necessary to deposit the electrodes on the semiconductor substrate. The pattern of the electrode, on which the organic molecules will be dropped, is realized with a shadow mask (Figure 27) whose dimension are:

- $Width : W = 50000\mu m$
- $Lenght : L = 30\mu m$

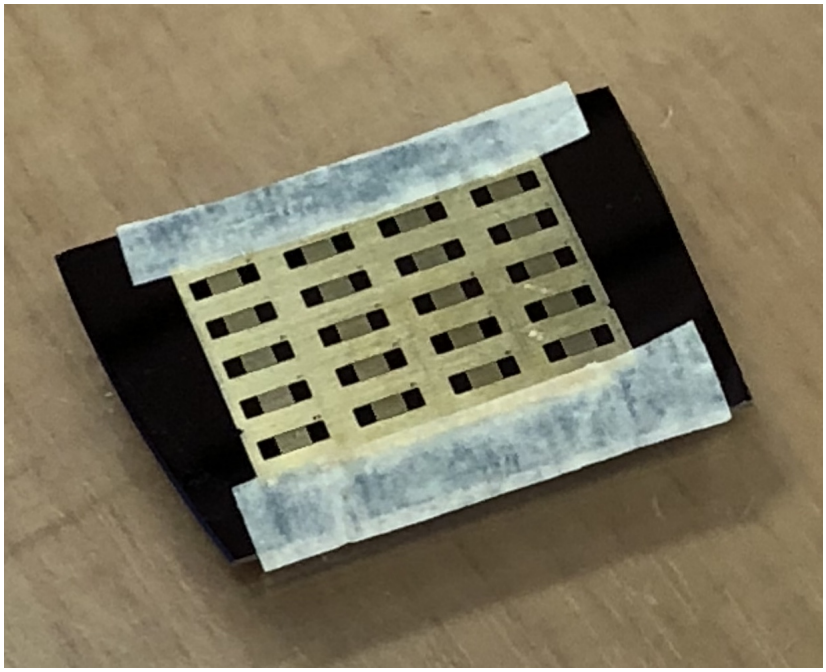

Figure 27 - Shadow mask placed on the substrate

The Pattern that has been realized for this study is called interdigitated; it reflects the shadow mask dimension in fact the Au interdigitated geometry on the SiO_2 substrate was $W = 50000\mu m$ and $L = 30\mu m$ and it is visible in Figure 28.

Figure 28 - Microscopic image of the interdigitated electrodes

In this specific case, for the evaporation process were used:

- 33gr of chromium (Cr)
- 207gr of gold (Au)

The evaporation process is held in a vacuum bell; Cr and Au are placed on a filament which is lighted on, making Au and then Cr evaporate for thermal emission(Figure29).

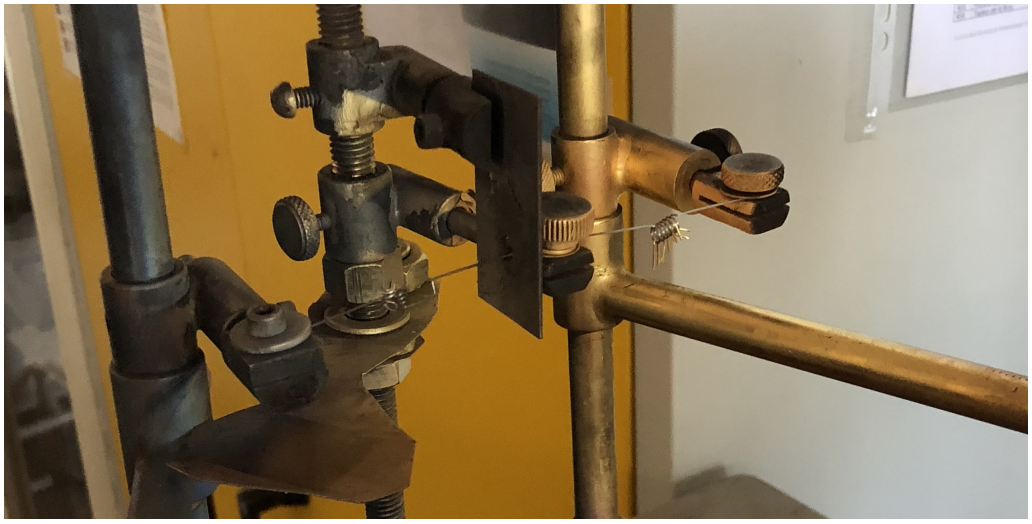

Figure 29 - Cr & Au placed on the filament before the evaporation process

The vapors, generated by the evaporation, deposit on the substrate recreating the pattern of the shadow mask(Figure 30a & Figure 30b).

The process of evaporation is not yet fully industrialized which means that the probability of an incorrect evaporation is real. In fact during the evaporation made for this study there were some reject due to the fact that the shadow mask wasn't perfectly adherent on the substrate.

The connections recreated by the evaporation were wrongly disposed on the substrate creating shortcuts in the devices.

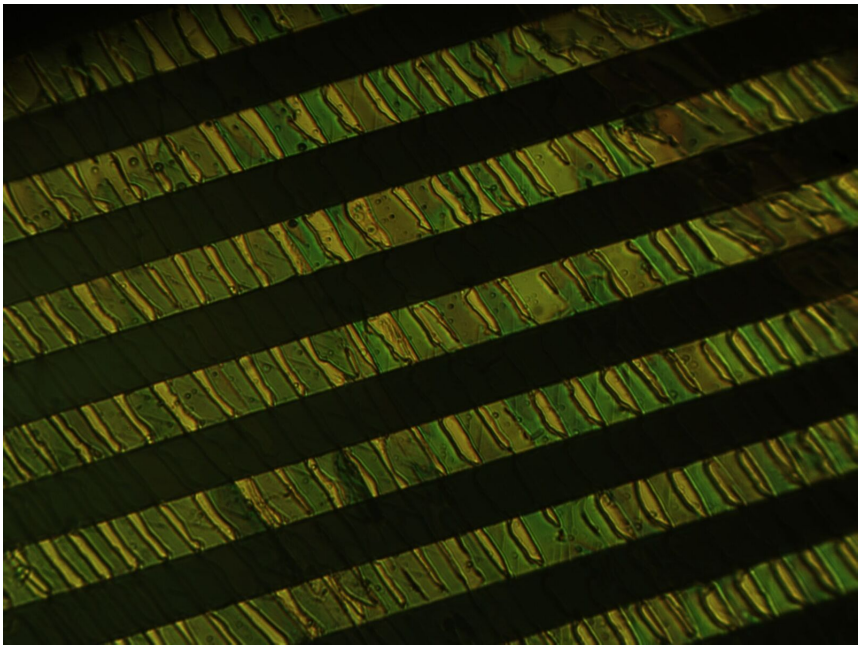

Figure 30a - Microscopic images of the interdigitated electrodes evaporated on PECVD substrate.

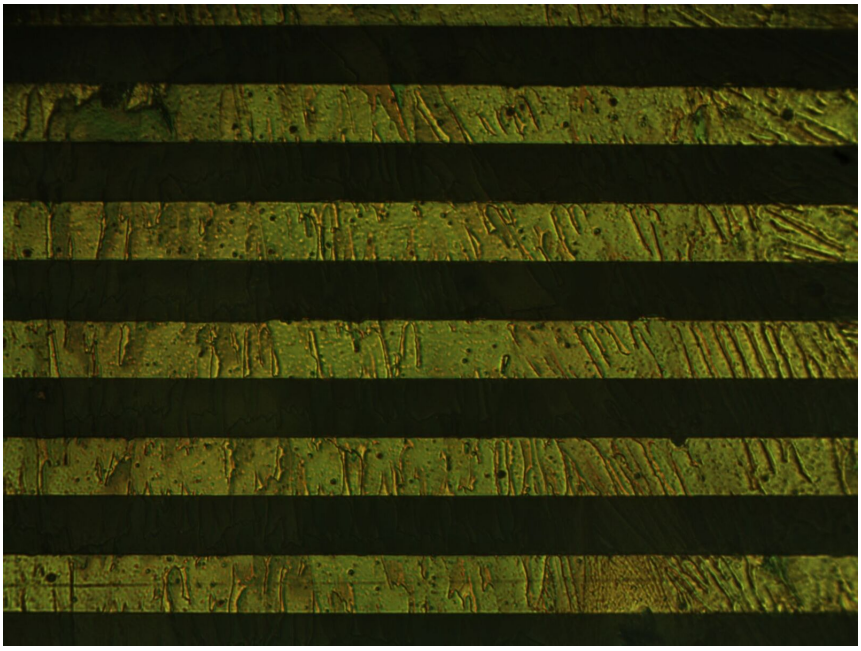

Figure 30b - Microscopic images of the interdigitated electrodes evaporated on TEOS substrate.

5.3 Organic thin films deposition

The organic molecules was dissolved in solution with a 0.5% of concentration in a Toluene solvent for the TIPS and TIPGe molecules.

The solution is then shuffled using ultrasounds and it is ready for the drop casting deposition on the different substrate.

5.3.1 Drop Casting

The optimized volume deposited was $3\mu l$ of the organic solution, drop casted over the substrate.

For the semiconductor deposition, the SAC (Solvent As- sisted Crystallization) method have been employed. This method consists in covering the samples for 1 hour next to $200\mu l$ of toluene at room temperature, immediately after the deposition.

This creates a saturated environment which slows the crystallization of the semiconductor, resulting in bigger crystals. After one hour resting in the saturated environment, the samples were annealed at 90 °C for 1 hour in order to evaporate the whole solvent which allows for a better electrical performance.

Those devices are highly sensible toward lights, in particular when exposed to visible radiation their current increases. For this reason, before the measurements, the samples stayed at rest protected from the light.

The drop casting has been made with both TIPS & TIPGe solution on the three different substrates. This part of the process of realization of the sample is critical mainly because it is still made manually; in fact it can happen that the solutions is not correctly dropped on the substrate or the amount of solution is greater or smaller with respect to the fixed quantity.

After the deposition, the devices are analized by an optical microscope. From the analysis of the images collected for the different devices is deductible that:

- Crystals over all substrates show good continuity between channel and electrodes;
- Both TIPS & TIPGe crystallize with grains; though in TIPGe they tend do be sorted and elongated while in TIPS they are disordered and thicker;
- TIPS & TIPGe crystallize in the same way regardless the substrate.

In some laboratories there are automated systems for the drop casting process which ensure that the correct amount of solution is correctly placed on the substrates. Such industrialization of the process of drop casting is necessary because it guarantees the repeatability in the realization of the devices. The fact that repeatability is not ensured in the manual process may introduce other sources of bias which are needed to be taken into account.

Chapter 6

Characterization of organic thin film devices for direct X-ray photoconversion

After the drop casting process is completed it is possible to start characterizing the samples as X-rays detector. The process of characterization is composed by:

- Electrical characterization (I-V)
- X-ray characterization

6.1 Electrical characterization

The first step consists of an electrical characterization or rather the study of the electrical behaviour and characteristics of the samples.

6.1.1 Experimental setup

Electrical characterization was performed using dual channel Keithley 2614B SourceMeter (Figure 31) and a custom made Labview software. The Tables 6.1 & 6.2, reports respectively the voltage and the current measurement accuracies of the SourceMeter, as a function of the range of measurement used and of the measurement itself, at a temperature of $(23 \pm 5)°C$.

Voltage measurement accuracy of Keithley 2614B SourceMeter

Range	Accuracy at $T_0 = (23 \pm 5)°C$
100 mV	0.015% ± 150 μ V
1V	0.015% ± 200 μ V
6V	0.015% ± 1 mV
40 V	0.015% ± 8 mV

Table 6.1: Voltage specifications for Keithley 2614B SourceMeter

Current measurement accuracy of Keithley 2614B SourceMeter

Range	Accuracy at $T_0 = (23 \pm 5)°C$
100 nA	0.005% ± 100 pA
1μA	0.025% ± 500 pA
10μA	0.025% ± 1.5 nA
100 μA	0.02% ± 25 nA
1 mA	0.02% ± 200 nA

Table 6.2: Current specifications for Keithley 2614B SourceMeter

In both cases, if the measurements are carried out at a different temperature is possible to obtain the accuracy applying the following equation:

$$A(T) = \frac{0,15 \times A(T_0)}{T} \tag{6.1}$$

Where $A(T)$ is the accuracy at temperature T and $A(T_0)$ is the accuracy at temperature $T0 = (23 \pm 5)°C$.

Figure 31 - Keithley 2614B SourceMeter

6.1.2 Results

This task is accomplished making an "I - V" characterization in the range between -1V - 1V. In the Figure 32 are presented the data related to some of the best devices tested at the laboratories of the Department of Physics and Astronomy of Bologna, realized on PET substrates.

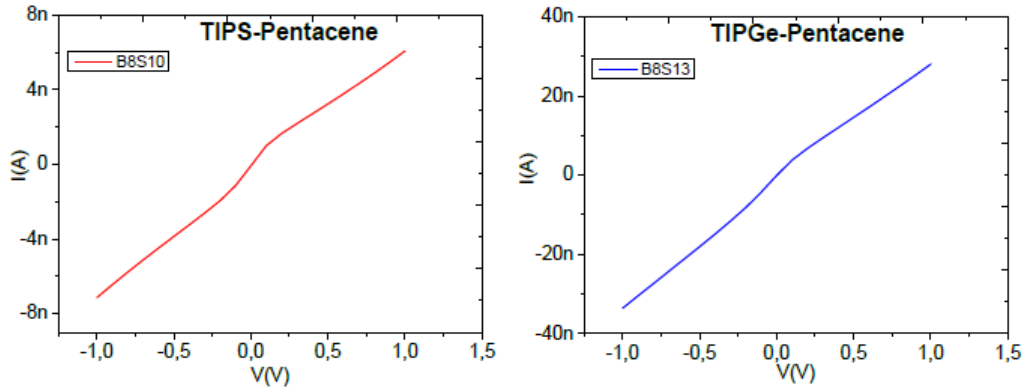

Figure 32 - Data collected at the Department of Physics and Astronomy of Bologna

Looking at the Figure 32 it is possible to notice that the TIPGe sample is able to achieve an higher current at 1V, compared to the TIPS sample. This fact means that the TIPGe device has a higher range of current, as expected.

The average resistance values for the samples previously tested at the Department of Physics and Astronomy of Bologna [15] are (Table 6.3):

R for TIPGe (Ω)	R for TIPSi (Ω)
$(32,2 \pm 0.3) \times 10^6$	$(142 \pm 1) \times 10^6$

Table 6.3: Average resistance values of the samples tested at the Department of Physics and Astronomy of Bologna

For each device the sheet resistivity was calculated: using the centre-to-centre distance along the current path (L) as the sample length and the distance between voltage probes perpendicular to the current path as the sample width (W), the sheet resistivity $\rho_{\square}$ was calculated as:

$$\rho_{\square} = \frac{R \times W}{L} \tag{6.2}$$

Dr. Maria Elias Lopes Pereira found out, during the "I-V characterization" held at the laboratorries of the Department of Physics and astronomy of Bologna the following results for the sheet resistivity of the two samples previously mentioned[43](Table 6.4):

TIPGe $\rho_{\square}(\Omega)$	TIPS $\rho_{\square}(\Omega)$
$(2.25 \pm 0.02) \times 10^{11}$	$(1.10 \pm 0.01) \times 10^{12}$

Table 6.4: Sheet resistivity of the samples tested at the Department of Physics and Astronomy of Bologna

where R is the resistance of the device calculated as the ratio between voltage V and current I at 1V.

In the following table (6.5, 6.6, 6.7, 6.8, 6.9) and figures (33, 34, 35, 36, 37) are presented the data for all the devices characterized:

Organic Molecule	Substrate	$\rho_{\square}(\Omega)$
TIPS	Glass	$(9.63 \pm 0.07)10^{11}$
TIPS		$(5.29 \pm 0.05)10^{10}$
TIPS		$(4.33 \pm 0.05)10^{10}$
TIPGe	Glass	$(6.10 \pm 0.04)10^{9}$
TIPGe		$(4.93 \pm 0.04)10^{9}$
TIPGe		$(3.61 \pm 0.03)10^{9}$

Table 6.5: Data collected for TIPS & TIPGe molecule on Glass substrate

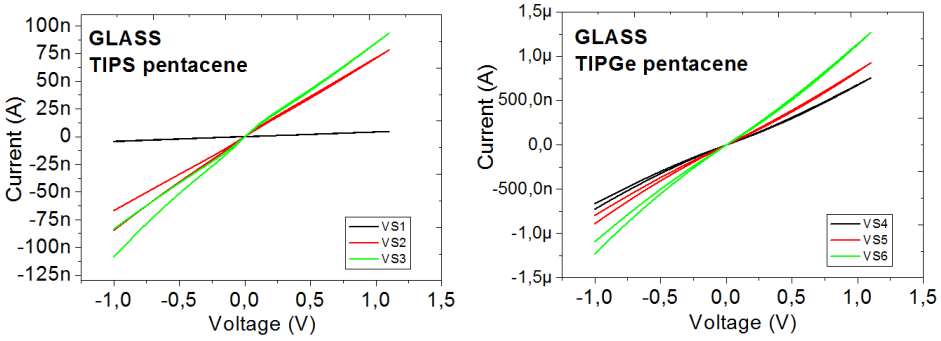

Figure 33 - Graph "I-V" for TIPS & TIPGe on GLASS substrate

Organic Molecule	Substrate	$\rho_{\square}(\Omega)$
TIPS	PECVD	$(7.42 \pm 0.06)10^{10}$
TIPGe		$(2.18 \pm 0.01)10^{9}$
TIPGe		$(2.86 \pm 0.05)10^{9}$

Table 6.6: Data collected for TIPS & TIPGe molecule with PECVD SiO_2 growth process

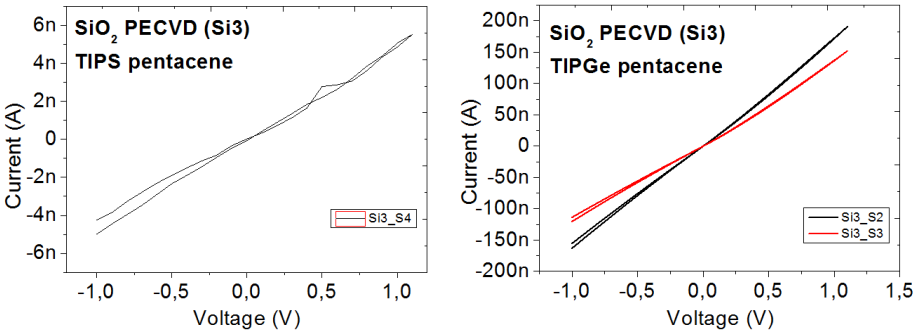

Figure 34 - Graph "I-V" for TIPS & TIPGe with PECVD SiO_2 growth process

Organic Molecule	Substrate	$\rho_{\square}(\Omega)$
TIPS	TEOS	$(8.78 \pm 0.02)10^{10}$
TIPS		$(7.23 \pm 0.03)10^{10}$
TIPS		$(1.49 \pm 0.02)10^{11}$
TIPS		$(1.40 \pm 0.01)10^{11}$
TIPGe	TEOS	$(5.71 \pm 0.09)10^{9}$
TIPGe		$(4.01 \pm 0.04)10^{9}$

Table 6.7: Data collected for TIPS & TIPGe molecule with TEOS SiO_2 growth process

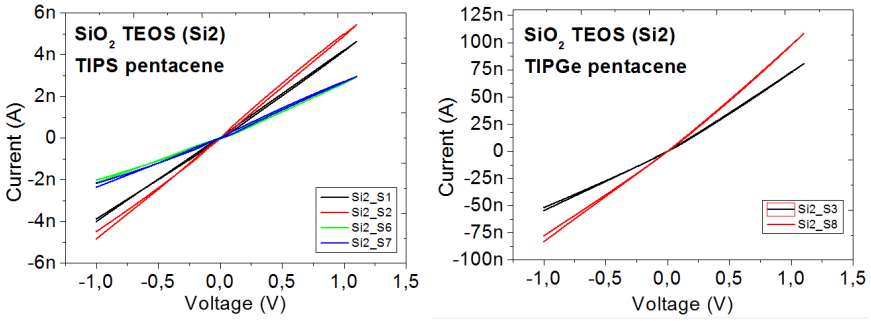

Figure 35 - Graph "I-V" for TIPS & TIPGe with TEOS SiO_2 growth process

Organic Molecule	Substrate	$\rho_{\square}(\Omega)$
TIPS	Thermal	$(1.61 \pm 0.01)10^{10}$
TIPS		$(3.57 \pm 0.02)10^{10}$
TIPS		$(2.63 \pm 0.02)10^{10}$
TIPGe	Thermal	$(3.475 \pm 0.007)10^{6}$
TIPGe		$(2.378 \pm 0.002)10^{6}$
TIPGe		$(4.586 \pm 0.003)10^{8}$

Table 6.8: Data collected for TIPS & TIPGe molecule with Thermal SiO_2 growth process

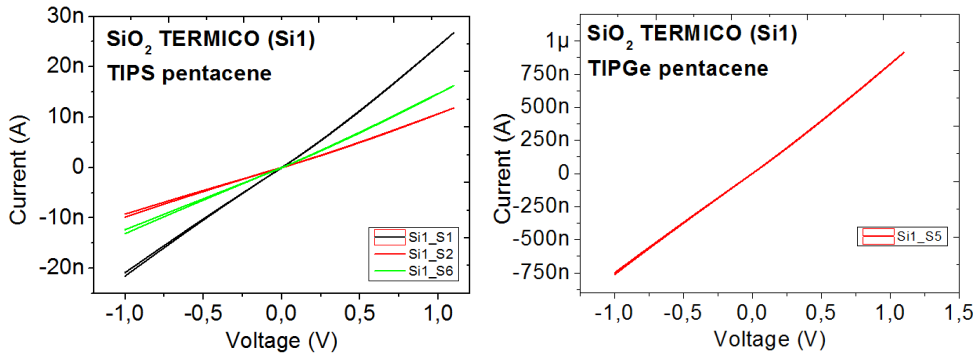

Figure 36 - Graph "I-V" for TIPS & TIPGe with Thermal SiO_2 growth process

Organic Molecule	Substrate	$\rho_{\square}(\Omega)$
TIPS	PEN	$(7.9 \pm 0.1)10^{10}$
TIPS		$(5.86 \pm 0.08)10^{10}$
TIPGe	PEN	$(3.98 \pm 0.03)10^{9}$
TIPGe		$(5.86 \pm 0.02)10^{9}$

Table 6.9: Data collected for TIPS & TIPGe molecule on PEN substrate

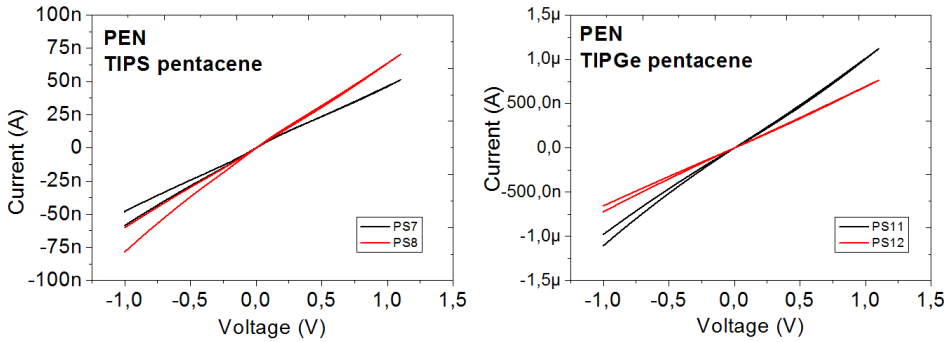

Figure 37 - Graph "I-V" for TIPS & TIPGe on PEN substrate

The results obtained show that the average resistivity of the TIPS devices over 5 different samples typology (PEN & Glass belong to an other batch of production) is smaller then the one of TIPGe samples. The values of resistivity obtained are quite high as requested for good detectors.

However there should be a compromise in this parameter because the resistivity cannot be high to the point where there is no current in the device (even in the exposure).

Below is graphically presented the trend of the sheet resistivity (Ω) over all the samples analyzed (Figure 38).

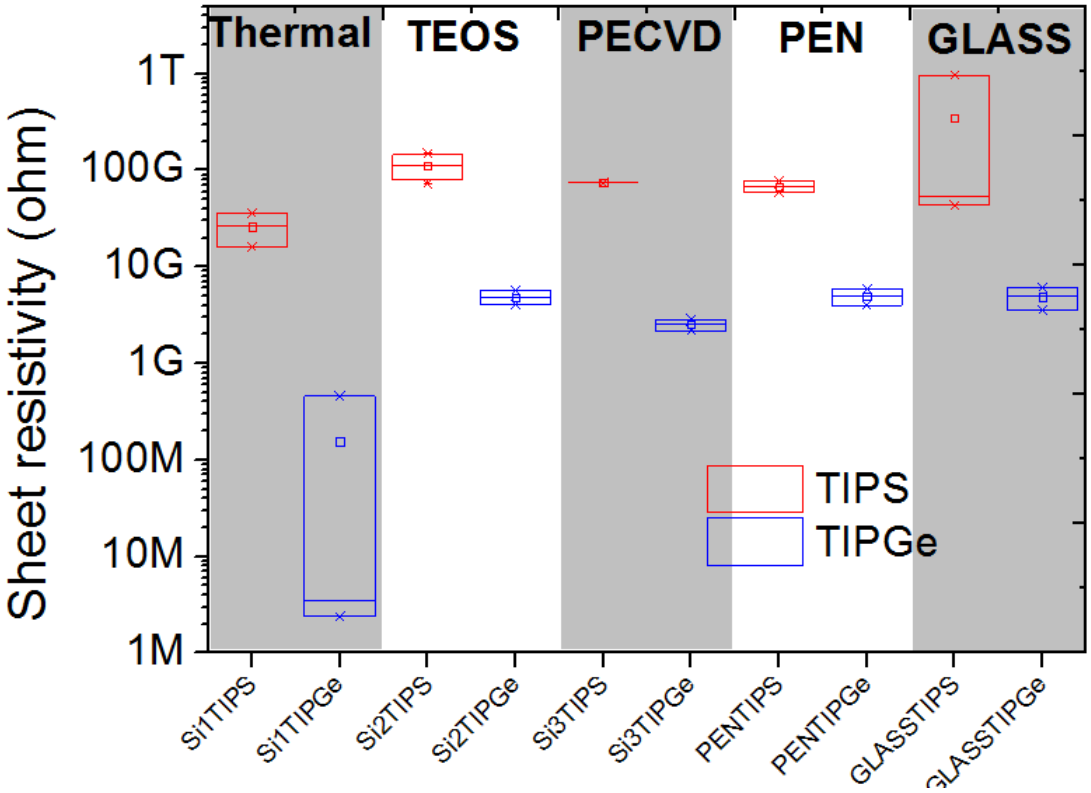

Figure 38 - Sheet resistivity of the different samples in logaritmic scale

6.2 X-rays characterization

The X-rays characterization is necessary to analyze the dynamical behaviour of the photocurrent of the device under X-rays exposure at different dose rates. It also acts as a seasoning test for the device.

The main parameters which can be obtained from the X-ray characterization are the sensitivity and an indication on the limit of detection of the device. The sensitivities of the organic thin film devices, expressed as $\frac{pC}{Gy}$ as a function of dose rate and induced photocurrent, are obtained from the derivatives of the curves obtained from these two quantities.

6.2.1 Experimental setup for X-rays characterization

The devices characterization under X-rays was performed using the dual channel Keithley 2614B SourceMeter and the custom made Labview software, already used for electrical characterization, with experimental setup depicted in the Figure 39. In addition, the metal Faraday cage was placed within a shielded area, containing also the X-rays tube.

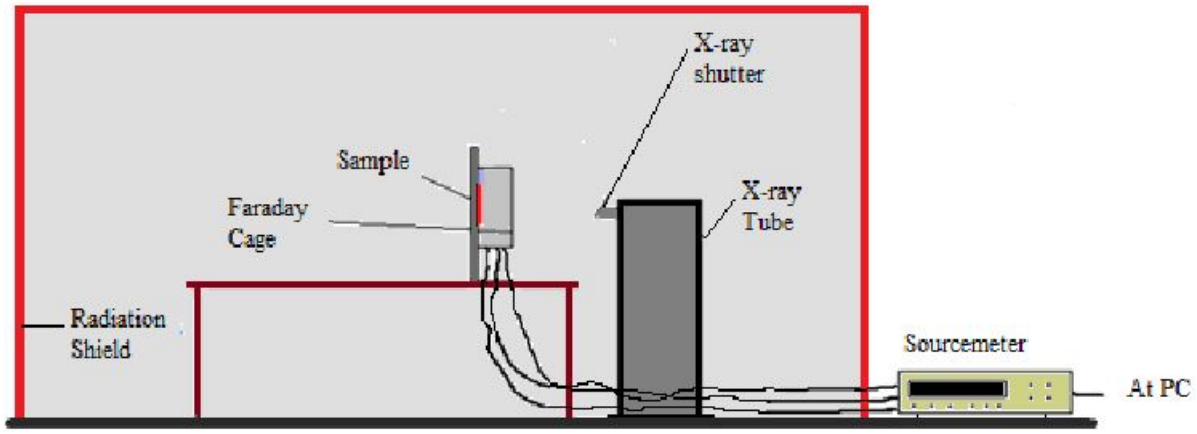

Figure 39 - Schematic view of the experimental setup for characterization under X-ray.

The X-ray tube is equipped with a shutter, that can be opened from the control unit manually or automatically, also by setting on/off cycles.

In the Figure 40 below is reported a picture of the experimental setup, within

the shielded area. It is possible to notice the Faraday cage with its connection cables and the X-ray tube.

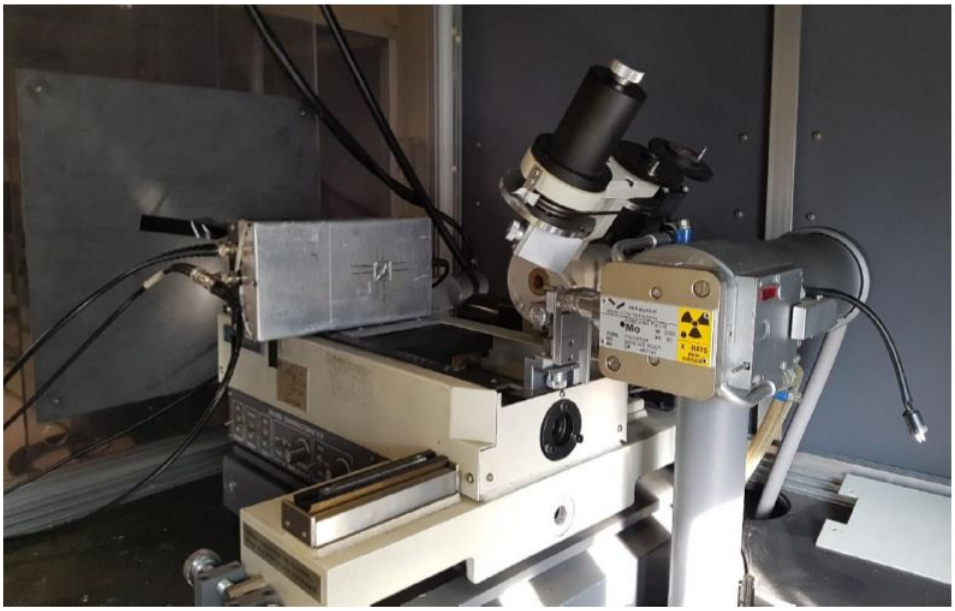

Figure 40 - Picture of the experimental setup for sample characterization under X-ray.

The X-rays tube is a Mo-tube (Figure 41a) (Kα=17.5keV, model PANalytical2 PW 2285/20), which operates at a voltage of 35 kV and at the current defined by the user in the range 5 mA - 30 mA. Its spectrum is reported in Figure 41.

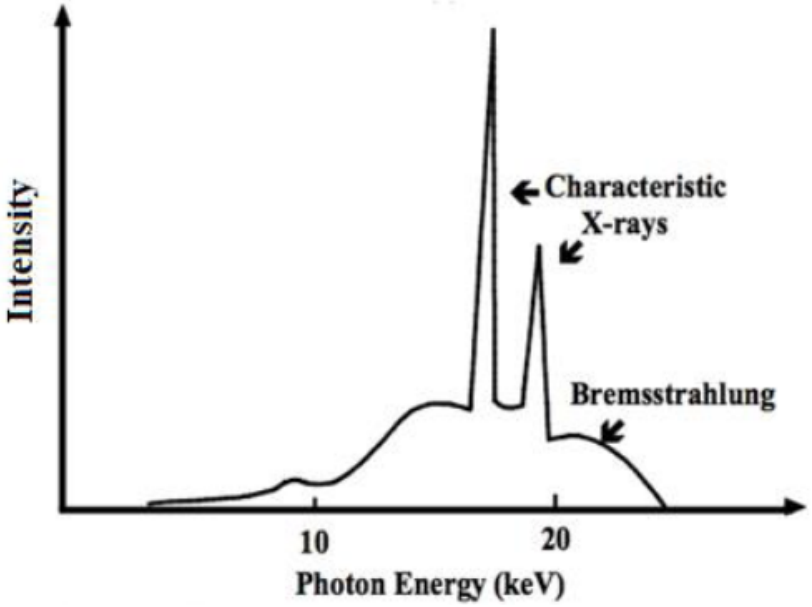

Figure 41 - Spectrum of Mo-target X-ray tube & Mo-Tube calibration

The X-rays Mo-tube was fixed at the distance of 33 cm from the studied device, that was irradiated with X-ray beams having different dose-rate, varying from 30mGy/s to 5mGy/s (30mGy/s, 20mGy/s, 10mGy/s and 5mGy/s). For each dose-rate the photocurrent was acquired during a cycle of four irradiation of 60s, each one followed by 60s without X-ray beam.

The dose rate of the Mo X-rays tube was previously calibrated employing the Barracuda dosimeter (RTI Group, Sweden).

In this procedure, the Barracuda probe was fixed at the radiation shield side, and the X-ray tube was powered at 35 kV and respectively 30mA, 25mA, 20mA, 15mA, 10mA, 5mA. For each current of the X- ray tube the corresponding dose-rate was measured. Then it was recalculated for the sample-tube distance by means of the equation:

$$D_r = D - rp\frac{r_p^2}{r_s^2} \tag{6.3}$$

Where

- D_r is the dose-rate impinging the sample

- D_{rp} the dose-rate at Barracuda probe
- r_p the distance Barracuda probe-X-ray tube
- r_s the distance sample-X-ray tube.

In order to have a detector which probes the dose rate in the faraday cage, at the same position of the devices under test, a Si-photodiode, that has a linear response to X-rays radiation, was calibrated by means of the Barracuda detector.

The photodiode current was measured with the Keithley 2614B SourceMeter during irradiation at same condition of previous tube calibration and with an applied voltage of -2V. The photodiode was installed in the Faraday cage, and shielded from visible light.

Below it is presented the relation between anodic current & dose rate(Table6.10 & Figure 42:

Anodic Current (mA)	Dose rate $\frac{mGy}{s}$
5	5.8
10	15.4
15	25.0
20	33.6
25	44.3
30	52.5

Table 6.10: Molibdenum X-rays tube calibration at the Department of Physics and Astronomy of Bologna

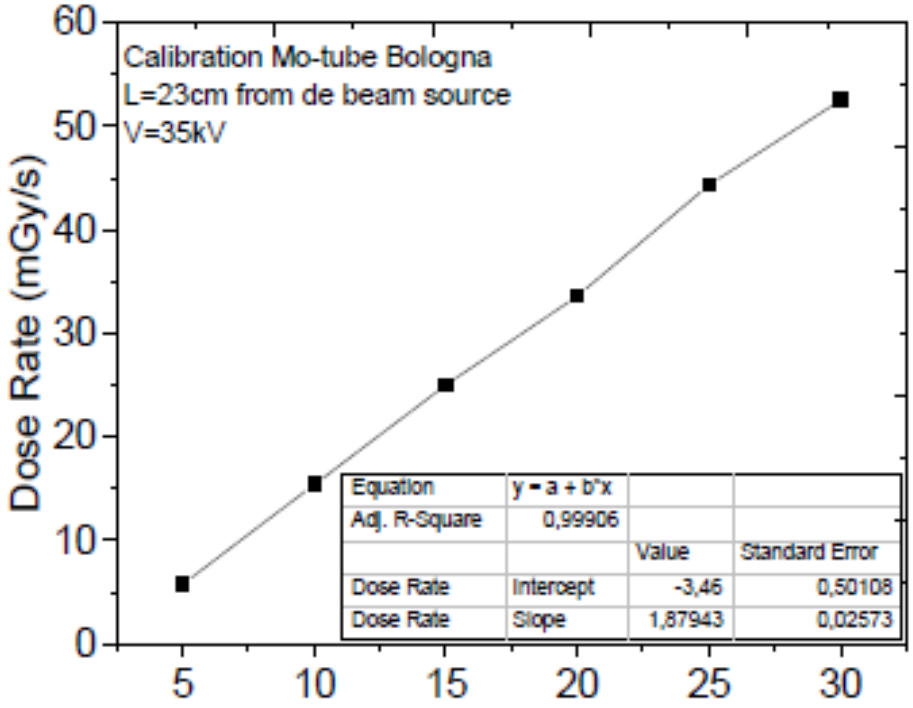

Figure 42 - Molibdenum X-rays tube calibration at the Department of Physics and Astronomy of Bologna

6.2.2 X-rays characterization's results

Once the calibration process is over it is possible to perform the X-rays characterization on the devices realized.

The data collected are plotted, analyzed and reported in the following table 6.11:

The sensitivity of the devices is calculated, as afore mentioned, as the slope of the line that relates the average photocurrent, having in consideration the 4 cycles OFF/ON of radiation exposure, with the respective dose rate [6]:

$$S = \frac{\partial I}{\partial D}$$

Every sample presents a different I-V characteristic before and after the X-ray exposure. This phenomenon can be interpreted as a results of the stressed

Molecule	Sample	Substrate	Sensitivity ($\frac{pC}{Gy}$)
TIPS	Thermal	Si1S1	400± 200
		Si1S2	300±200
		Si1S6	300±100
	TEOS	Si2S1	800±100
		Si2s2	1000±200
		Si2S6	450±50
		Si2S7	540±70
	PECVD	Si3S4	370±60
	PEN	PS7	$(16\pm3)10^3$
		PS8	$(28\pm5)10^3$
	GLASS	VS1	$(14\pm7)10^3$
		VS3	$(19\pm6)10^3$
Molecule	**Sample**	**Substrate**	**Sensitivity** ($\frac{nC}{Gy}$)
TIPGe	Thermal	Discharge	
	TEOS	High Dark Current	
	PECVD	Si3S2	$(4\pm2)10^3$
		Si3S3	$(3\pm2)10^3$
	PEN	PS11	$(42\pm2)10^3$
		PS12	$(33\pm6)10^3$
	GLASS	VS5	$(60\ \pm10)10^3$
		VS6	$(140\pm30)10^3$

Table 6.11: Data collected for the X-rays characterizatio

induced by the radiation in the device. Below are presented the graphs reporting the I-V characteristics, the X-ray characterization and the sensitivity per exposure(Figure 43, 44, 45, 46, 47, 48, 49, 50, 51):

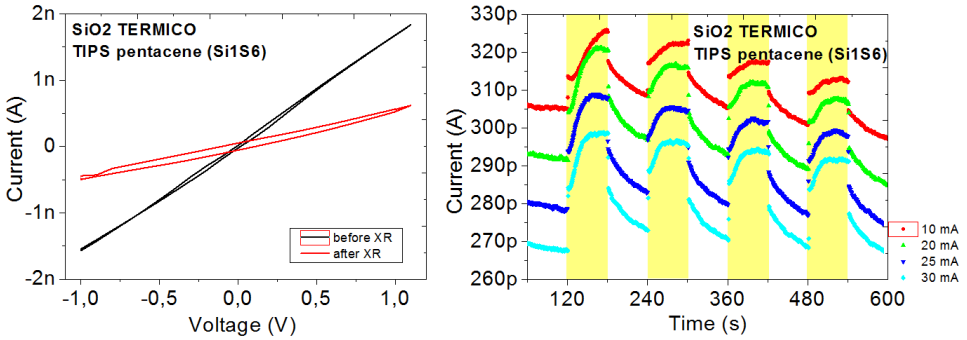

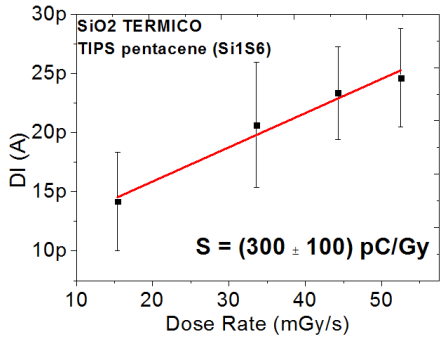

Figure 43 - TIPS sample SiS6 with thermal SiO_2 growth process, yellow regions indicate the exposures to X-rays

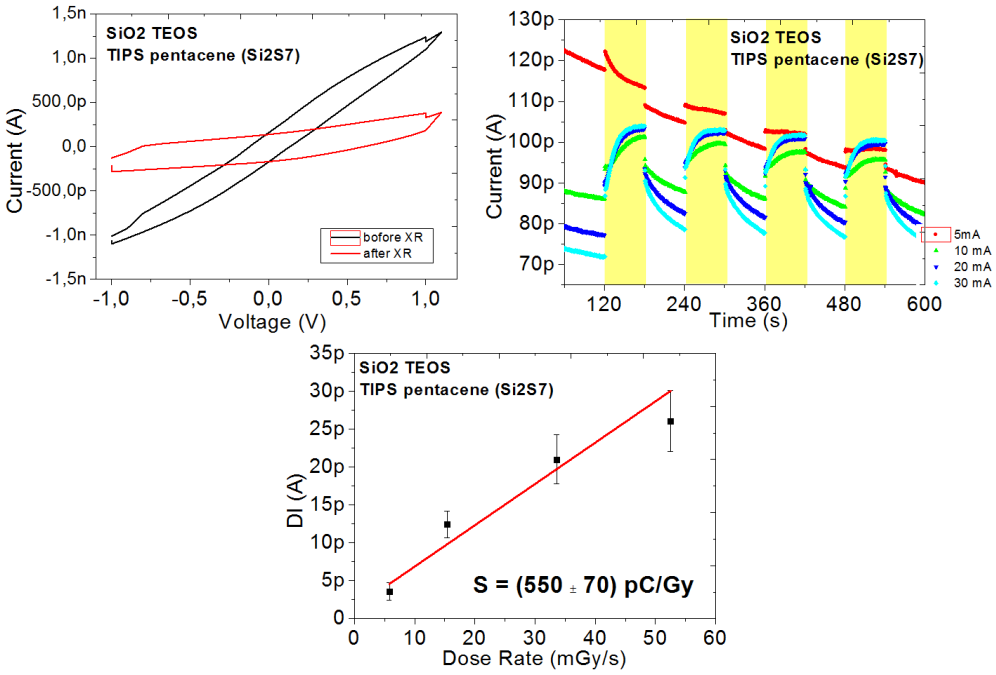

Figure 44 - TIPS sample Si2S7 with TEOS SiO_2 growth process, yellow regions indicate the exposures to X-rays

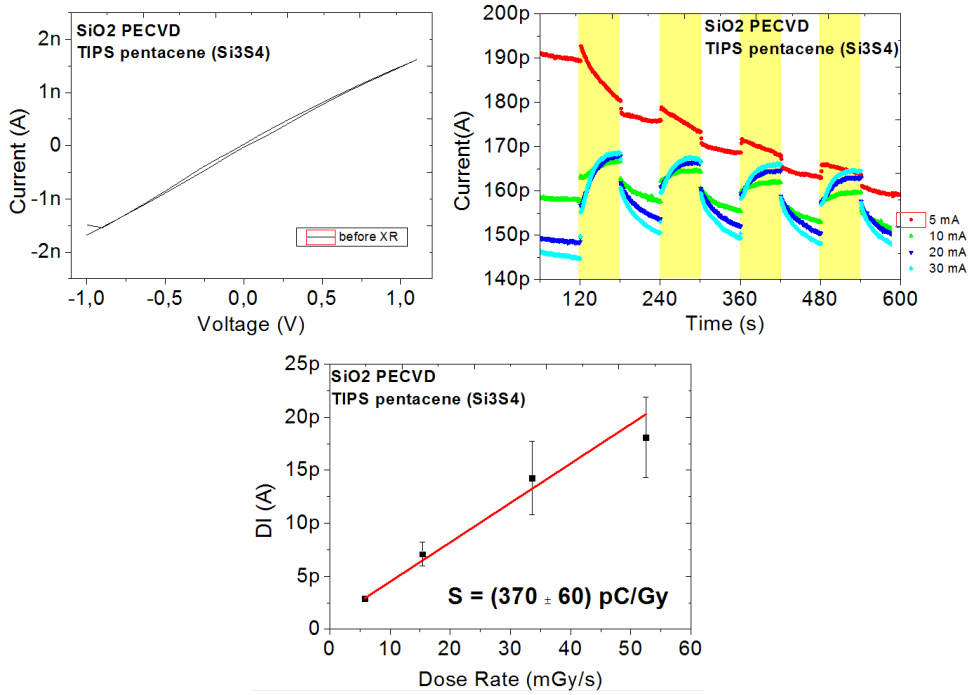

Figure 45 - TIPS sample Si3S4 with PECVD SiO_2 growth process, yellow regions indicate the exposures to X-rays

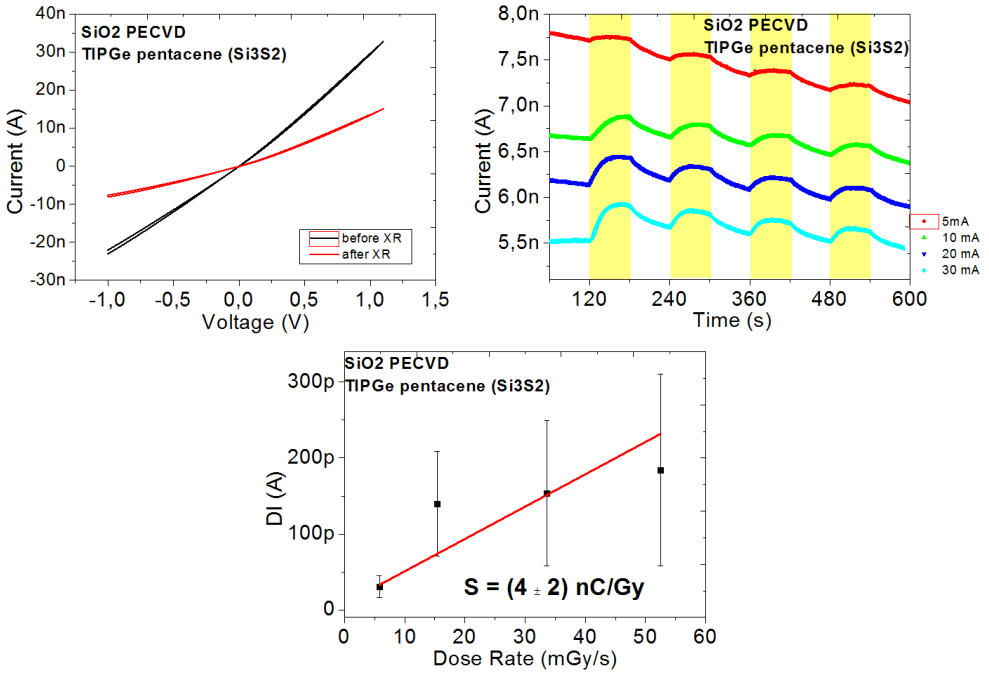

Figure 46 - TIPGe sample Si3S2 with PECVD SiO_2 growth process, yellow regions indicate the exposures to X-rays

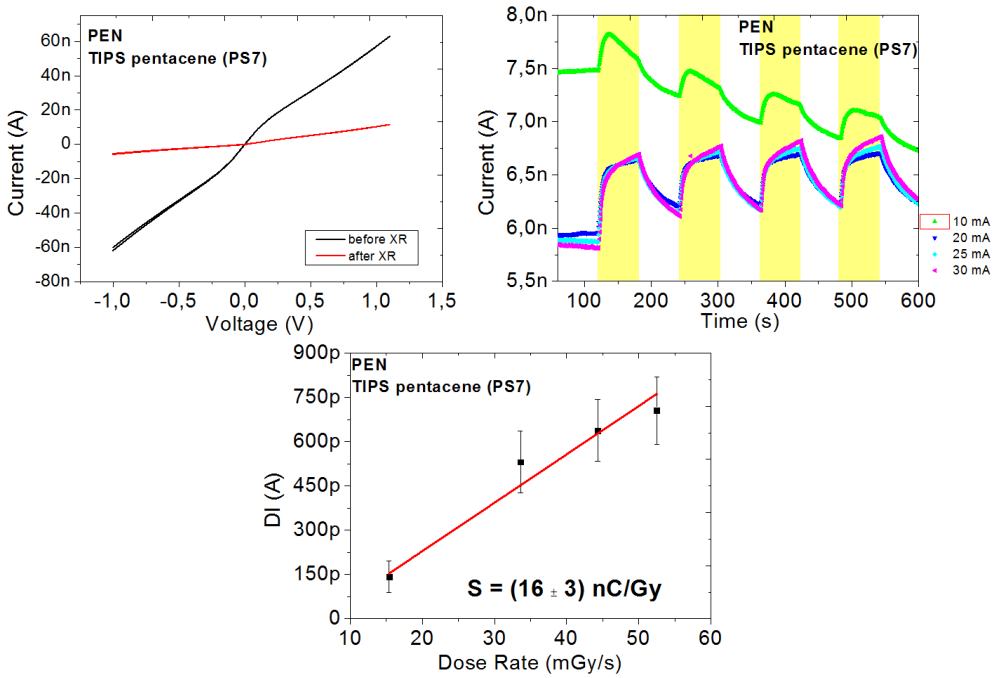

Figure 47 - TIPS sample PS7 on PEN substrate, yellow regions indicate the exposures to X-rays

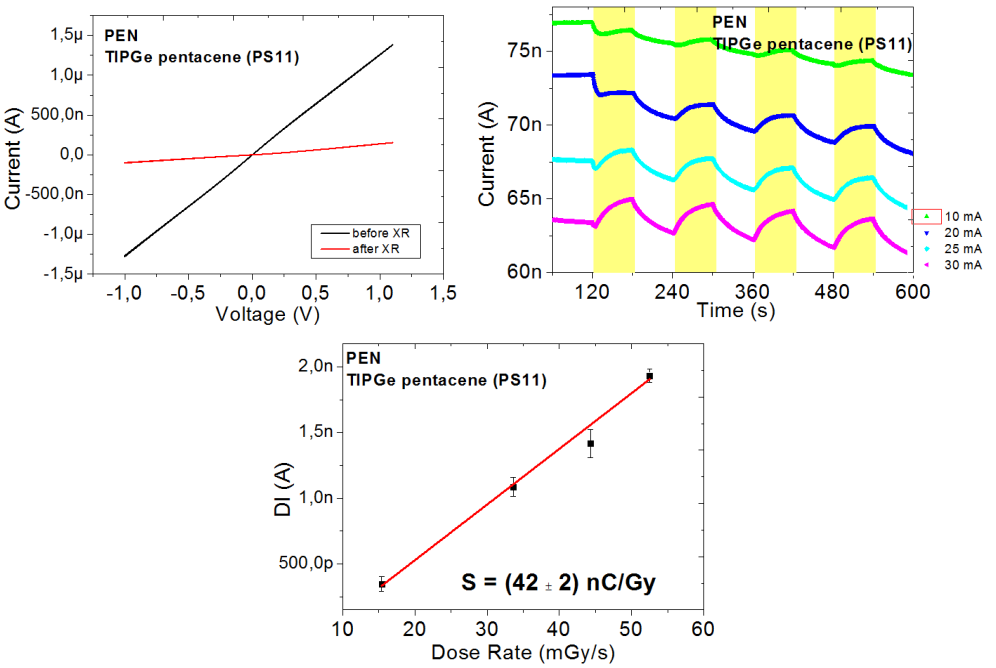

Figure 48 - TIPGe sample PS11 on PEN substrate, yellow regions indicate the exposures to X-rays

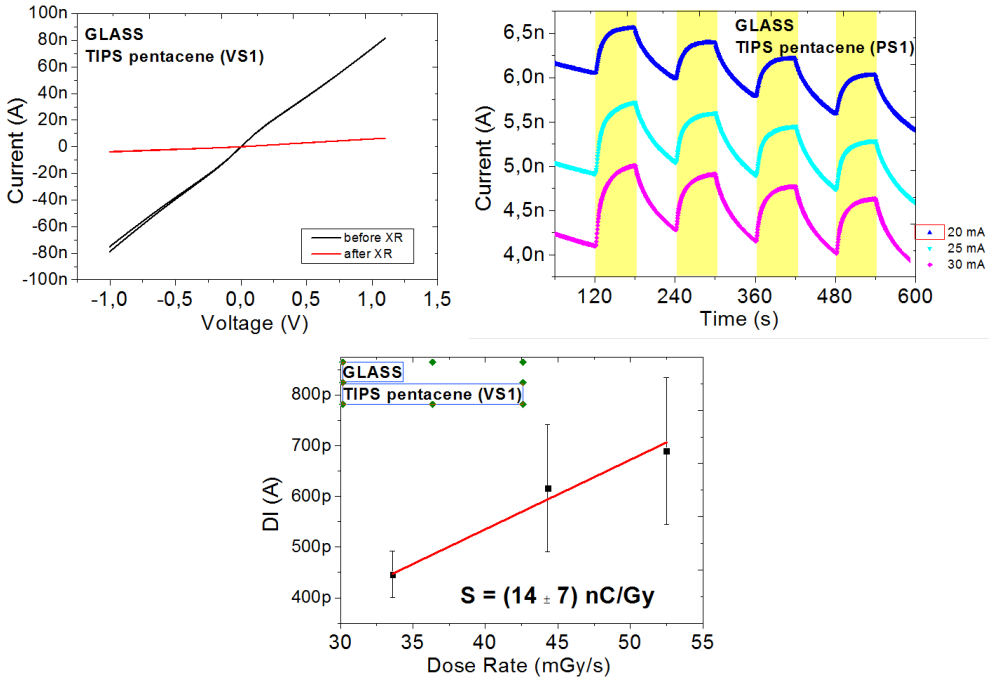

Figure 49 - TIPS sample PS1 on GLASS substrate, yellow regions indicate the exposures to X-rays

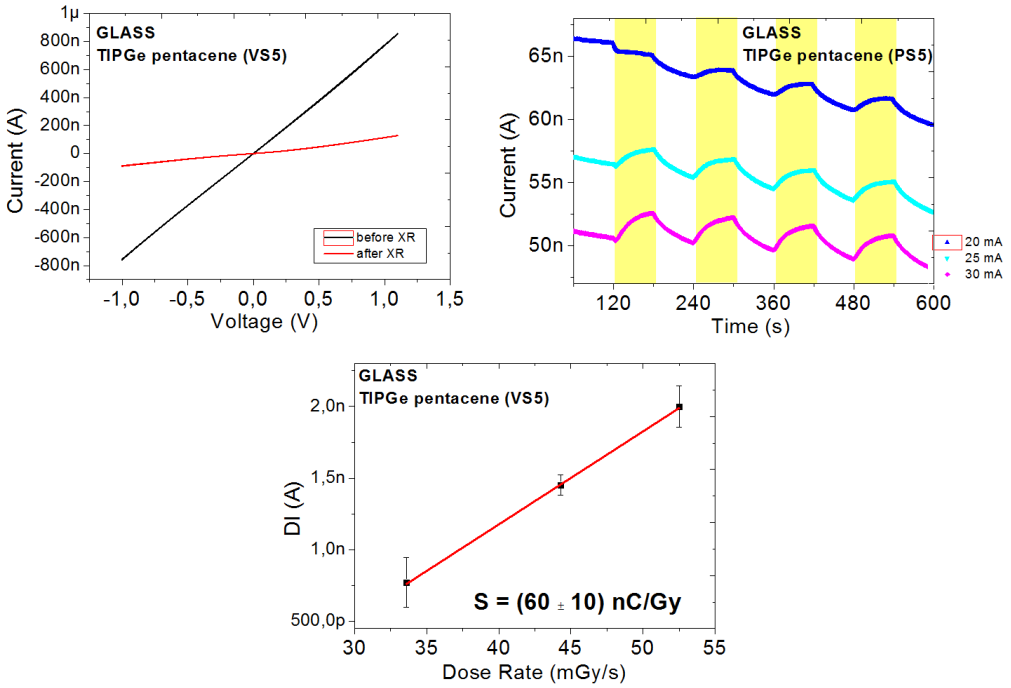

Figure 50 - TIPGe sample PS5 on GLASS substrate, yellow regions indicate the exposures to X-rays

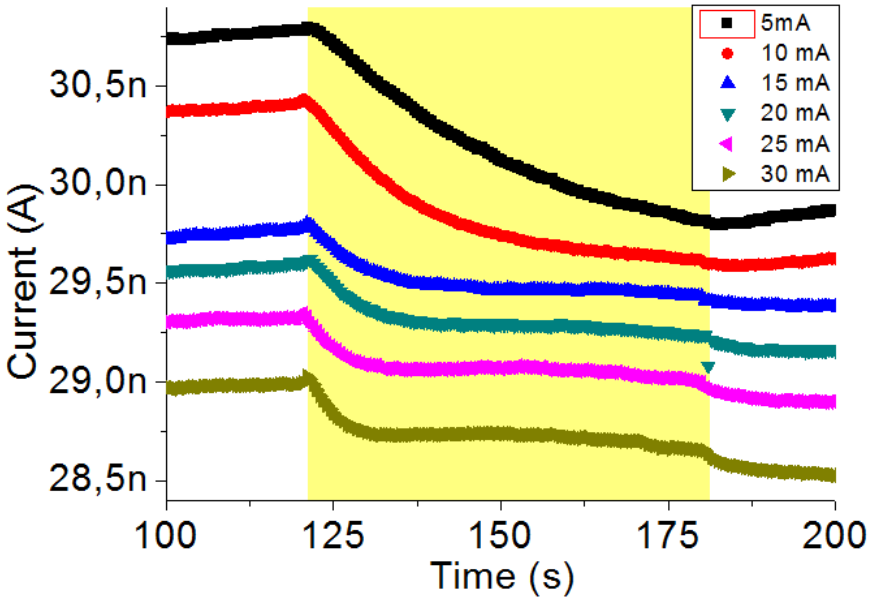

Figure 51 - Discharging TIPGe sample with thermal SiO_2 growth process, yellow regions indicate the exposures to X-rays

Devices previously realized and tested at the Department of Physics and Astronomy of Bologna reports sensitivity's values in the order of $180\frac{nC}{Gy}$ and was obtained for long exposure times and low dose rates with TIPS over a PET substrate [6].

The results obtained with the devices object of this study are quite different as theoretically expected; in fact, this evidence, shows partly the effect of the substrate on the device.

However the data collected for the TIPS & TIPGe samples with PEN substrates are consistent with the one calculated at the Department of Physics and Astronomy of Bologna by Dr. Maria Elias Lopes Pereira [43] with TIPS & TIPGe devices, on a PEN substrates, belonging to a different batch.

As stated before, every device was tested at different dose rate: in particular the measurements have been done from 35kV 5mA to 35kV 30mA with increments of 5mA per cicle.

Every sample, except for the PEN TIPS, showed arcs in the first exposures. Most of them began to behave properly after the arc. However several TIPGe

samples drop casted on SiO_2 weren't able to start responding adequately to X-rays radiation.

The sensitivity of the TIPGe samples is always greater than the one of TIPS devices. This result, together with the sensitivity's value for the samples over PEN and GLASS substrates, confirm the results obtained by Dr. Maria Elias Lopes Pereira with samples belonging to other batches of production [43]. This evidence can be evaluated as a proof of the repetatability of the process of fabrication.

Looking at the graphs in Figure 52, it is evident how the devices realized on PEN & GLASS substrates are charaterized by a better sensitivity respect to the one realized over SiO_2 substrates (no matter if Thermal TEOS or PECVD).

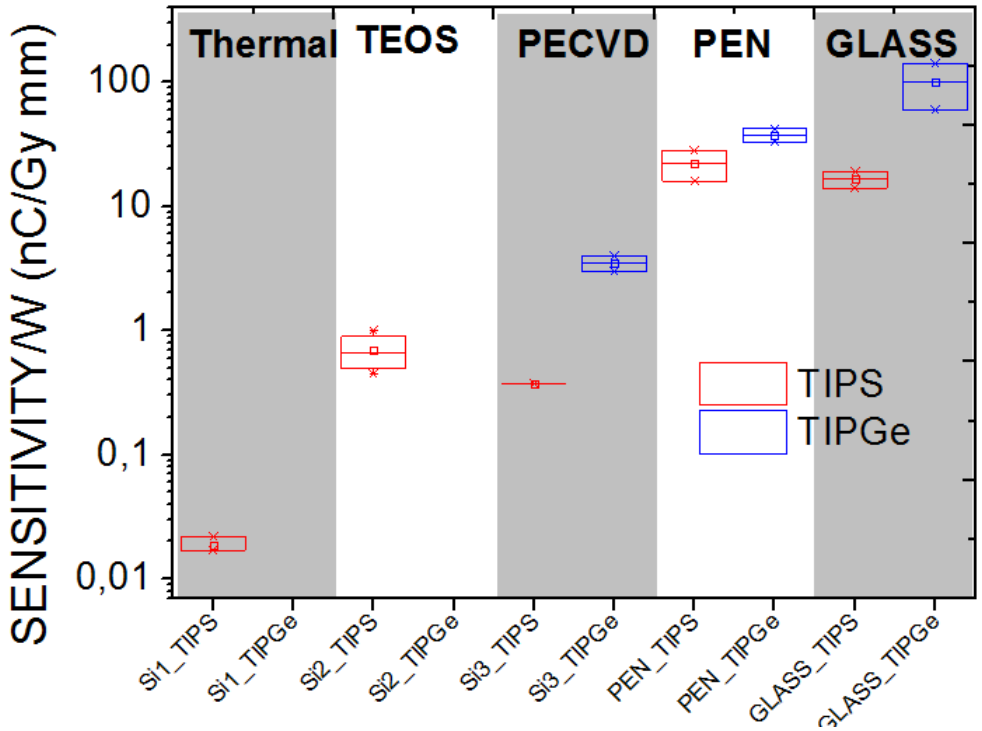

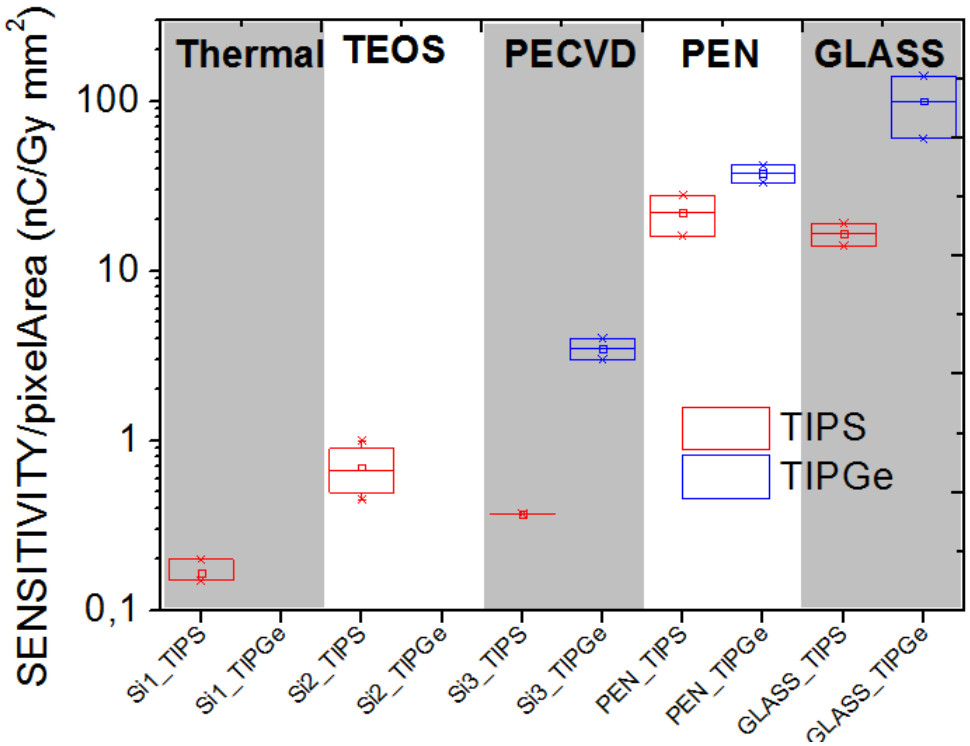

Figure 52 - Sensitivity respectively normalized with respect to the width of the channel and to the pixel area

To conclude this chapter, in the Figure 53 is presented a comparison between sheet resistivity and sensitivity of the devices analyzed.

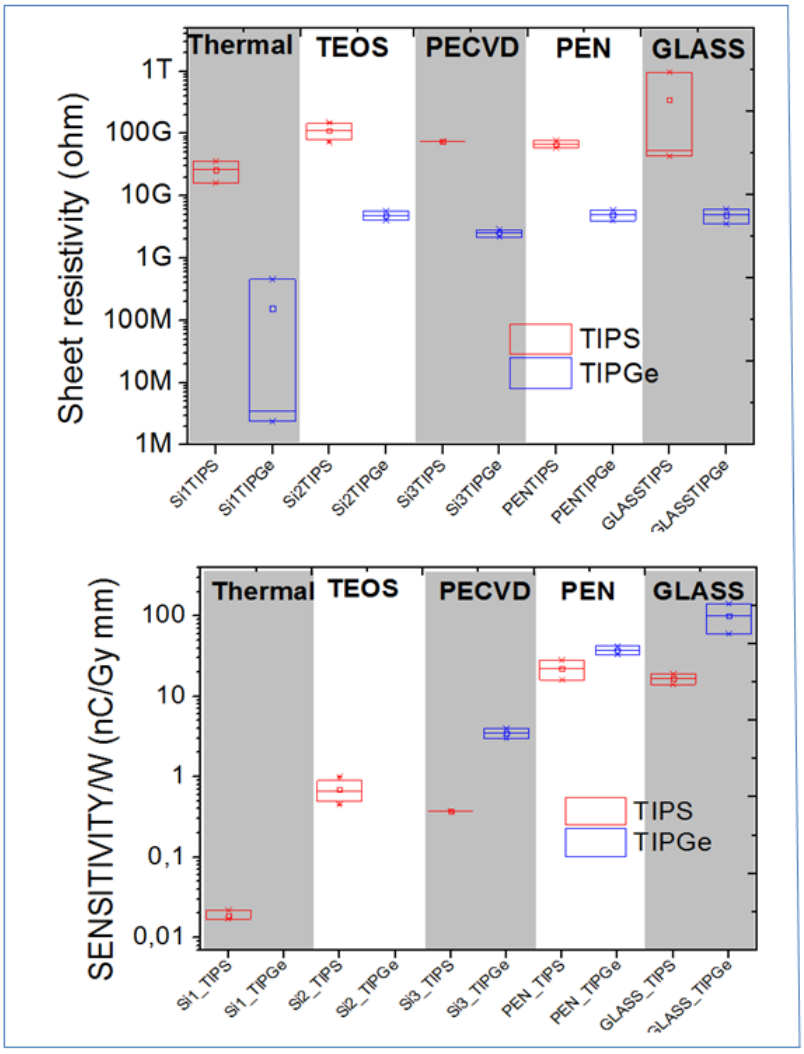

Figure 53 - Comparison graphs between sheet resistivity and sensitivity

It is possible to verify that, with each substrates, both for TIPS & and TIPGe, the better is the electrical conductivity the better is the sensitivity toward radiation X.

In the table 6.12 & table 6.13 below are presented all data grouped together:

Molecule	**Substrate**	**Resistivity** $\rho_{\square}(\Omega)$	**Sensitivity** $(\frac{nC}{Gy})$
TIPS	Glass	$(9.63 \pm 0.07)10^{11}$	$(14\pm6)10^3$
TIPS		$(4.33 \pm 0.05)10^{10}$	$(19\pm7)10^3$
TIPGe	Glass	$(4.93 \pm 0.04)10^9$	$(60\pm10)10^3$
TIPGe		$(3.61 \pm 0.03)10^9$	$(140\pm30)10^3$
Molecule	**Substrate**	**Resistivity** $\rho_{\square}(\Omega)$	**Sensitivity** $(\frac{nC}{Gy})$
TIPS	PECVD	$(7.42 \pm 0.06)10^{10}$	370±60
TIPGe		$(2.18 \pm 0.01)10^9$	$(4\pm2)10^3$
TIPGe		$(2.86 \pm 0.05)10^9$	$(3\pm2)10^3$
Molecule	**Substrate**	**Resistivity** $\rho_{\square}(\Omega)$	**Sensitivity** $(\frac{nC}{Gy})$
TIPS	TEOS	$(8.78 \pm 0.02)10^{10}$	800 ±100
TIPS		$(7.23 \pm 0.03)10^{10}$	1000±200
TIPS		$(1.49 \pm 0.02)10^{11}$	450±50
TIPS		$(1.40 \pm 0.01)10^{11}$	540±70
TIPGe	TEOS	$(5.71 \pm 0.09)10^9$	High Dark Current
TIPGe		$(4.01 \pm 0.04)10^9$	High Dark Current
Molecule	**Substrate**	**Resistivity** $\rho_{\square}(\Omega)$	**Sensitivity** $(\frac{nC}{Gy})$
TIPS	Thermal	$(1.61 \pm 0.01)10^{10}$	400±200
TIPS		$(3.57 \pm 0.02)10^{10}$	300±100
TIPS		$(2.63 \pm 0.02)10^{10}$	300±100
TIPGe	Thermal	$(3.475 \pm 0.007)10^6$	Discharge
TIPGe		$(2.378 \pm 0.002)10^6$	Discharge
TIPGe		$(4.586 \pm 0.003)10^8$	Discharge
Molecule	**Substrate**	**Resistivity** $\rho_{\square}(\Omega)$	**Sensitivity** $(\frac{nC}{Gy})$
TIPS	PEN	$(7.9 \pm 0.1)10^{10}$	$(16\pm3)10^3$
TIPS		$(5.86 \pm 0.08)10^{10}$	$(28\pm5)10^3$
TIPGe	PEN	$(3.98 \pm 0.03)10^9$	$(42\pm2)10^3$
TIPGe		$(5.86 \pm 0.02)10^9$	$(33\pm6)10^3$

Table 6.12: Data collected for the devices tested

Third Part

Chapter 7

Experimental measurements held at Skan-X Radiology Devices S.p.A.

Skan-X Radiology Devices S.p.A is a company situated in San Lazzaro di Savena (BO) which produces X-ray stationary anode tubes since 1956. Its production counts more than 30 different types of X-rays tubes moving from microfocal spot tubes, through panoramic and CBCT tubes, ending with 160kV tubes used for industrial inspection.

Figure 54 - Tubes from Skan-X Radiology devices S.p.A.

Skan-X is always looking forward for those technologies which can represent the future in the world of X-rays, not only under the aspect of X-rays producion (tubes) but also in the field of X-rays detection.

The collaboration between the Department of Physics and astronomy of Bologna and the Skan-X Radiology Devices S.p.A offered the possibility to characterized and test a TIPGe device, previously realized at the University,

using different type of X-rays tubes in many different configuration.

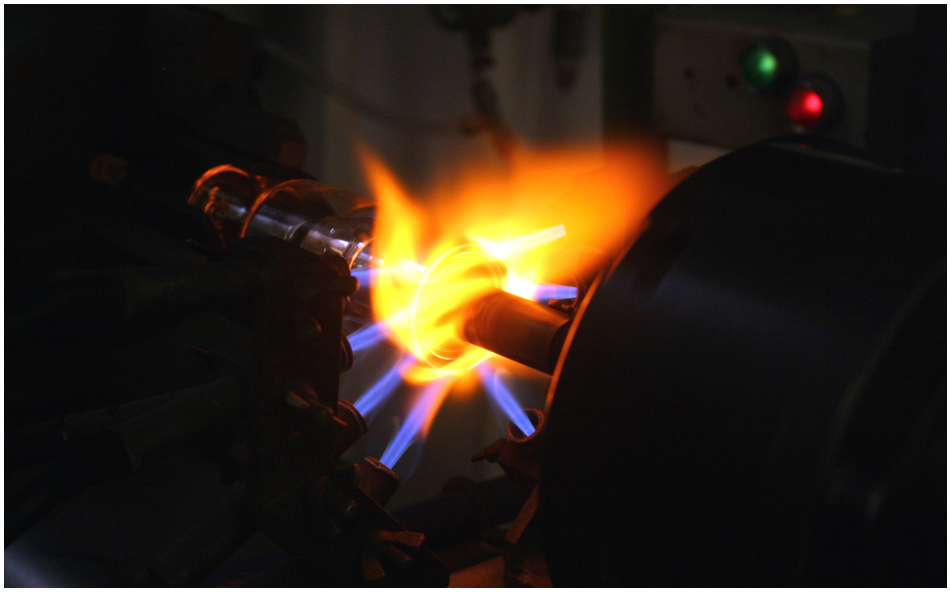

Figure 55 - Anode soldering in Skan-X Radiology Devices S.p.A.

7.1 Experimental setup

The experimental setup is composed by:

- Organic thin film detector: TIPGe over PEN substrate
- Vacudap dosimeter
- Barracuda multimeter
- X-rays tube OPX/105 Serial Number: 681502
- Keithley 2614B SourceMeter

As mentioned before, the sample used for the experimental measurements held at Skan-X Radiology Devices S.p.A. is not belonging to the batch 10 analyzed in the previous chapters. The device, subject of this chapter is a TIPGe sample with PEN substrate.

It was realized at the laboratories of the Department of Physics and astonomy of Bologna, shielded and kept close in a metal box to avoid deterioration from light sources and to reduce its dark current(Figure 56) . This devices was

chosen also because of its high stability and its better sensitivity compared to the one of the device presented in the previous chapter.

Figure 56 - Device tested at Skan-X Radiology Devices S.p.A.

The sample were placed, together with the "Barracuda dosimeter", at a distance of 465mm from the focal spot of the X-rays tube while the "Vacudap dosimeter" were placed at 300mm(Figure 57).

Figure 57 - Barracuda Dosimeter and VacuDap Dosimeter

Data were collected in four configuration:

- Increasing kV in the range (35-90)kV, fixed mA, fixed exposure time
- Fixed kV, increasing mA in the range (0.25-6.5)mA, fixed exposure time
- Fixed kV, fixed mA, increasing exposure time in the range (2-60)s
- Long exposure of fixed time interspersed by the same time off, fixed kV, fixed mA

Here the data collected are presented for each configuration.

7.2 Voltage sweep: increasing kV, fixed mA, fixed exposure time

In this set of measurements the main purpose was to verify both the limit of detection of the device and its behaviour at higher anodic voltage. Even if we higher voltage would have been possible, to keep the device safe (scared of discharged from the tube), 90kV was set as the maximum value.

Looking at the data (Table7.1), as theoretically predictable, the dose varies quadratically with increasing kV as shown in the graph of Figure 58:

kV	mA	time	exp	Vacudap ($\mu Gy \times cm^2$)	Barracuda ($\frac{\mu Gy}{s}$)
35	5	5	2	0.55	9.82
40	5	5	2	1.15	11.80
45	5	5	2	2.05	14.76
50	5	5	2	3.10	18.22
55	5	5	2	4.40	22.51
60	5	5	2	5.85	27.29
65	5	5	2	7.65	33.22
70	5	5	2	9.20	38.33
75	5	5	2	11.00	44.26
80	5	5	2	13.00	50.85
85	5	5	2	15.35	58.60
90	5	5	2	17.40	65.36

Table 7.1: Data collected during the voltage sweep

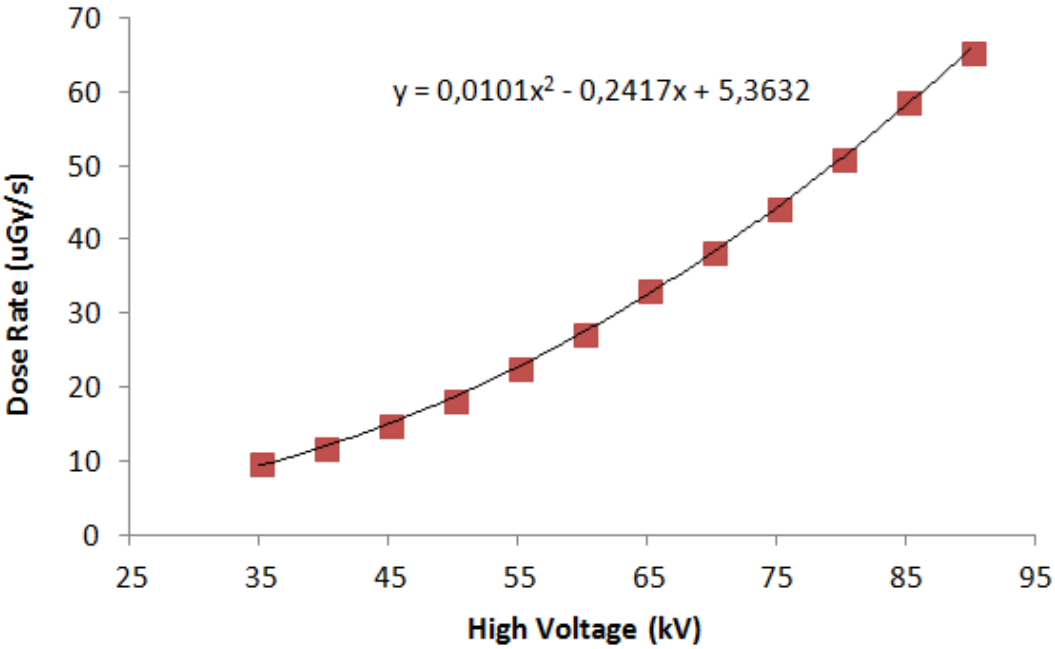

Figure 58 - Voltage sweep

7.3 Current sweep: fixed kV, increasing mA, fixed exposure time

The aim of the second set of measurements was to analyze the behaviour of the device when exposed to different doses for the same amount of time, imposing an anodic voltage which is comparable to the one used in dental radiography.

It is evident how the dose on the VacuDap dosimeter increases linearly with the anodic current according to the theoretical behaviour(Figure 59).

kV	mA	time	exp	Vacudap ($\mu Gy \times cm^2$)	Barracuda ($\frac{\mu Gy}{s}$)
70	0.25	5	2	0.30	8.99
70	0.75	5	2	1.20	11.96
70	1.25	5	2	2.30	15.59
70	1.75	5	2	3.25	18.72
70	2.25	5	2	4.10	21.52
70	2.75	5	2	5.05	24.65
70	3.25	5	2	6.15	28.28
70	3.75	5	2	6.96	30.97
70	4.25	5	2	8.05	34.54
70	4.75	5	2	8.90	37.34
70	5.25	5	2	9.85	40.47
70	5.75	5	2	10.60	42.94
70	6.25	5	2	11.60	46.24

Table 7.2: Data collected during the current sweep

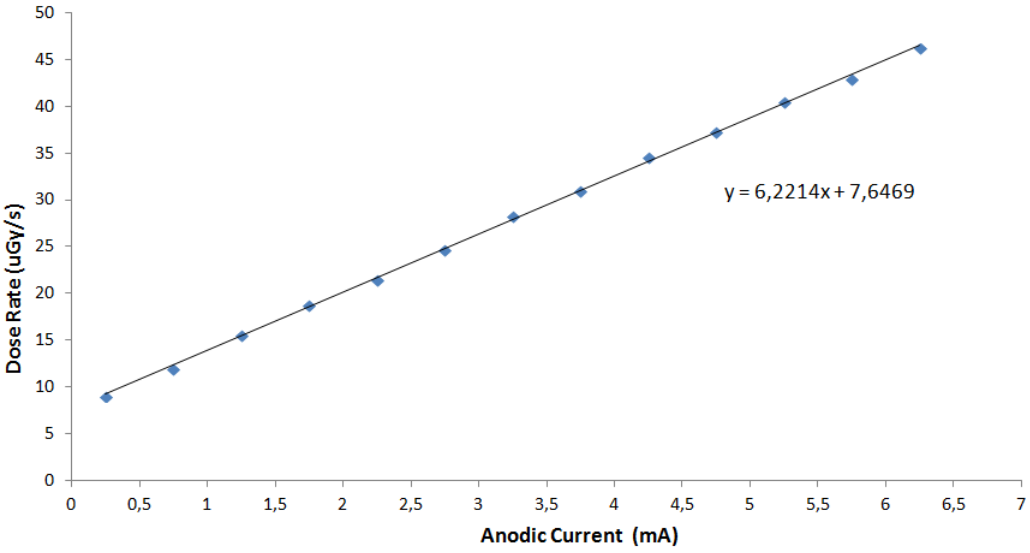

Figure 59 - Current sweep

7.4 Time sweep: fixed kV, fixed mA, increasing exposure time

In this set of measurements the main purpose was to analyse the behaviour of the sample under different exposure time to X-rays. According to the the-

oretical forecast the dose rate is almost linear due to the invariance of High voltage and anodic current(Figure 60).

The oscillations from the ideal behaviour can be justified by some imbalance during the emission from the X-ray tube.

These oscillations may be due to several reasons:

- Over Heating of the filament
- Oscillations of the filament voltage value
- Oscillation of the High Voltage value

Among them, the most probable one is the oscillation of the filament voltage value. This fact is partly due to the software which regulates the emission from the IGBT in the filament voltage generator. The software used to make the X-rayd emission is driven by a feedback logic; it reads the anodic current of emitted and retroact on the filament voltage value in order to obtain the desired emission with the specified tollerance.

Sometimes, while trying to find the correct value for the filament voltage, the anodic current can oscillate around the searched value. The intensity of the oscillation depends on many factors such as:

- Temperature of the filament
- Lenght of the filament
- Number of turns of the filament
- Thickness of the filament
- Short time exposure

kV	mA	time	exp	Vacudap ($\mu Gy \times cm^2$)	Barracuda ($\frac{\mu Gy}{s}$)
70	4	0.5	2	0.70	31.08
70	4	1	2	1.40	31.08
70	4	1.5	2	2.15	31.63
70	4	2	2	2.95	32.31
70	4	2.5	2	3.60	31.74
70	4	3	2	4.35	31.90
70	4	3.5	2	5.05	31.78
70	4	4	2	5.80	31.90
70	4	4.5	2	6.6	32.18
70	4	5	2	7.25	31.90
70	4	5.5	2	8.00	31.98
70	4	6	2	8.95	32.59
70	4	6.5	2	9.80	32.85

Table 7.3: Data collected during the time sweep

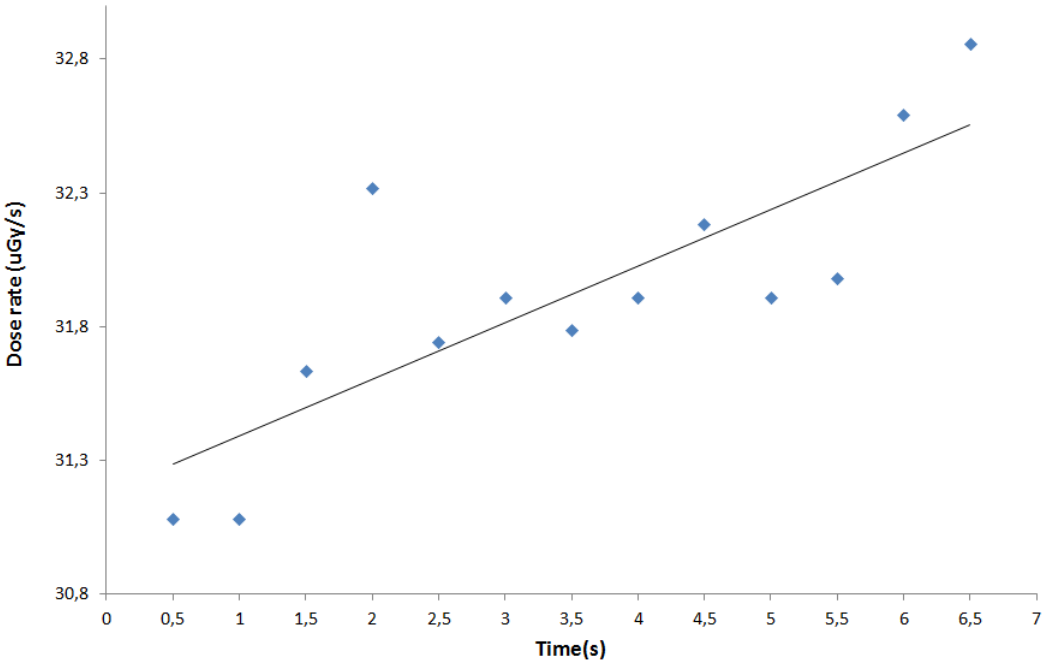

Figure 60 - Time sweep

7.5 X-rays cyclical exposures

In the last set of measurements, the aim was to check whether the respond of the device was coherent after long exposure to X-rays. It was simulated the same cycle used during X-ray characterization with anodic voltage and anodic current which are comprable to the one characterizing a radiography(Figure 61).

kV	mA	time	exp	Vacudap ($\mu Gy \times cm^2$)	Barracuda ($\frac{\mu Gy}{s}$)
70	5	60	1	90.80	32.94
70	5	60	1	91.30	33.08
70	5	60	1	92.90	33.52
70	5	60	1	89.00	32.45
70	5	60	1	91.00	33.00

Table 7.4: Data collected during the cyclical exposures

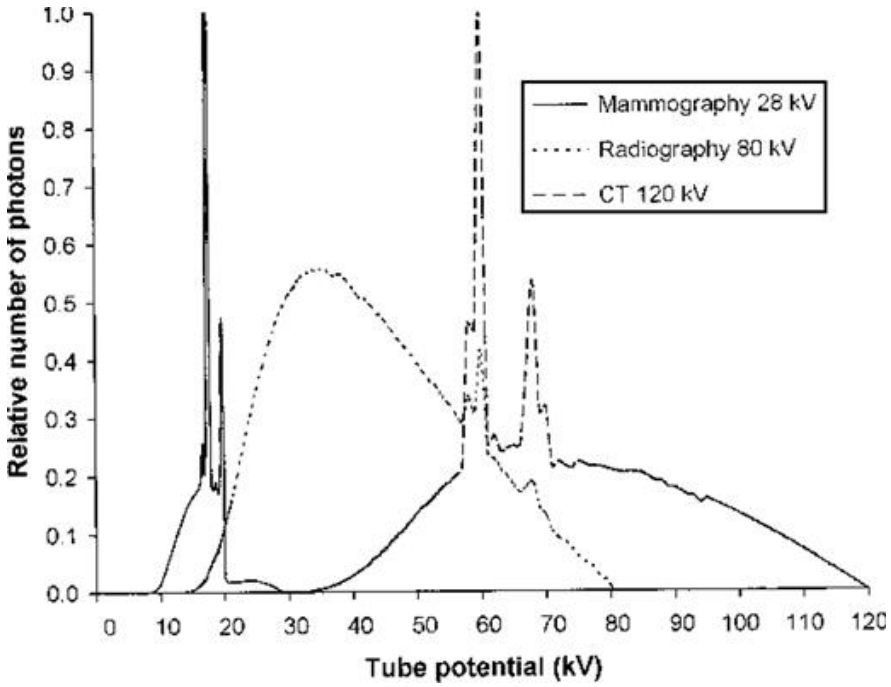

Figure 61 - Spectrum of a W-target radiography X-ray tube Vs Spectrum of a Mo-target mammography X-ray tube

The emission of an X-ray tube may change due to several reasons as previously mentioned; such oscillations in the X-ray exposure can slightly affect the data collected. Moreover the environment in which the measurements

were performed it is very harsh, in particular for electronic devices and electronic readings. These oscillation, whose nature is intrinsically stochastic, are unpredictable and difficult to quantify.

Chapter 8

Analysis of the data collected at Skan-X Radiology Devices S.p.A.

It is evident how the Dose rate detected from the VacuDap dosimeter and from the Barracuda Multimeter are quite different and inconsistent. Data obtained from the VacuDap dosimeter are difficult to deal with because of their unit of measure. This fact, together with the data previosuly collected at the laboratories of the Department of Physics and Astronomy of Bologna, suggested to study and elaborate the data obtained from the Barracuda Multimeter.

Using the software "OriginLab", the data collected have been analyzed in order to extract the sensitivity values of the sample according to different sets of measurements. In the following are presented the data collected, respectively, during the voltage sweep, the current sweep and the time sweep.

For each dataset the sensitivity of the device has been calculated. In the following paragraphs are presented the results obtained.

8.1 Data analysis for the voltage sweep measurements

The graph below (Figure 62) presents in the X-axis the photocurrent, expressed as the difference between $I_{ON} - I_{OFF}$, which represents the mere current induced by the radiation; I_{ON} is the total current which circulates in the device when it is exposed to X-rays radiation while I_{OFF} is the quiescent current when the device is not irradiated.

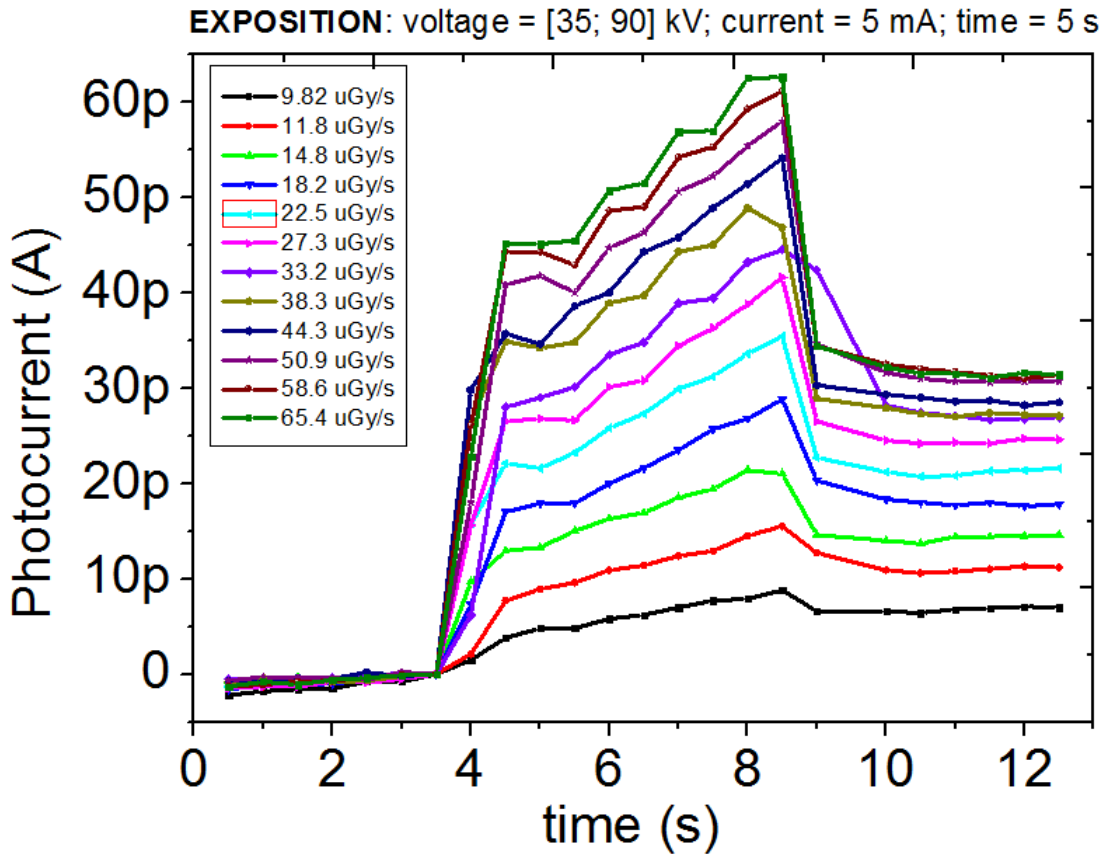

Figure 62 - Voltage sweep

The reason of this choice is that it helps to notice that an higher photocurrent is related to an higher dose rate. In the table 8.1 below are scheduled the data collected for the sensitivity calculation(Figure 63):

kV	mA	time(s)	Dose Rate ($\frac{\mu Gy}{s}$)	Photocurrent (pA)
35	5	5	9,82	9,9±0.5
40	5	5	11.80	15.5±0.1
45	5	5	14.76	21.2 ±0.3
50	5	5	18.22	28.1 ±1.0
55	5	5	22.51	33.7 ±2, 3
60	5	5	27.29	39.7 ±2, 6
65	5	5	33.22	44.5 ±2, 3
70	5	5	38.33	48.8 ±0.1
75	5	5	44.26	52.3 ±2, 5
80	5	5	50.85	56.9 ±1, 5
85	5	5	58.60	59.4 ±2, 3
90	5	5	65.36	59.9 ±3, 7

Table 8.1: Voltage sweep data analysis

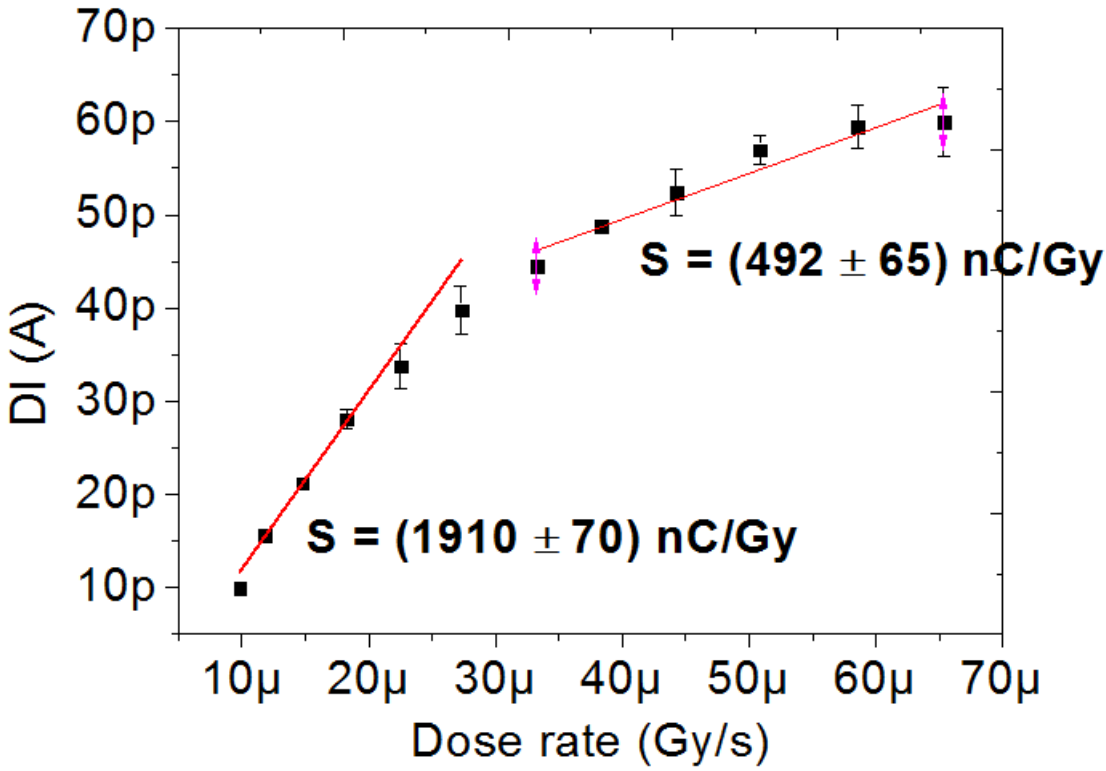

Figure 63 - Sensitivity calculated with respect to the voltage sweep dataset

8.2 Data analysis for the current sweep measurements

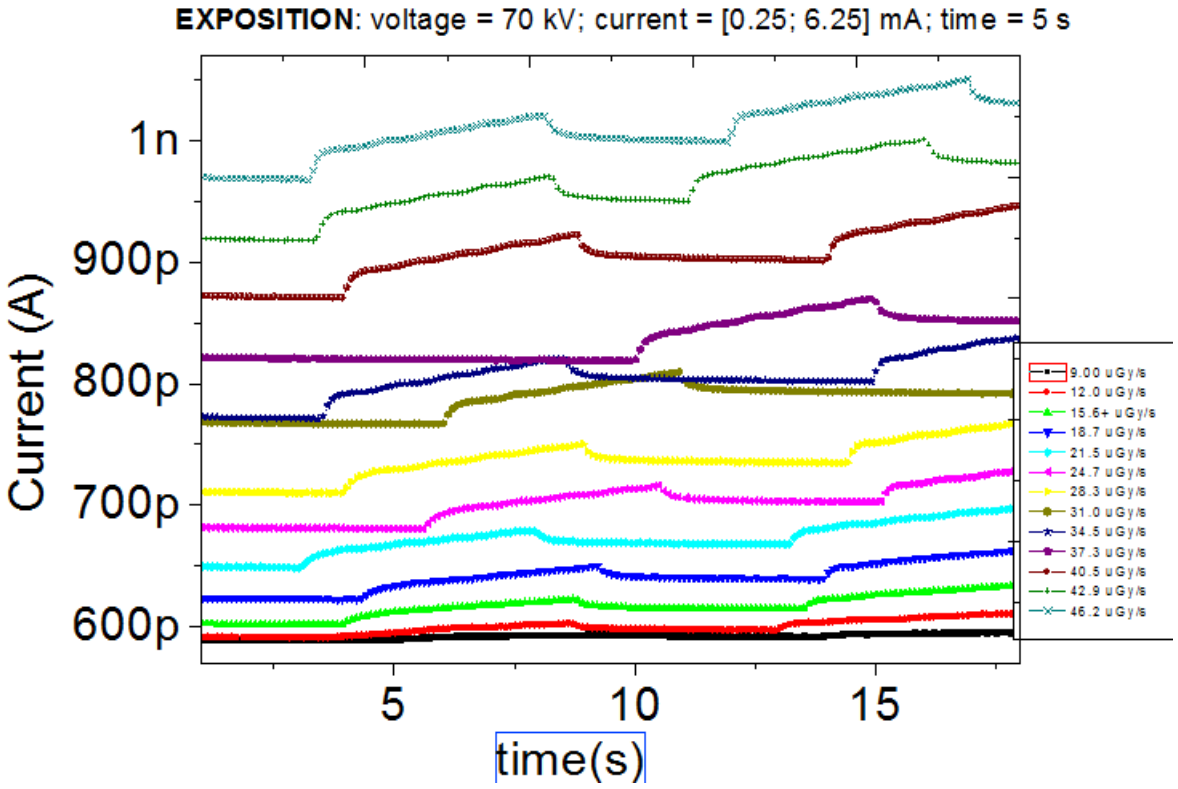

Figure 64 - Current sweep

In this case, on the Y-Axis, are reported the values of the current circulating in the device instead of the photocurrent. In fact the curves obtained (Figure 64) are not referred to zero but they are shifted after each exposure as a result of the stress due to the exposure to X-ray.

In the table 8.2 below are scheduled the data collected for the sensitivity calculation:

kV	mA	time(s)	Dose Rate ($\frac{\mu Gy}{s}$)	Photocurrent (pA)
70	0.25	5	8.99	4.2±0.2
70	0.75	5	11.96	12.8±1, 5
70	1.25	5	15.59	20.3±0.1
70	1.75	5	18.72	26.7±0.5
70	2.25	5	21.52	30.8±0.3
70	2.75	5	24.65	35.3±0.8
70	3.25	5	28.28	40.0±0.6
70	3.75	5	30.97	42.4±0.9
70	4.25	5	34.54	48.2±1, 9
70	4.75	5	37.34	49.9±0.1
70	5.25	5	40.47	51.1±0.4
70	5.75	5	42.94	51.6±1, 6
70	6.25	5	46.24	52.4±0.9

Table 8.2: Current sweep data analysis

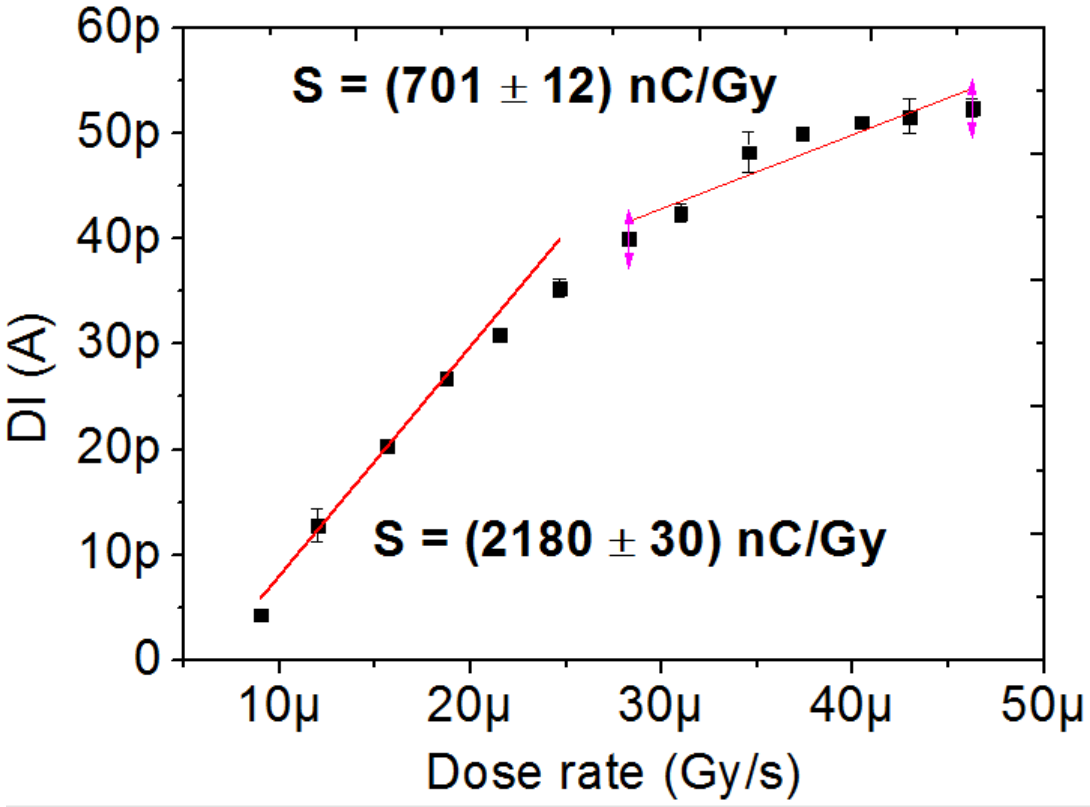

Figure 65 - Sensitivity calculated with respect to the current sweep dataset

8.3 Data analysis for the time sweep measurements

Here again is visible the effect of the X-rays radiation on the behaviour of the device. Exposure to X-rat considerably stressed the sample. In this case on the X-Axis it is reported the time expressed in seconds (Figure 66).

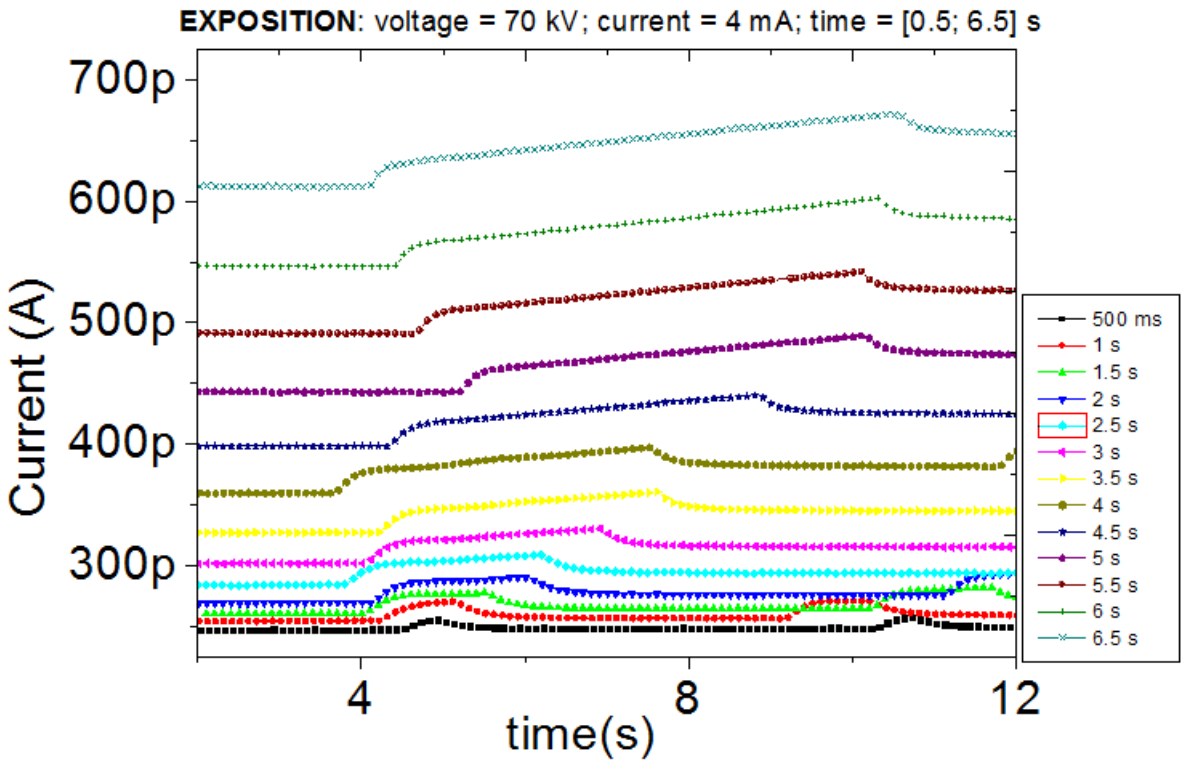

Figure 66 - Time sweep

In the table 8.3 below are scheduled the data collected for the sensitivity calculation:

kV	mA	time(s)	Total Dose (μGy)	Photocurrent (pA)
70	4	0.5	15,54	8.2±0.7
70	4	1	31,08	15.2±0.9
70	4	1.5	47,44	17.4±0.2
70	4	2	64,63	21.4±1.0
70	4	2.5	79,35	25.3±0.6
70	4	3	95,71	28.9±0.5
70	4	3.5	111,25	33.2±0.5
70	4	4	127,62	37.4±0.1
70	4	4.5	144,81	41.9±0.1
70	4	5	159,53	46.4±0.3
70	4	5.5	175,89	50.8±0.2
70	4	6	195,55	56.1±0.2
70	4	6.5	213,56	58.4±2, 6

Table 8.3: Voltage sweep data analysis

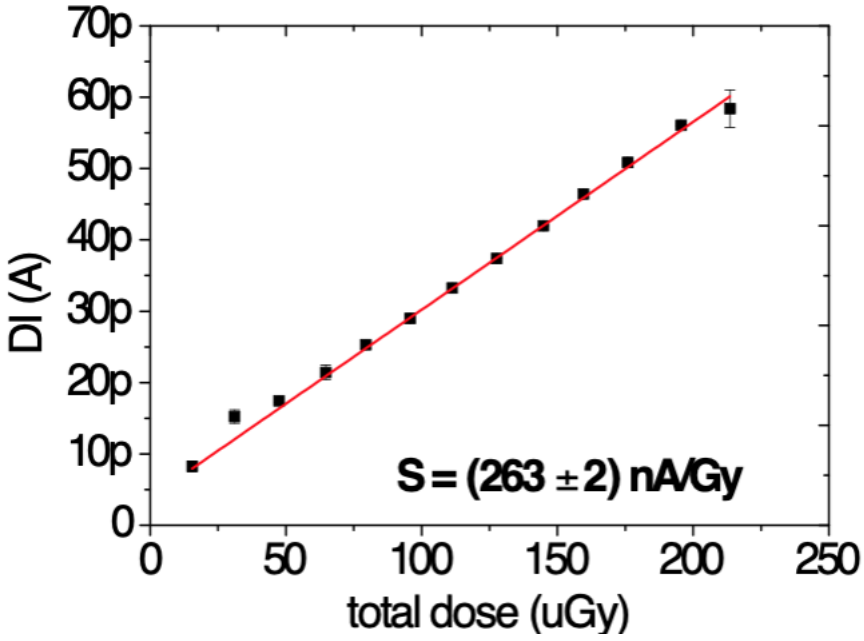

Figure 67 - Sensitivity calculated with respect to the time sweep dataset

8.4 Comparison between Skan-X's measurements and Unibo's measurements

Looking at the graphs previosuly presented (Figure 62, 64, 66), it is clear how the device is able to detect X-rays radiation when its doses is comparable with the one used in medical inspection, in particular in dental and panoramic analysis.

Moreover, it is an evidence that the device is detecting X-rays radiation both in case of short exposure (order of hundreds of mS) and low level of dose rate (order of some $\frac{\mu Gy}{s}$) .

The data shows a relevant increase in the sensitivity of the device. This fact, if confirmed by further measurements, could represents a crucial aspect in future developments of the techonology.

The increment of the "Signal to Noise Ratio" and of the limit of detection, together with the increased sensitivity can be ascribed to the reduction of the dark current, obtained keeping the device away from light sources.

However it is also true that the measurements made at Skan-X Radiology Devices S.p.A. represent the first attempt of X-ray characterization with such small doses and time of exposure. Moreover the energy spectrum of the radiation X used in the laboratory's measurements is completely different from the one emitted by the X-ray tube used in the factory.

Most of the results achieved during the X-ray characterization in Skan-X Radiology Devices S.p.A. can be probably ascribed to the fact that the device tested was kept in the dark for several months. This condition induced a net reduction of the dark current of the device.

Looking at the graphs previously reported, it is evident how these devices are subject to a considerably stressed while they are irradiated by radiation X. This stress is quantifiable with an increment in the darkcurrent of the device.

One of the most important results obtained from the data collected dur-

ing the measurements in the X-ray tube company is that the characteristic (Photocurrent Vs Dose Rate) shows a decrescent exponential trend.

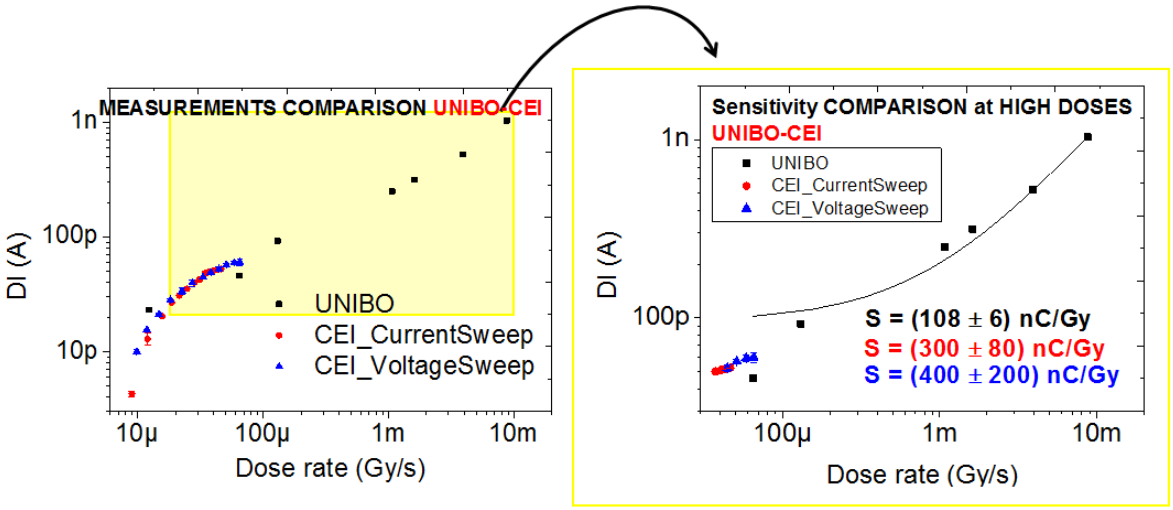

Figure 68 - Comparison charts for the measurements held at UNIBO % Skan-X

According to the experimental data it looks like there is a saturation effect at higher doses; in fact, in this region, the sensitivity's value obtained from the measurements held at the Department of Physics and Astronomy of Bologna are comparable, within the experimental error, with the one obtained from the measurements held at Skan-X Radiology Devices S.p.A. as shown in Figure 68.

Because of this saturation effect, it could be necessary to evaluate the sensitivity of the device using the Non-linear model presented in Dr. Laura Basirico's article[6]. In fact the data collected during the measurements held at Skan-X Radiology Devices S.p.A. present a saturating trend which suggests the practical definition of a "low dose sensitivity" and a "high dose sensitivity" as evidenced in the graphs in Figure 63 & Figure 65.

Chapter 9

Conclusions

The purpose of this thesis was to study the effect of different substrates on the behaviour of the organic device and assess the permormance of organic X-rays detectors at energies, dodes and exposure time typuical of Medical Radiography. To accomplish this task 5 different "substrates" were analyzed both with TIPS & TIPGe solution. Secondly, as a part of this study, thanks to the collaboration with the Skan-X Radiology Devices S.p.A, it was possible to test under different condition (Energy, distance, focalization of the X-ray beam) a TIPGe device which was shielded and protected from light sources for several months.

Data confirms that the TIPGe devices present a better sensitivity toward radiation X followed by a better electrical conductivity. It is important to proceed testing other devices in the future, in order to verify if there is a correlation between the sheet resistivity and the sensitivity of the samples.

The importance of the measurememts held at Skan-X Radiology devices S.p.A. resides mostly in the possibility of testing the devices in a complete different environment. First of all the energy spectrum was completely different; moreover the X-ray beam wasn't focalized such as the one used for the laboratory's X-ray characterization. Secondly it was encouraging to notice that the device tested wasn't to much sensible to the noise generated by the environment itself.

In details, it was surprising to notice that the TIPGe device was able to detect radiation X characterized by a dose rate smaller of a factor 10 with

respect to the one of the laboratory's measurements. This fact is not completely understood; howvere it can be assumed that the energy spectrum of the radiation X plays a key role in the phenomenon of the photoconductive gain.

According to the data collected in previous studies and compared to the ones subject of this work, it is evident that keeping the device away from light sources helped a lot to reduce the dark current.

The reduction of the dark current can be considered the principal cause to the increment of sensitivity, Signal to Noise Ratio (SNR) and limit of detection, in the TIPGe device tested at Skan-X Radiology Devices S.p.A.

It was evidenced that the devices are subject to a considerably stress whenever they are irradiated by radiation X; it is necessary to study in depth when, the increment of dark current due to this phenomenon of X-ray stress, will make the device unusubale or rather unreliable.

Further developments

The role of the substrate on the detection is not completely understood. It will be necessary to verify whether the problem related to some of the SiO_2 substrated can be ascribed to the process of device's realization or whether they are related to something more complex.

The industrialization of the process of realization of the devices is mandatory in order to minimize the possibility of problem related to fabrication mistakes,in particular the drop casting and the deposition process.

It will be important to test other devices which have been kept in the dark for long time such as the TIPGe subject of this study. It showed very interesting and encouraging results which needs to be replicated.

It should be newsworthy to test the TIPGe device with other radiological machine such as "intraoral X-ray tubes machine" or "panoramical X-ray tubes machine" where it is possible to have focalized X-ray beam and exposures

which last no more than some tens of milliseconds.

In order to move towards the realization of a prototype of X-ray detector it will be necessary to scale the dimension of the pixel, checking that the reduction of the dimensione of the device will not influence its behaviour.

The realization of a large area flexible detectors represents one of the main target of the project; data obtained in this work and the above mentioned conclusions deserve to be investigated in future studies to provide additional data.

Bibliography

[1] Fraboni B. Ciavatti A. Basiricò L. Fraleoni-Morgera A. *Organic semiconducting single crystals as solid-state sensors for ionizing radiation.* Faraday Discuss. 174, 219–234, 2014.

[2] Matsunage Akamatu Inokuchi. "rganic Semiconductors with High Conductivity: Complexes Between Polycyclic Aromatic Hydrocarbons and Halogens". In: *Bull.Chem.Soc.Jap. 29* ().

[3] Kang-Jun Baeg et al. "Organic light detectors: photodiodes and phototransistors." In: *Advanced materials (Deerfield Beach, Fla.)* 25.31 (Aug. 2013), pp. 4267–95. DOI: 10.1002/adma.201204979.

[4] Hongzhen Lin Fenglian Bai. *Electronic Process in Organic Solids*. Wiley, 2013.

[5] *Barracuda multimeter Datasheet.*

[6] Laura Basiricò et al. "Inkjet printing of transparent, flexible, organic transistors". In: *Thin Solid Films* 520.4 (Dec. 2011), pp. 1291–1294. ISSN: 00406090. DOI: 10.1016/j.tsf.2011.04.188.

[7] Weiss Borsenberger. "Organic Photoreceptors for Xerography". In: *arcel Dekker Inc. New York.* ().

[8] Wolfgang Brütting. *Physics of organic semiconductors*. Wiley. com, 2006.

[9] Richard H. Bube. *Photoelectronic Properties of Semiconductors*. Cambridge University Press, Cambridge, 1992.

[10] P. et al. Büchele. *X-ray imaging with scintillator-sensitized hybrid organic photodetectors.* Nat. Photonics 9, 843–848, 2015.

[11] Brown Burroughes Bradly. "Light-Emitting Diodes Based on Conjugated Polymers". In: *Nature* ().

[12] M B Casu et al. “A high-resolution near-edge x-ray absorption fine structure investigation of the molecular orientation in the pentacene/poly(3,4-ethylenedioxythiophene):poly(styrenesulfonate) pentacene/system.” In: *The Journal of chemical physics* 128.1 (Jan. 2008), p. 014705. DOI: 10.1063/1.2812649.

[13] MH Choo, WS Hong, and Seongil Im. “Characterization of pentacene organic thin film transistors fabricated on SiN x films by non-photolithographic processes”. In: *Thin Solid Films* 421 (2002), pp. 492–496.

[14] LL Chua et al. “General observation of n-type field-effect behaviour in organic semiconductors”. In: *Nature* 434.March (2005), pp. 194–199. DOI: 10.1038/nature03293.1..

[15] “Direct X-ray photoconversion in flexible organic thin film devices operated below 1V”. In: *Nature Communication* (2016).

[16] “Electrochemical polymerization of pyrrole”. In: *Journal of the Chemical Society, Chemical Communications* ().

[17] Thompson Forrest Bradley. “Measuring the efficiency of organic light-emitting devices”. In: ().

[18] Beatrice Fraboni et al. “Organic semiconducting single crystals as next generation of low-cost, room-temperature electrical X-ray detectors.” In: *Advanced materials (Deerfield Beach, Fla.)* 24.17 (May 2012), pp. 2289–93. DOI: 10.1002/adma.201200283.

[19] Schrieffer Heeger Kivelson. “Solitons in Conducting Polymers”. In: ().

[20] A Intaniwet et al. “Heavy metallic oxide nanoparticles for enhanced sensitivity in semiconducting polymer x-ray detectors.” In: *Nanotechnology* 23.23 (June 2012), p. 235502. DOI: 10.1088/0957-4484/23/23/235502.

[21] P. Lodomez J. Fink H. Krüger and N. Wermes. “Characterization of charge collection in CdTe and CZT using the transient current technique”. In: *Nuclear Instruments and Methods in Physics* (Nov. 2000).

[22] editor. J. Lilley. *Nuclear Physics: Principles and Applications.* Wiley. com, 2001.

[23] J.A.Seibert. *X-Ray Imaging Physics for nulear Medicine technologist.* 2004.

[24] Peter Proctor John McGinness Corry. “Amorphous Semiconductor Switching in Melanins”. In: *Science* ().

[25] Pope Kallmann. “Bulk Conductivity in Organic Crystals”. In: *Nature* ().

[26] Pope Kallmann. “Surface-Controlled Bulk Conductivity in Organic Crystals”. In: *Nature* ().

[27] Sano Pope Kallmann. “Recombination Radiation in Anthracene Crystals”. In: *J. Chem. Phys. 14* ().

[28] N Karl. “Charge carrier transport in organic semiconductors”. In: *Synthetic Metals* 133 (2003), pp. 649–657.

[29] *Keithley SourceMeter 2614B Datasheet.*

[30] G. F. Knoll. *Radiation detection and measurement*. Wiley, 2000.

[31] C Koidis and S Logothetidis. “Optimization of active nanomaterials and transparent electrodes using printing and vacuum processes”. In: *Handbook of Flexible Organic Electronics: Materials, Manufacturing and Applications* (2014), p. 253.

[32] Erich Krestl. *Imaging Systems for Medial Diagnostis*. Siemens.

[33] J H Lee et al. “Organic thin-film transistors fabricated on plastic substrates with a polymeric gate dielectrics”. In: *Jpn. J. Appl. Phys. Part 2 - Lett.* 42 (2003), pp. L523–L525.

[34] Chu-Hsuan Lin and Chee Wee Liu. “Metal-insulator-semiconductor photodetectors.” In: *Sensors (Basel, Switzerland)* 10.10 (2010), pp. 8797–826. DOI: 10.3390/s101008797.

[35] Mang Mang Ling and Zhenan Bao. “Thin film deposition, patterning, and printing in organic thin film transistors”. In: *Chemistry of materials* 16.23 (2004), pp. 4824–4840.

[36] C. Melzer. *Characterization of organic semiconductors and optoelectronic elements*. University Library Groningen][Host], 2004.

[37] A. G. Feucht. Milnes. *Heterojunctions and Metal-Semiconductor Junctions*. Academic Press, New York, USA, 1972.

[38] Herbert Naarmann. “Polymers, Electrically Conducting”. In: *Ullmann’s Encyclopedia of Industrial Chemistry* ().

[39] Douglas Natelson. “Organic semiconductors: Carrier characteristics.” In: *Nature materials* 9.9 (Sept. 2010), pp. 703–4. DOI: 10.1038/nmat2845.

[40] HT Nicolai et al. “Unification of trap-limited electron transport in semiconducting polymers”. In: *Nature Materials* (2012).

[41] W J Oosterkamp. “Evolution of the x-ray tube.” In: *Röntgenpraxis; Zeitschrift für radiologische Technik* 23.11 (Nov. 1970), pp. 252–60.

[42] E Ishmael Parsai, Diana Shvydka, and Jun Kang. "Design and optimization of large area thin-film CdTe detector for radiation therapy imaging applications." In: *Medical physics* 37.8 (Aug. 2010), pp. 3980–94.

[43] Maria Elias Lopes Pereira. *Characterization of direct X-ray Detectors based on Organic Semiconductor thin films*. 2018.

[44] Andreas Pahlke Peter Lechner. "Novel high-resolution silicon drift detectors." In: *X-ray spectrometry* ().

[45] Jose G. Rocha and Senentxu Lanceros-Mendez. "Review on X-ray Detectors Based on Scintillators and CMOS Technology". In: *Recent Patents on Electrical Engineering* (Apr. 2011).

[46] G C Sanderink and D A Miles. "Intraoral detectors. CCD, CMOS, TFT, and other devices." In: *Dental clinics of North America* 44.2 (Apr. 2000), pp. 249–55, v.

[47] Kallmann Sano Pope. "Electroluminescence and Band Gap in Anthracene". In: *J. Chem. Phys. 43* ().

[48] J. Anthony Seibert. "Flat-panel detectors: how much better are they?" In: *Pediatric radiology* 36 Suppl 2 (Sept. 2006), pp. 173–81.

[49] M Spahn, V Heer, and R Freytag. "[Flat-panel detectors in X-ray systems]." In: *Der Radiologe* 43.5 (May 2003), pp. 340–50.

[50] "Superconductivity in a synthetic organic conductor". In: *Journal de Physique Lettres. 41* ().

[51] "Synthesis of electrically conducting organic polymers: halogen derivatives of polyacetylene". In: *Journal of the Chemical Society, Chemical Communications* ().

[52] Van Slyke Tang. "Organic Luminescent Diodes". In: *Appl. Phys. Lett. 51* ().

[53] Albert C. Thompson. *X-Ray Data Booklet*.

[54] Sie-Chin Tjong. *Nanocrystalline Materials: Their Synthesis-Structure-Property Relationships and Applications*. Elsevier, 2013.

[55] *VacuDap dosimeter Datasheet*.

[56] Pfeifer Walzer Maennig. "Highly efficient organic devices based on electrically doped transport layers". In: ().

[57] W.T.Sproull. *X-Rays in practice*. McGraw Hill, 1946.

[58] J. Yaffe and J. A. Rowlands. "X-ray detectors for digital radiography". In: *Imaging Research Program, Sunnybrook Health Science Centre,* (Apr. 1996).

[59] S. et al. Yakunin. *Detection of X-ray photons by solution-processed lead halide perovskites.* Nat. Photonics 9, 444–449, 2015.

[60] Hee Taek Yi et al. "Ultra-flexible solution-processed organic field-effect transistors." In: *Nature communications* 3 (2012), p. 1259. DOI: 10.1038/ncomms2263.

[61] Roland J.A. Zhao W. "X-ray imaging using amorphous selenium: feasibility of a flat panel self-scanned detector for digital radiology." In: *Medical Physics* ().

Aknoledgments

My sincere thank goes to Professor Beatrice Fraboni, supervisor of the thesis, who gave me the possibility to accomplish this study. I want to thank Dr.Andrea Ciavatti & Dr.Ilaria Fratelli which helped me with advice, tips and their knoledge. I want to thank my colleague and General Operation Manager of Skan-X Radiology Devices S.p.A, Ing. Carlo Dalla Val, co-supervisor, which allowed me to dedicate part of my time to develop this project. I want to thank my colleague and Research & Development responsible, Dr.Lorenzo Giuliani, co-supervisor, who is sharing with me everyday his deep knowledge of the world of X-ray. I would also like to thank all my colleague, both from the University and from the company, even the smaller advices have always been important.

A special thank goes to my friend which sustained me during these intense two years of working and studying at the same time. A true and deserved thank goes to my girlfriend who has endured me in the last months. Last but not least, I want to thank my brother and sister for their unconditional support.

Finally, my heartfelt thank goes to my parents who have made this possible.